2011

Synthesis and binding studies of peptide mimetics, anion receptors, and kinase inhibitors

Nanditha G. Nair

Department: Chemistry

SYNTHESIS AND BINDING STUDIES OF PEPTIDE MIMETICS, ANION RECEPTORS, AND KINASE INHIBITORS

by

NANDITHA GOVINDAN NAIR

A DISSERTATION

Presented to the Faculty of the Graduate School of the

MISSOURI UNIVERSITY OF SCIENCE AND TECHNOLOGY

In Partial Fulfillment of the Requirements for the Degree

DOCTOR OF PHILOSOPHY

in

CHEMISTRY

2011

Approved by

V. Prakash Reddy, Advisor

Subhendar Kapila

Yinfa Ma

Ekkehard Sinn

Oliver C Sitton

Jeffrey G. Winiarz

ABSTRACT

A series of novel purine-based fluoroaryl triazoles were synthesized and assayed for their neuroprotective effects of hippocampal slice culture exposed to amyloid beta (Aβ) oligomers. A monofluorinated triazole has been identified which has comparable neuroprotective effect as that of flavopiridol and roscovitine against the Aβ induced neurotoxicity.

Carnosine and histidine are biologically interesting antioxidants. In order to probe whether they exert their antioxidant effect through metal ion chelation, the Cu(II) ion chelating abilities of these compounds were measured by UV–vis spectroscopy.

Amyloid beta, the major component of senile plaques in Alzheimer's disease, is known to complex transition metal ions through histidine residues. In this study, using ^{1}H NMR titration experiments, it was shown that histidine binds strongly to Zn(II), Cu(II), and Fe(III) ions at a biologically relevant pH (pH 7.4), with a stoichiometry of Zn(II): histidine binding of 1:2.

Fluorinated boroxines, tris(2,6-difluorophenyl)boroxin (DF), tris(2,4,6-trifluorophenyl)boroxin (TF), and tris(pentafluorophenyl)boroxin (PF) were synthesized and investigated for their fluoride anion binding affinity using multinuclear Nuclear magnetic resonance (NMR) and tandem mass spectroscopic techniques. DFT calculations show that the fluoride ion complex of DF prefers unsymmetrical, covalently bound structure over the symmetrically bridged species by 12.5 kcal/mol.

ACKNOWLEDGMENTS

I am indebted to many people in my life for helping me achieve this work. I begin by expressing my gratitude to Prof. Reddy for his invaluable guidance in my research all through these four years. He shaped the researcher in me by giving me the freedom to think and work independently. Moreover, he offered me the best opportunities in my life. I am thankful to Prof. Kapila, Prof. Ma, Prof. Sinn, Prof. Sitton and Prof. Winiarz for being part of my advisory committee. I am grateful to Department of Chemistry at Missouri S&T for supporting my research. My journey to Missouri S& T wouldn't have been complete without the encouragement from my undergraduate and graduate professors; of whom Dr. S. Prathapan deserves special mention. Collaboration with many scientists complemented this research work. I acknowledge Dr. Mario Blanco at CalTech, Dr. William West at JPL and Dr. Mark Smith at Case Western university. I take pleasure in thanking all the present and past members of Prof. Reddy's group for their help. Words cannot render the love, appreciation and gratefulness I have towards my family and friends for the unconditional love and support they have extended to me during my research.

TABLE OF CONTENTS

LIST OF FIGURES

LIST OF SCHEMES

LIST OF TABLES

1. PURINE-BASED FLUOROARYL-1,2,3-TRIAZOLES: Aβ OLIGOMERS AND CELL CYCLE PROTEIN INHIBITORS IN ALZHEIMER'S DISEASE

1.1 CELL CYCLE INHIBITORS IN ALZHEIMER'S DISEASE

Amyloid beta plaques (Aβ), Neurofibrillary tangles (NFTs), neuronal loss and dysfunction are the major pathological hallmarks of Alzheimer's disease (AD). Aβ plaques consists of mainly Aβ which derives from Aβ precursor protein(APP). Neurofibrillary tangles are made up of hyperphosphorylated forms of the microtubule associated protein tau. Neuronal loss results in cognitive impairment in neurodegenerative disease. Several hypotheses, such as the Aβ hypothesis and oxidative stress, have been proposed to explain the contributing aspect of Alzheimer's disease (AD). In recent years the concept of abnormal neuronal cell cycle re-entry is gaining increasing attention, as a major causative factor for AD.[1-2] AD brain is characterized by over expression of cell cycle regulating proteins,[3] indicating that neuronal cells are reentering the cell cycle leading to neuronal cell death.

Cell cycle is the cellular process, leading to proliferation and differentiation of cells. The cell cycle is regulated by a group of protein kinase called cyclindependent kinase (Figure 1.1). The four main phases of the cell cycle are, S phase where the DNA replication take place, M phase where cell division happens and G1 phase where cells increase in size and get ready for DNA replication, G2 phase, the gap between DNA replication and mitosis. When a cell is in any phase of the cell cycle other than mitosis, it is often said to be in interphase. Cells that have temporarily or reversibly stopped dividing are in a state of quiescence called G_0 phase. The neuronal cells in adult

hippocampus are an example of quiescent cells. Such terminally differentiated cells are generally incapable of reentering in to the cell cycle. They will continue their function in G0 phase. Under physiological conditions neurons are subjected to a variety of stimuli and signals. They include mitogenic signals that promote reentry in to the cell cycle and antimitogenic factors which strive to maintain the neurons in the G0 phase. However, conditions such as brain injuries can alter the balance, leading to cell cycle entry. It has been shown that cell cycle proteins are over expressed in AD patients with mild cognitive impairments. These are over expressed even before the appearance of Aβ plaques indicating that cell cycle reentry happens at the early stage of disease.

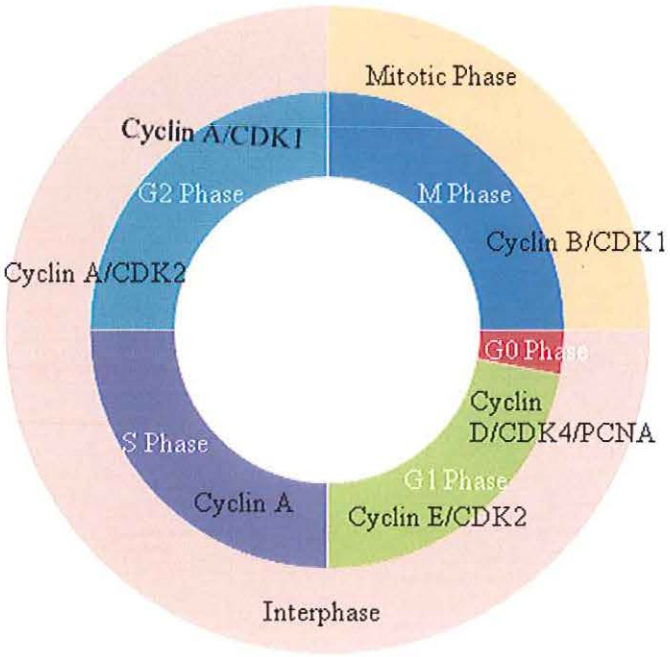

Figure 1.1 Cell cycle proteins and CDKs which are involved in the different phases of the cell cycle.

1.1.1 Cell Cycle and Cyclindependent Kinases. Each phase of the cell cycle is regulated by a group of cell cycle proteins and cyclin dependent kinases (CDKs) (Figure 1.1). They are a group of serine/threonine kinases that are regulated by subunits cyclins. Several CDKs are involved in the process of cell cycle. Mainly CDK4, CDK6, CDK1 and CDK2 cooperate to drive cells through the cell cycle by binding to appropriate cyclins along with other cell cycle proteins (e.g. PCNA). Reentry of cells in the G0 phase to the G1 phase are activated by CyclinD/CDK4/ PCNA(proliferating cell nuclear antigen) complexes.[4]Cyclin E/CDK2 complexes are involved in the transition of G1 phase into S phase. cyclin A binds to CDK1 in G2 and, together with CDK1–cyclin B, lead to an entry into mitosis. Cell cycle progression from the G2 phase into Mitotic phase is controlled by the presence or absence of Cyclin A. Absence of Cyclin A may lead to redifferentiation of the cells by returning to the G0 phase.[5-6]

1.1.2 CDK5 and Neurodegeneration. CDK5 is essential for both neuronal differentiation and cell cycle inhibition.[7] CDK5 is not directly involved in cell cycle regulation. CDK5 activity increases, when neurons exit the cell cycle during the differentiation. Loss of CDK5 leads to both failure of neuronal differentiation and loss of cell cycle control.[8-10] CDK5 is present in all cell types, but its activity has been detected only in the central nervous system (CNS). The cellular activity of CDK5 is regulated naturally by other kinases, phosphates and inhibitory peptides. Binding of CDK5 to cyclin-like p35, a neuron specific protein, leads to activation of the kinase. Normal functions of CDK5/p35 include neurite outgrowth/ differentiation, regulation of dopamine signaling through phosphorylation of DARPP-32 and regulation of presynaptic

neurotransmitter release.[11-14] Over activated CDK5 is able to phosphorylate tau protein leading to the formation of neurofibrillary tangles which is the main morphological features of Alzheimer's brain. Membrane-bound p35, when activated by molecules like amyloidβ converts into CDK5/p25 and relocalizes in to cytoplasm leading to neurotoxicity. Its expression in the CNS is converse to the expression levels of the cell cycle kinases. As neurons differentiate, CDK2 and CDK1 are downregulated, while CDK5 expression increases.[15] There are excellent reviews on role of CDK5 in neurodegenration.[16-18] CDK5 shares a high degree of homology with CDK1 and CDK2 and selective inhibition is highly important in therapeutic treatment.CDK5 activity is increased following axon injury and regeneration [19] and treatment with roscovitine (2) and olomoucine (3) reduces the extent of regeneration.

1.1.3 Aβ Oligomers and Cell Cycle Reentry. It has been shown that although cell cycle proteins are over expressed, this factor alone doesn't cause cell cycle reentry. It needs stimuli from the molecules like Aβ, reactive oxygen species, nitric oxide and others. Elevated levels of these molecules induce mitogenic signal cascades and when this exceeds beyond a threshold neurons exit the G0 state and reenter the cell cycle (Figure 1.2). Aβ oligomers are more toxic than Aβ plaques, which are present around the dying neurons. There are many theories on how Aβ can be neurotoxic. A recent study using transgenic mice show that (R1.40 Tg) neurons reenter in to cell cycle, even 6 months before the appearance of Aβ plaques.[20] Experiments in transgenic mice which lack BACE show that the cell cycle proteins are not expressed. BACE is a protein that is necessary for the production of Aβ from its precursor. These results indicating that cell

cycle reentry happens at early stages of AD. The formation of Aβ plaques occurs in the later stage. When neurons, *in vitro* are subjected to Aβ oligomers, but not monomers, there is increase in DNA synthesis, giving further evidence for the importance of Aβ oligomers on cell cycle reentry. The neuronal cells that reenter the cycle undergo apoptosis before reaching the Mitotic stage. Evidences show that Aβ induced neurons proceed to the S phase and replicate DNA. Thus the neurons entering the cell cycle are trapped in or before the s phase. They neither finish dividing nor enter in to the G0 phase.

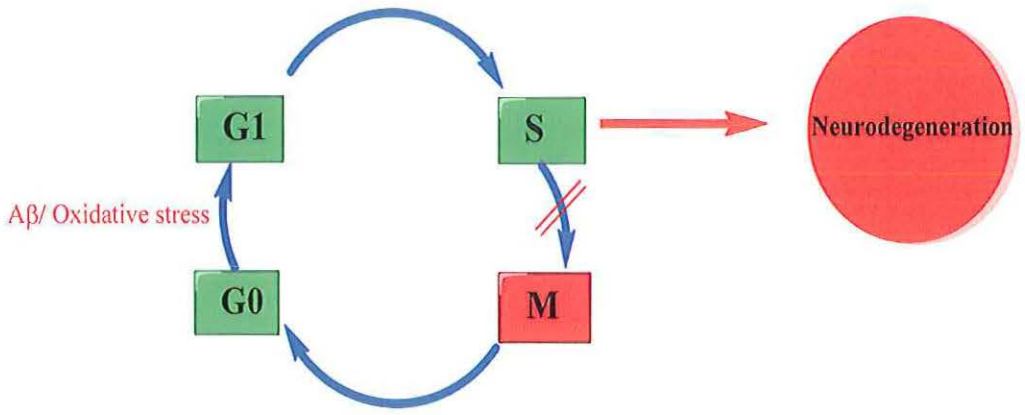

Figure 1.2. Aβ induced neurons proceed to S phase and replicate DNA.

1.1.4 Aβ and CDK5. Aβ plaques occur around the neuron, when the balance of Aβ generation and clearance is altered. Aberrant activation of kinases and inhibition of phosphatases results in elevates the levels of Aβ and Neurofibrillary tangles. Overactivation of CDK5, mediated by A β results in tau-hyperphosphorylation, decreased

levels of synaptic markers, and cell cycle reactivation leading to substantial neuronal loss.[21-22] In turn CDK5, in association with aberrantly formed protein p25 (by cleavage of p35), is responsible for Neurodegeneration. P25 accumulation may precede the formation of NFT in AD brain. Even though the involvement of the p25 in the intracellular neurofibrillary tangle (NFT) formation is not well established,[23] its role in neuronal cell-cycle re-entry and resultant neuronal cell death is widely established.[24-25] Aβ induces the cleavage p35-p25 in primary cortical neurons.[26] Accumulation of p25 and overactivation of CDK5 resulted in elevated levels of Aβ-42 in APP transgenic mice.[27-28] Inhibition of CDK5 activity inhibits the Aβ induced neuronal cell death, indicating that aberration in CDK5 activity and formation of Aβ plaques are related to each other.[29] There are conflicting reports on the role of CDK5 on APP processing. CDK5 inhibitors injected in to the transgenic mouse brain increased the level of Aβ in the brain[30] and inhibition of CDK5 in APP transfected HEK293 cells elevated the Aβ secretion.

1.1.5 Cell Cycle Proteins and Cyclin Dependent Kinases as Targets for the Treatment of AD. Terminally differentiated neuronal cells are not capable of proliferating by entering in to mitotc stage, where tumor cells entering the cell cycle are capable of proliferating. Pathological evidence of AD shows the entry of neurons in G0 phase to G1 phase or beyond.[31-33] Neurons undergo cell cycle progression in AD, to the point that DNA replication occurs.[34-35] AD neuron exhibits over expression of cyclins, CDKs and other cell cycle regulating factors (e.g. PCNA).[3] [31-32] Since cell cycle reentry leads to neuronal death in neurodegenerative disease and cell proliferation in

cancer, cell cycle inhibition prevents neuronal cells from dying as well as proliferation of tumor cells. Thus cell cycle inhibition is a therapeutic strategy for both neurodegenerative disease and cancer.[36] Several molecules are involved in cell apoptosis and Neurodegeneration.[37] A number of chemical inhibitors of neuronal apoptosis targeting a variety of different proapoptotic proteins, including c-jun N-terminal kinase (JNK), glycogen synthase kinases (GSK3), and p53 were investigated.[37] The main focus of this review is inhibitors of cyclin dependent kinases.

Two distinct CDK pathways may have a role in the neuronal loss responsible for AD. One pathway involves aberrant reactivation of the cell cycle, whereas a second involves dysregulation of CDK5.[38] Cell cycle inhibition by inhibiting CDKs was first used in cancer therapy. The concept of inhibition of cell cycle reentry in neurodegenerative disease got attention in recent years. Thus there are not many drug discovery programs in this area targeting AD. Structurally diverse compounds including indole,[39-42] imidazole,[43-44] pyrazolopyridine,[45] pyridopyrimidines,[46] piperidine,[47] and purine[48-55] derivatives have been tested as CDK inhibitors.[56-57] But not many of these were tested for CNS disorder. Although many CDK inhibitors are under clinical trial for tumor, no clinical trials of CDK inhibitors are reported for CNS disorder.

The class of CDK inhibitors which are reported for neurodegenerative diseases include the nonselective CDK inhibitor, flavopiridol(1); selective inhibitors of CDK1, 2, and 5 such as roscovitine(2), olocomucine(3), and butyrolactone 1 (4); the selective inhibitor of CDK5, GW8510 (5),[58-59] selective inhibitor of CDK5 and CDK2, Quinazolines(6),[60-61] 4.aminoimidazole(7),[62] indurubins (8),[63] 6-oxo-1,6-dihydropyridines(9).[64] So far there is not a single CDK inhibitor which is selective for a

particular CDK or other protein kinases. Most of them collectively inhibit either a group of CDKs or other protein kinases.

Several CDK inhibitors have been developed over the past decade (Figure 1.3). The first CDK inhibitor to reach clinical trial is Falvopiridol (1). Flavopiridol (1) Roscovitine (2), olomoucine (3) are the most widely studied CDK inhibitors.[65-66] Flavopiridol (1) is a broad spectrum CDK inhibitor where are purine derivatives are more specific. The neuroprotective effect of flavopiridol (1) was suggested to be due to its inhibition of CDK5 and to some extent CDK2.[67] However, flavopiridol (1) also inhibits other kinases, at higher concentrations. Additionally, disruption of RNA polymerase II-mediated transcription by flavopiridol (1) has been reported.[68] Flavopiridol (1) may have also role in inhibition of gene expression [69] . Recent evidences show that 1.methyl-4.phenylpyridinium (MPP) induced neuronal cells undergo cell cycle reentry in to S phase of the cell cycle. But in the presence of flavopiridol (1) and Olomoucine (3) the neuronal cell cycle re-entry and apoptosis were attenuated.[67, 70] Flavopiridol (1) and Roscovitine (2) were also reported to be neuroprotectors in colchicines-induced cell apotosis.[71] *In vitro* studies using HIV neurotoxicity model show that roscovitine (2) act as a neuroprotector by inhibiting CDK5 activity.[72] In a model of focal ischemia, (S)-roscovitine (2) was able to cross the blood brain barrier and prevent Cerebral increase of CDK5/p25 activity protecting the neurons *in vivo*.[73]

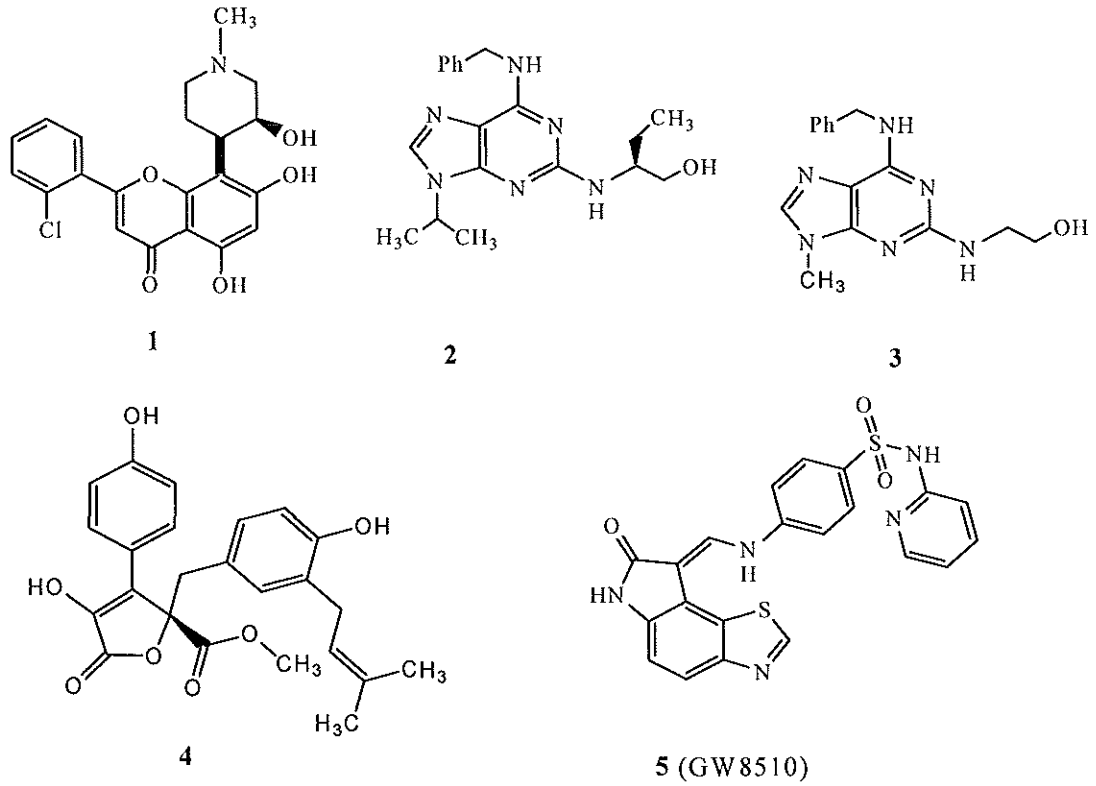

Figure 1.3. CDKs inhibitors which are currently under preclinical trial for treatment of AD.[63]

Butyrolactone-I (4) is a selective inhibitor of cyclin dependent kinases, particularly CDK5.[74] Butyrolactone-1(4) displays a selectivity profile similar to the purine analogues (e.g. inhibits CDKs 1, 2, and 5), and inhibits CDK 5 with an *in vitro* IC50 of 0.49 μM. Butyrolactone I(4) prevent memory consolidation by decreasing baseline CDK5 activity within the septo-hippocampal circuitry.[75] The neurotoxic effect of Aβ on primary cultures of hippocampal cells decreased on co-incubation of the butyrolactone I.[29]

A number of other 3.substituted indolones have also been found to inhibit neuronal death.[59, 76] GW5074 is a 3.substituted indolone (Figure 1–4), completely inhibits the death of cultured neurons induced by a variety of different apoptotic stimuli,[76] but it doesn't have any effect on any of the CDKs. Structurally similar compound GW8510 (5) (Figure 1.3) inhibits CDKs *in vitro* but has a weak effect on classical CDKs in cultured cells . GW8510(5) was discovered to be a potent inhibitor of CDK2 (IC50 = 60 nM) when tested *in vitro*.[77] In addition to CDK2, Davis and co-workers reported that GW8510 also inhibited other CDKs, including CDKs 4 and 6, at a higher concentration. Besides CDKs 2, 3 and 5, moderate inhibition of CDK1 and Gsk3b was also observed. In contrast CDK5 is inhibited by GW8510 both *in vitro* and *in vivo*. Since GW8510 is not inhibiting the cell cycle CDKs, the neuroprotection may be by other alternative mechanisms.[59]

Several 2.arylidine and 2.hetarylidin derivatives. of the 1,4.benzoxazines class of compounds (ASK2a and HSB-13) (Figure 1.4) are shown to be highly protective in tissue culture models of Neurodegeneration. ASK-2a was found to be neuroprotective in primary granule neurons. *Invitro* CDK inhibition studies of both Ask 2a and HSB-13 shows that HSB-13 inhibits CDK1, CDK2, and CDK5. HSB-13, but Not ASK-2a. HSB-13 is Protective against Oxidative Stress (Homocysteic Acid (HCA)-induced Neuronal Death. HSB-13 protects hippocampal neuroblastoma HT22 cells and neurons against HCA.[78] ASK 2a is not neuroprotective on oxidative stress induced cell death. This suggests that inhibition of CDKs is essential for protection against HCA-induced neurotoxicity. HSB-13 reduced striatal degeneration and improved behavioral performance in a chemically induced mouse model of Huntington's disease, and it

protects against APP toxicity in flies. The ability of HSB-13 to protect cortical neurons against Ab-toxicity and against oxidative stress (HCA) and flies against the detrimental effects of mutant APP suggests that this compound could have value in the treatment of AD. The protection displayed by HSB-13 in an in vivo model of HD suggests broad neuroprotective efficacy.

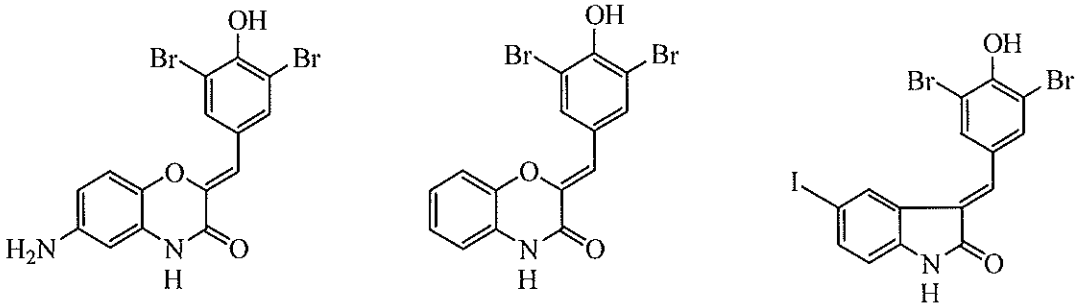

Figure 1.4. 3-substituted indolens for neuroprotection.

Indirubin and its derivatives were shown to be inhibits CDK5/p25 (IC50 =10 nm) and GSKb3(IC50 = 2 nm).[63] Indirubin-3'-monoxime (8, Figure 1.5) rescues spatial memory deficits and attenuates Aβ associated neuropathology in a mouse model of AD. Indirubins are very potent inhibitors of CDK5/p25. Furthermore, indirubin-3.monoxime inhibits tau phosphorylation *in vitro* and *in vivo* at AD-specific sites.[79] It also inhibits Aβ-induced neurotoxicity in neuroblastoma.[80]

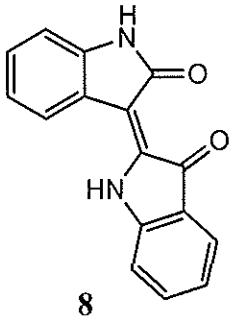

8

Figure 1.5. Structure of Indirubin - 3 '- monoxime.

The accumulation of p25 results in overactivation of CDK5 was related to Aβ toxicity. N-acetylcysteine (Figure 1.6) acts as a neuroprotector against the Aβ toxicity in cultured cortical neurons by an increase in p35/CDK5 activity and attenuation of p35 proteolytic degradation.[81]

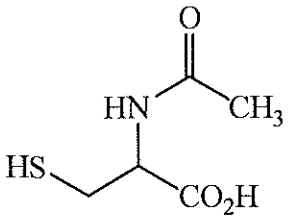

N-acetylcystein

Figure 1.6. Structure of N-acetylcystein.

Although there are several recent reports of CDK5 inhibitors for potential treatment of neurodegenerative disease, many of them are not extensively studied for their neuroprotection and selectivity towards kinases. In recent times, compounds based

on Quinazolines (6),[60-61] 4.aminoimidazole (7),[62] 6-oxo-1,6-dihydropyridines (9),[64] 3,6-diamino-1H-pyrazolo[3,4.bpyridine derivative (10),[82] has been investigated for their CDK5 inhibition and Aβ toxicity (Figure 1.7).

Based on the crystallographic data of 12/CDK2 complex, Rzasa and coworkers synthesized a series of 3,4.dihydro-1*H*-quinazolin-2.ones (6, IC50 = 79nm) as potent CDK5 inhibitors.[83] The 4.pyridyl moiety in these molecules form H-bonding to the Asp144.Lys33 salt bridge to the inhibition of CDK5. They are good inhibitors of CDK2 as well. The selectivity of these compounds over CDK5 is less to moderate.[83]

The derivative of 4- aminoimidazole (7, IC50 = 64 nm and 11, IC50 = 9 nm) compound has been shown to selectively inhibit the CDK5 over CDK2.[62] X-ray crystal structure of compound 11 with CDK2 shows that [62] the amide carbonyl accept a hydrogen bond from Lys33 and it interacts with a water molecule that bridges to the NH of Asp145. Lys33 and Asp145 (Asp 144 in CDK5) are the amino acid residue which in present in the phosphate binding region of ATP. The compound 3,6-diamino-4.phenyl-1H-pyrazolo[3,4.b]pyridine-5-carbonitrile 10 inhibits CDK5(IC50 =0 .4nM) and GSK-3β (IC50 = 1.5nM).[82]

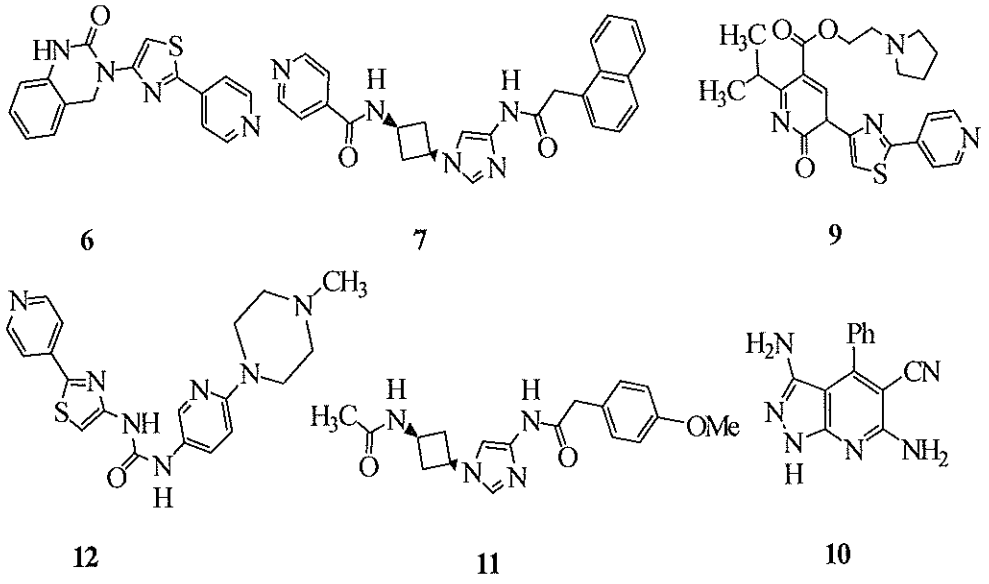

Figure 1.7. CDK5 inhibitors, which are potential drugs in neurodegenerative diseases.

1.1.6 Cyclin Dependent Kinases: Structural Consideration. Cyclin-dependent kinases (CDKs) are a family of 16 serine/threonine kinases that are key regulators of the mammalian cell cycle.[66] CDK5 is the main cyclin dependent kinase which is targeted in AD. Due to it similarity with CDK1 and CDK2 selective inhibition is a challenging problem. An understanding of structure of CDK5 and its mode of binding will give an insight in to develop better drugs. Crystal structure of CDK5/p25 cleared the mechanism of activation of CDK5 by p25.[84]

The classical mechanism of CDK activation include binding of the cyclin box fold and the phosphorylation of the activation loop known as T loop[85] by the CDK activating kinase[86-87]. p25 contains a highly divergent CBF domain which elicits an active conformation of CDK5 in the absence of phosphorylation[84]. Mapelli and coworkers co-crystalized CDK5/p25 and three kinase inhibitors, (R)-roscovitine (Figure 1.3) (2),

aloisine –A (Figure 1.8) and indurubin-3'-oxime(Figure 1.5).[66] These molecules ATP competitive binders which bind to the well conserved catalytic loop of the kinase. Their IC50 values are in the range of 0.1.0.2 mM. Smaller molecules such as aloisine A doesn't fit to the back cleft of the ATP binding pocket resulting in reduced shape complimentarily.

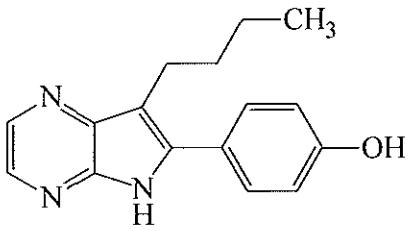

Aloisine-A

Figure 1.8. Structure of Aloisine-A.

Inhibitors affinity mainly arises due to the formation of hydrogen bonds and hydrophobic interactions. In CDK5, the back bone carbonyl and amide of Cys83 serve as a hydrogen bond acceptor and donor respectively. Crystals of CDK2 with inhibitors such as roscovitine (2), olomoucine (3) and purvalanol B (Figure 1.13) showed similar pattern of binding. But the orientation heterocyclic ring of these molecules in their complexes is different. These orientations are different from adenine ring in APT/CDK2 complexes itself. Different amino acids in binding loops of CDK5 are involved in the binding of different inhibitors to CDK5.

1.1.7 Structural Basis of CDK Inhibition. Cyclin dependent kinases belong to a super family containing eukaryotic protein kinase (ePK) catalytic domain.[88-90] Most of the protein kinases belong to this family have bilobal structure with N terminal domain of approximately 85 residues, C terminal domain of approximately 170 amino acid residues and a ATP binding cleft between the two lobes.[91-92] They bind to γ phosphate of ATP though serine\ threonine\tyrosine hydroxyl groups. Activation of kinases belong to ePK family are regulated by folding process of ePK domain.[93] In activation and deactivation of the kinases the active loop (T loop) under goes a conformational change to form a platform for the interaction of kinase with substrate. Activation loop is an approximately 20 amino acid residue located in the centre of N lobe and C lobe, where cyclin binding and phosphorylation takepalce. N lobe is reconstructed to generate a conformation to fit the ATP in the kinase active site.[94]

CDKs are an ePK subfamily of Serine/Threonine kinases. CDKS are activated by binding to cyclins a regulatory subunit. Another process in the activation of CDKs is the phosphorylation of the activation loop at a conserved threonine residue.[86, 95-96] This is the case with most of the members of CDK family, including CDK2, CDK1, CDK4 and CDK6.[97] CDK5 differs from others activation mechanism. The binding of CDK5 cyclins (cyclin D and E) doesn't lead to activation. Its activity is triggered by homologous proteins p35 and p39, which are expressed only in neurons and a few other cell types.[98-100] CDK5 is also not activated by the phosphorylation of potential site Ser159 (Thr 160 of CDK2) residue in the activation loop. [101-102]

In the case of CDK2, binding Cyclin A, remodels the kinase N lobe allow the correct orientation of amino acid residues with ATP. [94] For example, it pushes C helix

(PSTAIRE helix) [103] of N lobe facilitating the interaction Lys33 and Glu51 is with α and ß-phosphates of ATP. Cylin A also locks the conserved Asp-Phe-Gly motif (DFG) to a conformation that supports the function of this motif in the orientation of the α-phosphate of ATP via a magnesium ion. Another step in the activation process is the remodeling of the activation loop triggered via the phosphorylation of Thr160 by CDK-activating kinase.[96] CDK2 is deactivated by phosphorylation of T14 and Y15, in the glycine rich loop which is positioned opposite to the T loop.[103]

Cyclins interact with CDK2 through a 100 amino acid residue structural motif known as Cyclin box fold (CBF). Similarly p25 also has a CBF fold which binds the activation loop around PSAALRE (PSTAIRE in CDK2) helix. Similar to cyclins p25 also pushes the C helix to orient Lys33 and Glu51 for proper binding to ATP.

1.1.8 Mechanism of Binding of CDK Inhibitors. The majority of small-molecule kinase inhibitors that have been developed so far target the ATP binding site, with the kinase adopting a conformation almost identical to that used to bind ATP. Selectivity is a major issue in this strategy. In this the molecules inhibit the kinase by binding to the active DFG in conformation. A large conformational change for the residues in the conserved Asp-Phe-Gly (DFG) motif in the active site of kinase is required for the binding of the inhibitor. In all of the Ser/Thr kinase protein structures the DFG motif assumes a conformation with the Phe residue buried in a hydrophobic pocket in the groove between the two lobes of the kinase (DFG in conformation). The residues in the pocket are highly conserved among the kinases. On binding to inhibitors the Phe residue will move resulting in another conformation called DFG out conformation.[104]

The adenine of ATP forms a crucial hydrogen bond with the hinge region of the kinases in between the N- and C-terminal lobes of the kinase domains while the end β and γ phosphates of ATP are coordinated by a complex network of ionic and hydrogen bonding interactions with several structural elements, including Mg^{2+} or Mn^{2+} ions, the Asp side chain of the conserved DFG motif, and amino acid residues in the glycine-rich loop located above the ATP binding cleft.

Adenine region of ATP forms hydrogen bonding with Glu81 and Leu 83 residue of CDK2 in the active site. The carbonyl group of Gln 131 and Asp 86 act as a hydrogen bond acceptor to the hydroxyl group on sugar moiety in ATP. In addition to these hydrogen bonds, the phosphate groups engage in active hydrogen bonding with several amino acid residues in the active site (Figure 1.9).

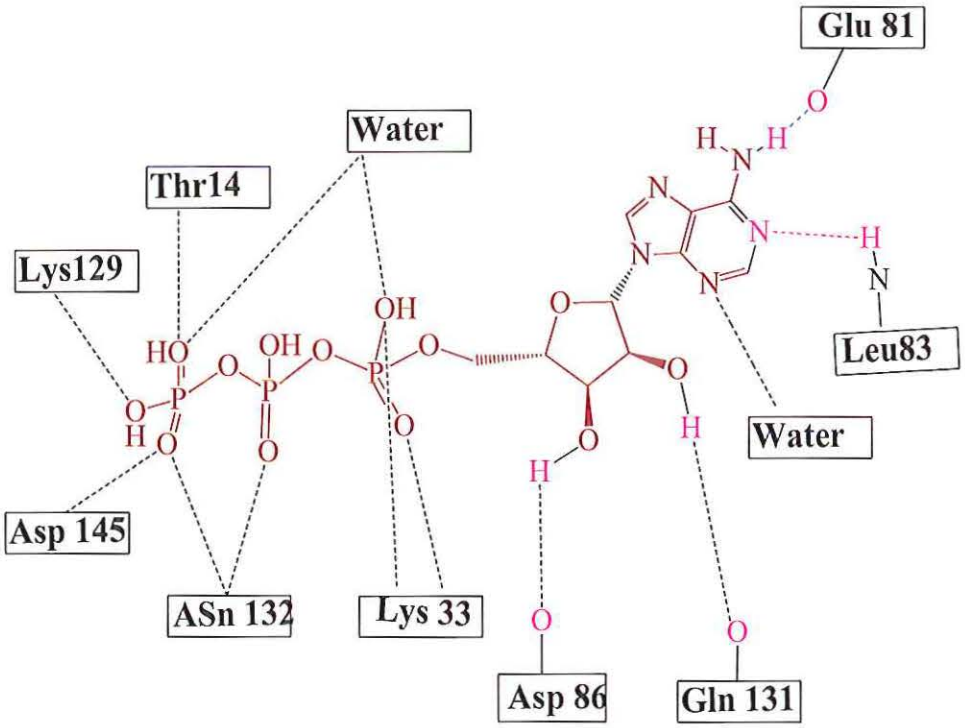

Figure 1.9. Major binding amino acid residues in CDK2 /ATP complex.

ATP competitive inhibitors typically form 1 to 3 hydrogen bonds with the kinase hinge residues. The binding region of inhibitors can be divided in to adenine region, ribose region, phosphate region and hydrophobic region. The adenine region can be occupied by all the inhibitors although with different orientations than ATP. The ability of inhibitors to extend in to hydrophobic region and other region is the key factor in the specificity. The co-crystal structures of roscovitine (2), olomoucine (3), aloisine, inirubin-3'-oxime (8) etc with CDK2 and CDK5/p25 have been reported (Figure 1.10 and Figure 1.11).[66, 105]

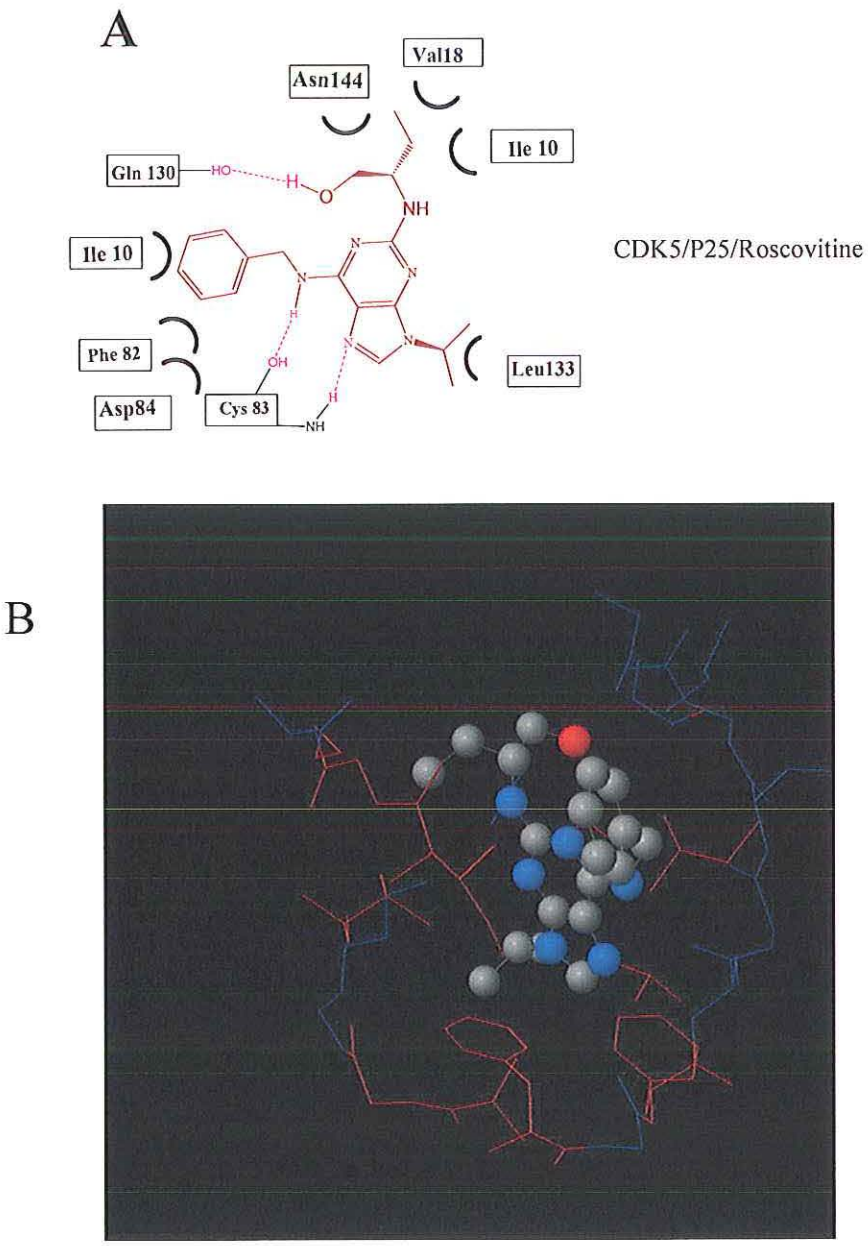

Figure 1.10. Schematic diagram of major aminoacids involved in binding of roscovitine (2) to CDK5/p25 (A). Crystal structure of CDK5/p25-roscovitine showing ligand binding pocket. Hydrophobic region is indicated in red (B)[66] (PDB, DOI:10.2210/pdb1unh/pdb).

A

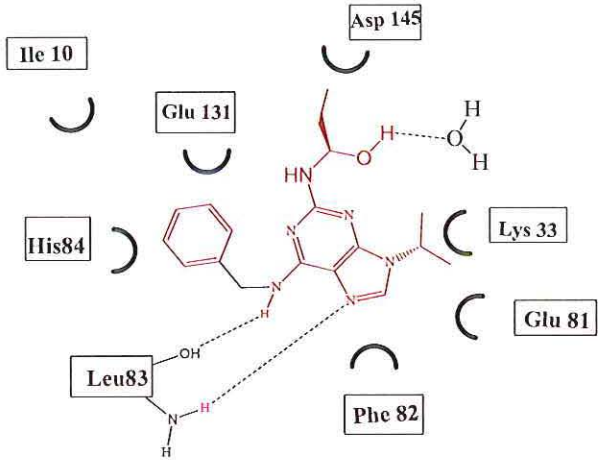

CDK2/Roscovitine

B

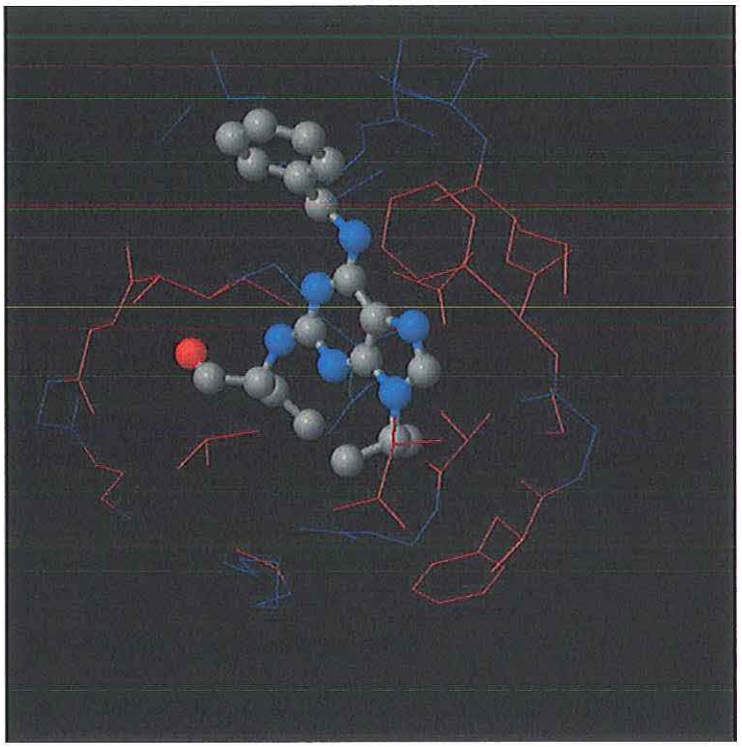

Figure 1.11. Schematic diagram of major aminoacids involved in binding of roscovitine (2) to CDK2 (A).Crystal structure of CDK2.roscovitine (2) showing ligand pocket. Hydrophobic region is indicated in red (B).[106]
(PDB, DOI:10.2210/pdb2a4l/pdb).

In the ATP pockets of CDK5 and CDK2 93% (27/29) of residues are conserved and the two differing amino acid residues (Cys83 and Asp84 in CDK5; Leu83 and His84 in CDK2) have side chains that project away from the ATP pocket, thus reducing their impact on inhibitor binding. Both CDK2 and CDK5 conserve the Phe80 residue of the hydrophobic pocket and maintain a Lys33.Asp144 salt bridge the binding pocket of CDK5.

In this CDK5/CDK2.inhibitor complexes different molecule have different orientation in the active binding pockets.[107] In this review we will be comparing the roscovitine (2) complexes of CDK2 and CDK5/p25, which is the most potent CDK5 inhibitor, currently under study. Roscovitine (2) is a planar molecule whose structure is highly complementary to ATP-binding cavity. In CDK5 the carbonyl and the amide of Cys 83 residue act as a hydrogen acceptor and donor respectively. The hydroxyl group of roscovitine (2) is hydrogen bonded to Gln 130 amino acid residue. The ethyl groups are buried in hydrophobic interactions with Ile10 and Val 18 (Figure 1.10).

The chiral C2-substiuent of roscovitine (2) in complexes with CDK5/p25 is rotated around 182^0 around the N-C bond compared to the C2 of roscovitine (2) in complexes with CDK2.[66] The large benzyl substituent is projected in to the hydrophobic pocket lined by Ile10 and Phe82. The cyclic nitrogen N7 act as a hydrogen bond acceptor to the NH of Cys 83. The backbone carbonyl oxygen act as a hydrogen bond acceptor to the NH of benzylamino group in the purine ring.

In CDK2 complexes of roscovitine (2), the hydroxyl group of roscovitine (2) is hydrogen bonded to water molecule. Leu 83 of CDK2 interacts with roscovitine (2) through two hydrogen bonds. One nitrogen N7 act on roscovitne as a hydrogen bond

acceptor for NH of Leu83 and the carbonyl group of Leu83 act as hydrogen bond acceptor to the NH of benzylamino group on roscovitine (2). CDK2 maintains 20 vander Waals interaction with the benzylaminogroup of roscovitine (2) in complexes[106] (Figure 1.11). This interaction is not shown by ATP in their complexes with CDK2. The main residues involved in these interactions are Ile10, Phe82 and His84. The ethyl group is interacting with hydrophobic environment.

1.1.9 Purine-Based Kinase Inhibitors. The purine derived cyclin dependent kinase inhibitors got much attention due to its structural similarity to ATP itself. Among them 2, 6, 9 substituted purines were found to be more active (Figure 1.12).

In 1973, Lionel Rebhun and co-workers discovered 6-dimethylaminopurine(6-DMAP, 13) as a protein synthesis enhancer which inhibited cell division in embryos.[108] In 1980's the compound 13 was largely used as a nonspecific protein kinase inhibitors.[109-110] Rialet and coworkes found the IC_{50} value of 6-DMAP as 120μM. The same group also found that plant hormone, N6-(γ,γ-Dimethylallyl)aminopurine, 14 (IC_{50}= 50μM, Table 1.1) another derivative of purine slightly more active that 6-DMAP.[111] In a continues effort to find out specific more active inhibitors, Jaroslav Vesely and coworkers studied the effect of the structural derivatives of 6-DMAP (13) and , N6-(γ,γ-Dimethylallyl)aminopurine (14) on protein kinases.

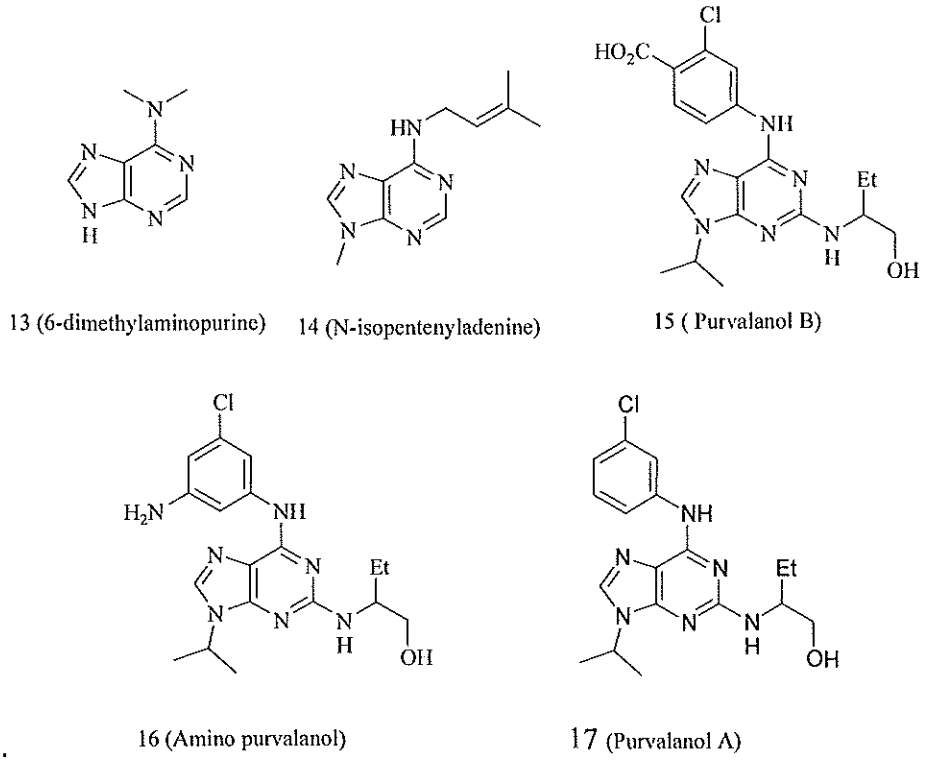

Figure 1.2. Structures of Purine based kinase inhibitors

But none of them showed any inhibitory effect (IC_{50}>500μM). Olomocine 3 (Figure 1.3) (2.(2.hydroxyethylamino)-6-benzylamino-9-methylpurine) and other C2, N6 and N9 substituted purines were found to exert strong inhibitory effect on CDK1, CDK2, CDK5, erk1 kinases but not on CDK4 and CDK6. [112]

Olomocine (IC_{50}=7μM) was found to be an antimitotic reagent and it act as a competitive inhibitor of ATP. Based on the structural activity relationship of more than 80 purine derivatives, Jaroslav and coworkers proposed the potential enzyme binding sites of 2, 6, 9substituted purine inhibitors. They proposed that N1, N3 and N7 are involved in hydrogen- bonding interaction and substitution at N9 and C2 are important

for hydrophobic interaction directly with CDKs. The purine ring may be involved in the hydrophobic interaction.[112]

Structural modification of Olomoucine (3) led to the development of Roscovitine, 2.{[(1.hydroxymethyl)propyl]amino}-6-benzylamino-9-isopropylpurine, 2 which was selective towards CDK1. Detailed analysis of molecular and cellular effects of purine CDK inhibitors, supported by co-crystal analysis, has motivated several scientific teams to continue with the synthesis and biological testing of 2, 6, 9-trisubstituted purines.[113-115] Gray and coworkers found that when benzyl amino group of roscovitine (2) is replaced with 3.chloroanilino group in purvalanol A (17), the inhibitory activity increased 100-fold roscovitine (2).[116]

The most potent compound known to date is purvalanol B. But it is inactive in cellular assays which may be due to its lack of cell permeability.[119]Although frequently considered as rather selective for some CDKs (CDK1, CDK2, CDK5, CDK7, CDK9), roscovitine (2) interacts with several other targets (DYRK1A, CK1, pyridoxal kinase), although with a lower affinity.[121-122] Moravec and coworkers found that 2, 6, 8,9-tetrasubstituted purines are not effective CDK inhibitors due to the rigid back part of the active site of CDK2.[123]

Table 1.1. IC50 (μM) of selected kinase inhibitors.

CDKs	CDK1/ CyclinB	CDK2/ CyclinA, E	CDK4/ CyclinD	CDK5/ p25
[105, 117]R-Roscovitine (2)	0.45	0.7	14.2	0.16
[117-118]Olomoucine (3)	7	7	>1000	3
[116]Purvalanol B	0.006	0.006(A), 0.009(E)	>10	0.006
[119]Aminopurvalanol	0.033	0.033(A), 0.028(E)	-	0.02
[120]Flavopiridol (1)	0.06	0.15	0.4	-
[118]NIsopentenyladenine	45	50(A)	>100	80

1.1.10 Conclusions. Although there are several reported CDK inhibitors in the literature for the treatment of other diseases such as tumor, not many of them are well studied for their neuroprotective effect. Many of the CDK inhibitors tested such as flavopiridol (1), roscovitine (2), butyrolactone 1 (4) and indirubins (8), although are very potent inhibitors of CDK5/p25, act on targets (GSK-3β), other than CDKs while inducing apoptosis. Whether their dual specificity with GSK-3β and CDK5/P25 is detrimental or beneficial is still under debate.[63, 124] No molecule which inhibits a single kinase has been found out. This can be due to the structural similarities of the cyclin dependent kinases.

Various side effects may arise because of the nonspecificty of those CDK inhibitors, which can act on other cell cycle regulating molecules. Thus achieving high selectivity will be one of the most important goals for the developments of new drugs.

1.2 PURINE-BASED FLUOROARYL-1,2,3.TRIAZOLES: SYNTHESIS AND EVALUATION AS CELL CYCLE INHIBITORS IN ALZHEIMER'S DISEASE

1.2.1 Introduction. The concept of abnormal neuronal cell cycle re-entry is gaining increasing attention in recent years, as a major causative factor for AD. Cell cycle dysregulation is accompanied by a variety of cascades including kinase upregulation, DNA replication, and eventually leads to neuronal apoptosis.[125-130] Cyclindependent kinases (CDKs) are the protein kinases which regulate cell cycle, among which CDK5 plays a major role in the neuronal cell death as a result of abnormal cell cycle re-entry. Overactivation of CDK5, mediated by A β (Aβ), results in tau-hyperphosphorylation, decreased levels of synaptic markers, and cell cycle reactivation leading to substantial neuronal loss.[21] CDK5 in association with its principal activation protein p35 is involved in functions such as neuronal differentiation and migration to synaptic transmission. Intracellular oxidative stress leads to a rise in Ca^{2+} levels that activate calpain resulting in the cleavage of p35 to p25.[131] Thus selective inhibitors of CDK5/p25 over CDK5/p35 are currently targeted, although there seems to be little success in this regard.[44, 131] A variety of CDK5 inhibitors are currently under development as potential therapeutics in AD and neuronal disorders. Structurally diverse compounds including indole,[39-42] imidazole,[43-44] pyrazolopyridine,[45] pyridopyrimidines,[46] piperidine,[47] and

purine[48-55] derivatives have been tested as CDK5 inhibitors. Among these compounds, flavopiridol (1) and roscovitine (2) are currently undergoing clinical trials as therapeutics in AD (Figure 1.13).[56-57]

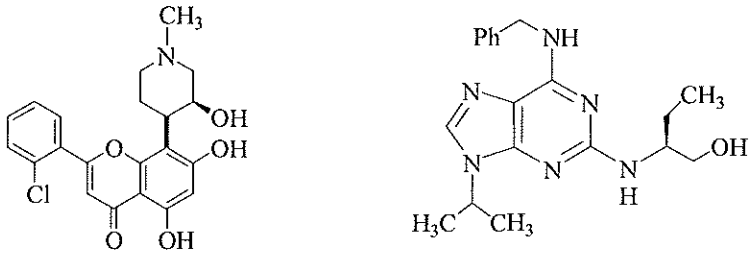

1 2

Figure 1.13. Structures of flavopiridol (1) and roscovitine (2)

Fluorinated compounds are a major focus of current pharmaceutical interest. Introduction of a fluorinated aryl groups into pharmaceuticals results in major improvement in their therapeutic efficacy, presumably due to the hydrogen bonding interactions with the fluorines at the enzyme active sites.[132-134] Further, fluorinated drugs have additional advantages such as their enhanced solubilities, metabolic stabilities and bioavailability. We have reasoned that by introducing a fluoroaryl group distant from the nucleoside moiety, their selective CDK5 inhibitory effect, and hence neuronal cell cycle suppression, could be improved. With that goal, we have now synthesized a series of fluorinated purine-based triazoles and we have assayed their neurotoxicity/neuroprotection in Aβ incubated hippocampal slice cultures, using fluorescence microscopy.

1.2.2 Results and Discussion. Selective inhibition of CDK5/p25 over CD5/p35 is a desired goal for the treatment of AD and other neurological disorders. Roscovitine (2) is currently undergoing preclinical trials as kinase inhibitor in AD, although it is not a selective inhibitor of CDK5.[57] Similarly, a flavone-derived compound, flaovopiridol has also been shown to be effective as a broad-spectrum CDK inhibitor.[135] Perhaps due to this nonspecificity to selective CDKs, it is more cytotoxic and has other harmful effects.[136-137] It is therefore, desirable to design selective CDK inhibitors that show neuroprotective effects, without attendant harmful side effects. We have anticipated that by attaching the fluoroaryl rings to the roscovitine (2) analogues through 1,2,3-triazole linkage, these compounds could be selective inhibitors of CDKs. Click chemistry[138-139] is a convenient technique for tethering fluorinated and variously substituted aryl moieties to purine derived alkynes. In this study, we have investigated the neuroprotective effects of the fluoroaryl substituted purine based 1,2,3.triazoles along with those of flavopiridol (1) and roscovitine (2), the current state-of-the-art pharmaceuticals[140] for AD and related neurological diseases.

The neurotoxicity of Aβ peptide arises primarily due to its overactivation of CDK5.[21, 125] In turn CDK5, in association with aberrantly formed protein p25 (by cleavage of p35), is responsible for neurodegeneration. Even though the involvement of the p25 in the intracellular neurofibrillary tangle (NFT) formation is not well established, its role in neuronal cell-cycle re-entry and resultant neuronal cell death is widely established.[24-25] Thus quest for kinase inhibitors is a reasonable alternative in the design of AD therapeutics.[141] We have identified a convenient assay for neuronal cell death, which could be artificially induced by incubation with Aβ oligomers. The binding of

propidium iodide (PI) with DNA of dead cells gives characteristic fluorescence which could be followed by fluorescence microscopy. Since PI is impermeable to live cell membranes, the observed fluorescence is indicative of the extent of dead cell populations. Using this technique, we have found that incubation of hippocampal neuronal cells with Aβ results in significant neuronal cell death after duration of 48 h (Figure1–15).

1.2.3 Synthesis. The triazole, 21, and its fluorinated derivatives, compounds 22.24, were prepared by the Cu(I) catalyzed 1,3.dipolar cycloaddition reactions of the corresponding alkyne and azide substrates (Scheme 1.1). As expected, the products show high 1,4.regioselectivity in these cycloadditions. Reaction of the commercially available 2,6-dichloropurine (18) with benzylamine gave 2.chloro-6-benzylaminopurine (19) using a reported procedure.[142] Under our conditions, the reaction was complete in 15 min at 60 °C instead of the reported time of 3 h at 110 °C. Propargylation of compound 19 using propargyl bromide in DMSO under mild conditions gave 2.chloro-6-benzylamino-9-(2.propynyl)purine (20) regioselectively in high yield. The Cu(I) catalyzed azide-alkyne click reaction[143] (the 1,3.dipolar cycloaddition) of the alkyne 20 with fluorinated benzyl azides, prepared in situ from their corresponding benzyl bromides, gave exclusively 1,4.disubstituted triazoles, 21-24.

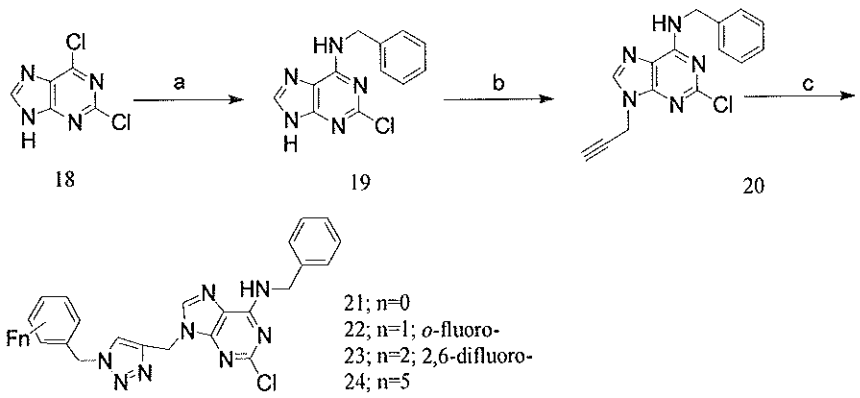

Reagents and conditions: [a]benzylamine; [b]propargyl bromide; [c]fluorophenylmethyl bromide (or phenylmethyl bromide), sodium azide, Cu(I)Br, Et_3N, DMSO, 10 min.

Scheme 1.1. Synthesis of purine-based fluoroaryl triazoles

The isomeric homogeneity of the product triazoles is readily verified through their ^{19}F NMR spectra (Figure 1.13). The pentafluoro triazole, 24, shows relatively shielded $\delta^{19}F$ absorptions as compared to the monofluoro and the difluoro triazoles, 22 and 23 respectively, in accordance with similar observations for the monofluoro-, difluoro-, and pentafluorotoluenes.[144]

Aβ is neurotoxic, and it can overactivate CDK5, which results in the tau-hyperphosphorylation, cell cycle re-entry, resulting in neuronal apoptosis. Thus, we have used Aβ oligomers as the trigger of neurotoxicity in vitro for convenient assay of the neuroprotective effects of the kinase inhibitors. Mouse hippocampal slice cultures were treated with Aβ oligomers in the presence of PI as the staining agent. The degree of hippocampal neuronal death was monitored by electron microscopic observation of the PI uptake.

The intensities of the fluorescence were conveniently analyzed using Scion images. The intensity of the PI fluorescence reflects the relative number of the dead cells as PI cannot permeate the live cell membranes. As shown in Figure 1.15, there is visible difference in the control (in the absence of Aβ oligomers) and the Aβ oligomers-treated cell cultures. Typically 48 h is required for the expression of the Aβ toxicity. These experiments were repeated using the established cell cycle inhibitors, roscovitine (2), flavopiridol (1), and the fluoroaryl substitued purine derived triazoles, compounds 22-24.

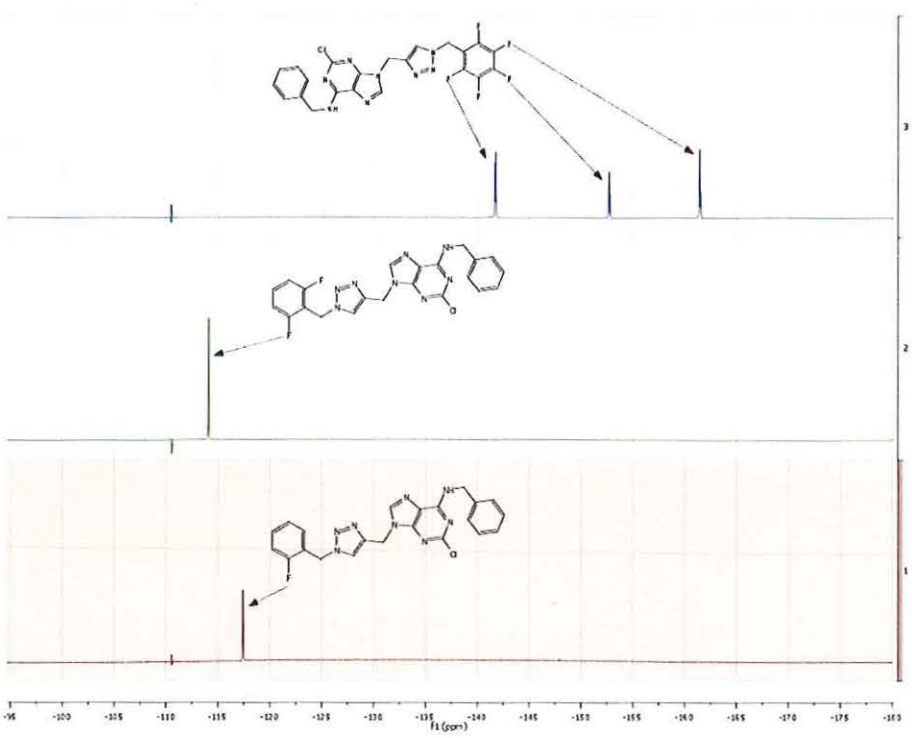

Figure 1.14. ^{19}F spectra of compounds 22, 23 and 24.

As can be seen in Figure 1.16, after 48 h of incubation time, roscovitine (2) and flavopiridol (1) and the *o*-fluorophenylmethyl-triazole, 22, have neuronal cell survival rates comparable to those of the control experiments, i.e., those corresponding to the cultures in the absence of the Aβ oligomers. Interestingly, the pentafluorotriazozle (24) has virtually no neuroprotective effect, and the 2,6-difluoro- (23) and the nonfluorinated- (21) derivatives have only marginal effects.

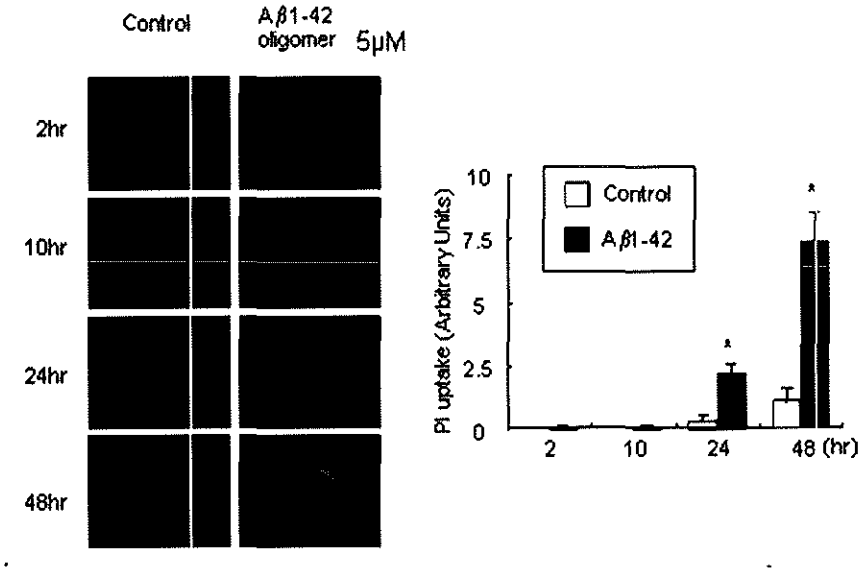

Figure 1.15. Time dependent response of PI uptake in hippocampal slices were recorded over 48 h incubation after exposing hippocampal slice cultures to 5 μM Aβ oligomers for the indicated times. The PI uptake responses were quantitatively analyzed and shown as graphs.

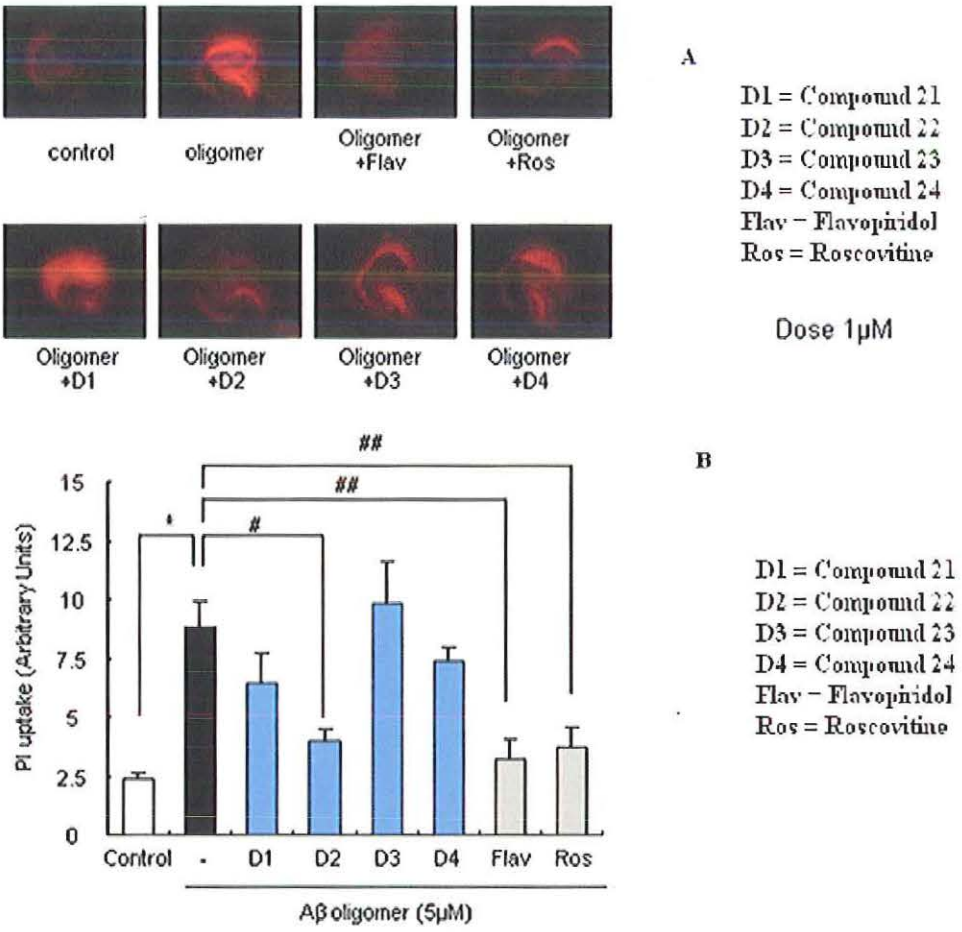

Figure 1.16. Hippocampal slices were incubated with compounds 21.24, or cell cycle inhibitors flavopiridol (1), roscovitine (2) (1 μM) for 1 h and then treated with 5 μM Aβ oligomers in the presence of PI for 48 h. PI uptake was analyzed with microscopy (panel A) to determine the effects of these pharmacological agents on Aβ oligomers-induced toxicity. The relative fluorescence intensities are expressed as arbitrary units of PI uptake (panel B).

1.2.4 Pretreatment of CBMFMT Suppresses the Neuronal Cell Cycle Reentry Caused by Aβ Oligomers. The alteration of cell cycle proteins expression with pretreatment of the monofluoro compound (CBMFMT) was analyzed. The treatment of CBMFMT significantly suppressed the induction of cyclin A and PCNA by Aβ oligomer, suggesting our new compound rescue Aβ oligomer-induced neurotoxicity by inhibiting cell cycle re-entry (Figure 1.17).

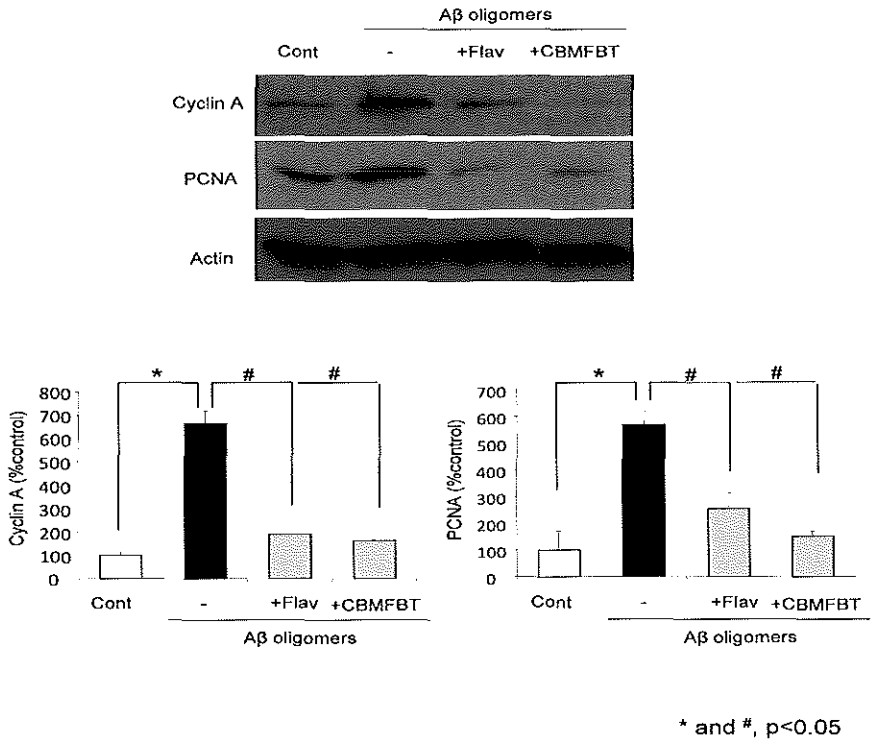

Figure 1.17. *CBMFMT* suppresses cell cycle activation in response to Aβ oligomer in hippocampal slices. (A) The effect of CBMFMT on Aβ oligomer-induced cell cycle activation. Slices were treated with CBMFMT (1 μM), or Flavopiridol (1 μM) before the incubation with Aβ oligomer for 24 h. Their pretreatment suppressed the increased expression of cell cycle protein induced by Aβ oligomer . Each number represents the mean ± S.E. from four different experiments. *, $p<0.05$ different from the Aβ oligomer-treated samples.

1.2.5 Conclusions. In summary, Aβ induced neurotoxicity in hippocamapal cell cultures could be readily followed by fluorescence microscopy using PI assay, and using this assay, we have demonstrated the Aβ-induced neurotoxicity in neuronal cell cultures. Through this fluorescence technique, we have shown that the roscovitine (2) and flavopiridol (1) are efficient neuroprotecting agents. Further, the neuronal toxicity, induced by the Aβ-oligomers treatment of the cell cultures, could be effectively suppressed in the presence of our mono-fluorinated purine based triazole, compound 22. The pentafluorinated version, compound 24, is ineffective as neuroprotector, while nonfluorinated triazole, compound 21, and difluorinated triazole, compound 8, although relatively less effective than triazole 22, show some attenuation of neurotoxicity. More importantly, the neuroprotective effect of compund 21 is comparable to those of the state-of-the-art pharmaceuticals, flavopiridol (1) and roscovitine (2). The monofluorocompound significantly suppressed the induction of cyclin A and PCNA by Aβ oligomer, suggesting our new compound protects the neuronal cells from Aβ oligomer-induced neurotoxicity by inhibiting cell cycle re-entry.

1.2.6 General Comments. Benzylamine (>99.5%), 1.butanol (anhydrous, 99.8%), benzyl bromide (reagent grade, 98%) triethylamine (>99.5%), dimethyl sufoxide (ACS reagent, >99.9%), potassium carbonate (ACS reagent, >99.9%), Copper(I)bromide (98%), 2.flurobenzyl bromide (98%), 2,6-difluorobenzylbromide (97%), pentafluorobenzylbromide (99%), and 2,6-dichloropurine (97%) were obtained from Aldrich and used as received.

^{1}H NMR spectra (400 MHz), ^{13}C NMR spectra (100 MHz), and ^{19}F NMR spectra (376 MHz) were obtained on a Varian Inova 400 MHz spectrometer in DMSO-D_6 solutions (Figure 1.18 – Figure 1.25). The digital resolution of the ^{1}H spectra was 0.26Hz and ^{13}C spectra was 0.83Hz. ^{19}F NMR spectra were referenced to $CFCl_3$ ($\delta^{19}F$ = 0), and ^{1}H, and ^{13}C NMR were referenced to the residual solvent signals or internal tetramethylsilane.All sample concentrations were ranged from 5mg to 30mg in a volume of 0.7mL of deuterated solvent.^{13}C spectra were obtained after 1024 scans and ^{1}H NMR spectra were obtained after 4 scans. EI/MS was obtained using solid probe on a Hewlett Packard HPs 5890 GC/MS instrument.

1.2.7 Synthesis Procedure. *2-Chloro-6-benzylaminopurine (19).* To a suspension of 2,6-dichloropurine (110 mg, 0.52 mmol) in n-butanol (3 mL), benzylamine (57 mg, 0.52 mmol) and triethylamine (72 mg, 0.79 mmol) was added. The mixture was stirred and heated at 60 °C for 15 min. The resulting precipitate was filtered, washed with water (20 mL) and methanol (10 mL), and air-dried overnight. Compound 19 (130 mg, 95%) was obtained as an off-white solid: mp 262 °C; EI/MS (m/z (relative %)): 259 (19, $M^{+\cdot}$), 260 (14), 261 (17 %), 106 (100), 91 (77); ^{1}H NMR (400 MHz, DMSO) δ 8.15 (s, 1 H), 7.25-7.34 (m, 5 H), 4.66 (d, J_{H-H}= 6 Hz, 2 H) ; ^{13}C NMR (100 MHz, DMSO) δ 155.0 (s) 153.1 (s), 150.7 (s), 140.2(d, $^{1}J_{C-H}$ = 200 Hz), 139.6 (s), 128.5(d, $^{1}J_{C-H}$ = 158 Hz, 127.5 (d, $^{1}J_{C-H}$ = 157 Hz), 127.0(d, $^{1}J_{C-H}$ = 158 Hz) 118.1 (s), 43.4 (t, $^{1}J_{C-H}$ = 139 Hz)).

2-Chloro-6-benzylamino-9-(2.propynyl)purine (19). A solution of 2.chloro-6-benzylaminopurine (1.1 g, 3.8 mmol), in DMSO (5 mL) was cooled to 0 °C, potassium carbonate (0.79 g, 5.7 mmol) and propargyl bromide (0.45 g, 3.8 mmol) was

added to the contents, and stirred for 1 h at 0 °C. Water (20 mL) was then added to the reaction mixture, and the resulting yellow precipitate was filtered and washed with excess water (50 mL). Compound 20 (1.1 g, 80%) was obtained as an off-white solid upon successive recrystallization from dichloromethane and ethyl acetate: mp 180 °C; EI/MS (m/z (relative %)): 297 (63, $M^{+\cdot}$), 298 (15), 299 (23), 258 (46), 91(100); ^{1}H NMR (400 MHz, DMSO) δ 8.23 (s, 1 H), 7.21– 7.38 (m, 5 H), 5.03 (bs, 2 H), 4.62 (d, J_{H-H}= 6 Hz, 1 H), 3.51 (s, 1 H). ^{13}C NMR (100 MHz, DMSO) δ 155.6 (s), 154.0 (s), 150.3 (s), 140.7 (d, $^{1}J_{C-H}$ = 214 Hz) 139.9 (s), 128.9 (d, $^{1}J_{C-H}$ = 159 Hz) , 127.9 (d, $^{1}J_{C-H}$ = 157 Hz), 126.8 (d, $^{1}J_{C-H}$ = 158 Hz), 118.1 (s), 78.5 (t, $^{2}J_{C-H}$= 9 Hz) 76.7 (dt, $^{1}J_{C-H}$= 252 Hz, $^{2}J_{C-H}$= 4 Hz), 43.8 (t, $^{1}J_{C-H}$= 126 Hz), 33.3 (t, $^{1}J_{C-H}$= 139 Hz).

2-Chloro-6-benzylamino-9-(1.benzyl-1H-1,2,3.triazol-4.yl-methyl)purine (21). Benzyl bromide (110 mg, 0.58 mmol) was added dropwise to a solution of sodium azide (42 mg, 0.64 mmol) in DMSO (5 mL, and stirred at room temperature for 15 min. Compound 20 (173 mg, 0.58 mmol), triethylamine (6 mg, 0.06 mmol) and CuBr (8 mg, 0.6 mmol) were added to the contents in that order, and the reaction mixture was stirred at room temperature for 30 min. The reaction mixture was poured into ice-cold water (20 mL), and the resulting off-white precipitate was filtered and washed with dilute NH_4OH (20 mL) and water (50 mL) to give the compound 21 (200 mg 80%) essentially pure by NMR; mp 235 °C. EI/MS (m/z (relative %)): 430 (32, $M^{+\cdot}$), 431 (11), 432 (13), 258 (54), (100); ^{1}H NMR (400 MHz, DMSO) δ 8.23 (s, 1 H), 8.15 (s, 1 H), 7.40-7.17 (m, 10 H), 5.56 (s, 2 H), 5.40 (s, 2 H), 4.62 (d, J_{H-H}= 6 Hz, 2 H); ^{13}C NMR (100 MHz, DMSO) δ 155.6 (s) , 153.9 (s), 150.3(s), 143.1(d, $^{1}J_{C-H}$ = 199 Hz), 141.9 (s), 139.9 (s) , 136.51(s), 129.4 (d, $^{1}J_{C-H}$ = 160 Hz) ,128.9 (d, $^{1}J_{C-H}$ = 159Hz), 128.8 (d, $^{1}J_{C-H}$ = 159 Hz) , 128.5 (d

, $^{1}J_{C-H}$ = 158 Hz), 127.9 (overlapping doublets), 127.4 (overlapping doublets), 124.4 (d, $^{1}J_{C-H}$ = 200 Hz) 118.6 (s) , 53.4 (t, $^{1}J_{C-H}$ = 145 Hz) , 43.7 ((t, $^{1}J_{C-H}$ = 135 Hz), 38.9 (t, $^{1}J_{C-H}$ = 139 Hz).

2-Chloro-6-benzylamino-9-[1.(2.fluorobenzyl)-1H-1,2,3.triazol-4.yl-methyl]purine (22). Compound 22 was obtained as an off- white solid (85%), using procedure A: mp 240 °C; EI/MS (m/z (relative %)): 448 (44, $M^{+\cdot}$), 449 (14), 450 (17), 258 (83), 109 (100), 91 (67); ^{1}H NMR (400 MHz, DMSO) δ 8.23 (s, 1 H), 8.17 (s, 1 H), 7.43 – 7.10 (m, 9 H), 5.60 (s, 2 H), 5.38 (s, 2 H), 4.60 (d, J_{H-H}= 6 Hz, 2 H); ^{19}F NMR (376 MHz, $CDCl_3$) -117.37 (dd, $^{1}J_{H-F}$ = 14 Hz, $^{2}J_{H-F}$ = 8 Hz); ^{13}C NMR (100 MHz, DMSO) δ 160.7 (d, $^{1}J_{C-F}$ = 248 Hz), 155.6 (s), 153.8 (s), 150.3 (s), 143.1 (d, $^{1}J_{C-H}$ = 199 Hz) , 142.0 (s), 139.9(s), 131.4 (d, $^{1}J_{C-H}$ = 165 Hz) 131.3 (d, $^{1}J_{C-H}$ = 160 Hz, $^{3}J_{CF}$ = 4 Hz), 128.9 (d, $^{1}J_{C-H}$ = 156 Hz) 127.9 (d, $^{1}J_{C-H}$ = 150 Hz) , 127.4 (d, $^{1}J_{C-H}$ = 160 Hz), 125.5 (d, $^{1}J_{C-H}$ = 150 Hz), 124.5 (d, $^{1}J_{C-H}$ = 200 Hz), 123.3 (d, $^{2}J_{CF}$ = 26 Hz), 118.6 (s), 116.2 (d, J_{CH} = 170 Hz, $^{2}J_{C-F}$ = 21 Hz) 47.6 (t, $^{1}J_{C-H}$ = 130), 43.8 (t, $^{1}J_{C-H}$ = 133 Hz) , 38.9 (t, $^{1}J_{C-H}$ = 143 Hz).

2-Chloro-6-benzylamino-9-[1.(2,6-difluorobenzyl)-1H-1,2,3.triazol-4.yl-methyl]purine (23). Compound 23 was obtained as an off white solid (84 %), using the procedure similar to that for compound 21: mp 239 °C; EI/MS (m/z (relative %)): 466 (52, $M^{+\cdot}$), 467 (19), 468 (22), 258 (77), 127 (100), 91 (73); ^{1}H NMR (400 MHz, DMSO) δ 8.20 (s, 1 H, purine CH), 8.16 (s, 1 H, triazole CH), 7.05 -7.47 (m, 8 H, phenyl), 5.60 (s, 2 H, benzylic CH_2 attached to triazole), 5.37 (s, 2 H, N9-CH_2), 4.61 (d, J = 5.5 Hz, 2 H, $NHCH_2$). ^{19}F NMR (376 MHz, $CDCl_3$) δ -114.10 (t, J = 7.0 Hz). ^{13}C NMR (100 MHz, DMSO) δ 162.5, 160.2, 155.4, 153.7, 150.3, 142.8, 141.8, 140.0, 132.4, 128.8, 127.9,

124.6, 118.4, 112.7, 112.4 (aromatic carbons) , 43.7 (benzylic-C attached to the amino group), 41.4 (benzylic-C attached to triazole ring), 38.6 (N9-CH_2).

2-Chloro-6-benzylamino-9-[1.(pentafluorobenzyl)-1H-1,2,3.triazol-4.yl-methyl]purine (24). Compound 24 was obtained as an off- white solid (89 %), using the procedure A: mp 225 °C; EI/MS (m/z (relative %)): 520 (24%, $M^{+\cdot}$), 521 (6), 522 (9%), 258 (73), 181 (69), 106 (64), 91(100); ^{1}H NMR (400 MHz, DMSO) δ 8.22 (s, 1 H), 8.23 (s, 1 H), 7.32.7.19 (m, 5 H), 5.73 (s, 2 H), 5.39 (s, 2 H), 4.61 (d, J_{H-H} = 5.5, 2 H); ^{19}F NMR (376 MHz, $CDCl_3$) δ -141.70 (dd, $^1J_{F-F}$ = 23.2, $^2J_{F-F}$ = 7.2 Hz, *ortho*-fluorines), -152.7 (t, J_{F-F} = 22 Hz, *para*-fluorine), -161.43 (dt, $^1J_{F-F}$ = 22.9, $^2J_{F-F}$ = 7.4 Hz, *meta*-fluorines); ^{13}C NMR (101 MHz, DMSO) δ 155.5 (s), 153.8 (s), 150.3 (s) , 145.6(dm, $^1J_{C-F}$ = 254 Hz), 143.14 (s), 142.01 (d, $^1J_{C-H}$ = 199 Hz,), 141.6 (dm, , $^1J_{C-F}$ = 259 Hz), 137.7 (d, $^1J_{C-F}$ = 249 Hz), 139.9 (s), 128.9 (dd, $^1J_{C-H}$ = 159 Hz, $^2J_{C-H}$ = 6Hz), 127.9 (dm, $^1J_{C-H}$ =154 Hz),127.5 (dt, $^1J_{C-H}$ = 164 Hz) , 124.8 (d, $^1J_{C-H}$ = 197 Hz,), 118.8 (s), 109.8 (t, $^2J_{C-F}$ = 18 Hz, $^3J_{C-F}$ = 3 Hz), 43.8 (t, $^1J_{C-H}$ = 139 Hz,), 41.1 (t, $^1J_{C-H}$ = 130 Hz), 38.8 (t, $^1J_{C-H}$ = 142 Hz).

1.2.8 Preparation of Aβ Oligomers. Soluble Aβ oligomers were prepared as described previously.[145] Briefly, 1.0 mg of Aβ1.42 peptide was dissolved in 120 μL of hexafluoroisopropanol for 60 min at room temperature, and placed back on ice for 5-10 min. Hexafluoroisopropanol was evaporated overnight in the hood at room temperature. The sample was dissolved in 100% DMSO by adding 20 μL fresh anhydrous DMSO (Sigma Hybri-Max) to 0.45 mg peptide, and diluted 5 mM peptide stock into medium. Diluted peptide was incubated at 4 °C for 24 h, and then centrifuged at 14,000 g for 10

min in the cold. Before treating slice culture with Aβ oligomers, the oligomers were incubated at room temperature for 20 h.

1.2.9 Preparation of Hippocampal Slice Cultures. Organotypic hippocampal slice cultures were prepared as described previously.[146] Briefly, hippocampal slice cultures were prepared from 7-10 day-old mouse pups. Slices were cut at 400 μm on a McIlwain tissue chopper, transferred to Millicell (Millipore Corp., Bedford, MA) membrane inserts (0.4 μm), and placed in 6-well culture plated. The upper surfaces of the slices were exposed to a humidified 37 °C atmosphere containing 5% CO_2. Slice culture media consisted of basal Eagles medium with Earle's balanced salt solution, 20% heat-inactivated horse serum, enriched with glucose to a concentration of 5.6 mM. The medium was changed every other day. Slices were examined periodically for viability, and any dark or abnormal slices were discarded.

1.2.10 Experimental Treatment of Aβ Oligomers to Organotypic Hippocampal Slice Culture. The effects of Aβ oligomers were tested in the slices which had been maintained for 15-20 days *in vitro*. All reagents were added to serum free medium (no horse serum). Aβ oligomers were added to cultures in serum free medium. Vehicles were treated the same way except with no peptide. The slices were pretreated with compounds 21, 22, 23, 24 or cell cycle inhibitor flavopiridol (1) or roscovitine (2) (1 μM) for 1 h before Aβ oligomers treatment.

1.2.11 Assessment of Neuronal Cell Death by PI Staining. To analyze the degree of hippocampal neuronal cell death, hippocampal slices were stained by adding Propidium Iodide (PI) into slice culture medium at a concentration of 5 μg/mL. At indicated times after Aβ oligomers treatment, the degree of hippocampal neuronal death was evaluated by microscopic observation of PI uptake as described previously.[53] Images were acquired through an AxioCam camera on an Axiovert 200M microscope (Zeiss, Thornwood, NY). The intensity of the fluorescence was quantitatively analyzed using Scion Image. The images were expressed as an arbitrary unit of PI uptake.

1.2.12 Protein Extraction and Western blot Analysis. The western blotting analysis was performed as described previously [147]. After Aβ oligomer treatment, these slices were rinsed twice with ice-cold PBS and then lysed in ice-cold lysis buffer. The protein concentration was determined by the method of BCA (Pierce). Equal amounts of sample proteins were separated according to their molecular weight on 10 or 12% SDS-polyacrylamide gel and transferred onto polyvinylidene difluoride membranes. The blots were blocked with 10% milk in TBS-T for 1 h at room temperature, and then treated with primary antibodies diluted with 1% milk and incubated overnight at 4 °C. The following antibodies were used: anti-PCNA (1:1000; Santa Cruz), anti-cyclin A (1:1000; Abcam).

1.2.13 Statistical Analysis. Data were expressed as the means ± S.E. of the values from the number of experiments indicated in the corresponding figures. Differences between groups were examined for statistical significance using one-way analysis of variance with an unpaired Students t-test. A p value less than 0.05 denoted statistical significance.

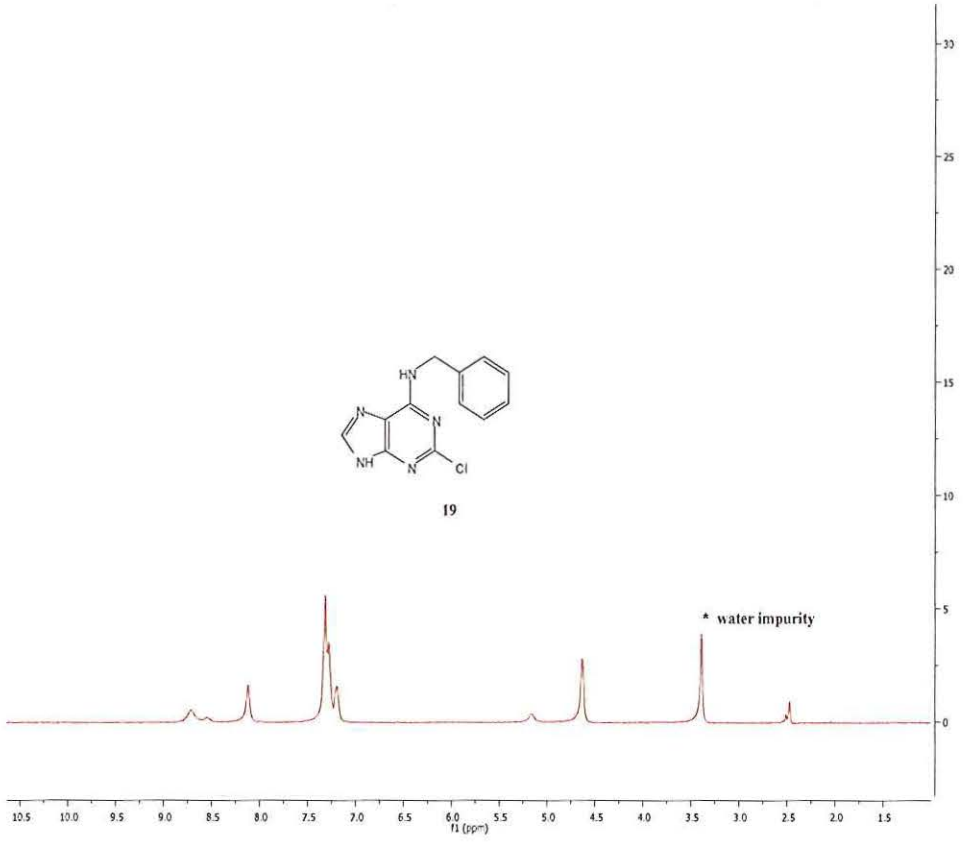

Figure 1.18. ^{1}H NMR (400MHz) spectra of 2-Chloro-6-benzylaminopurine (19)

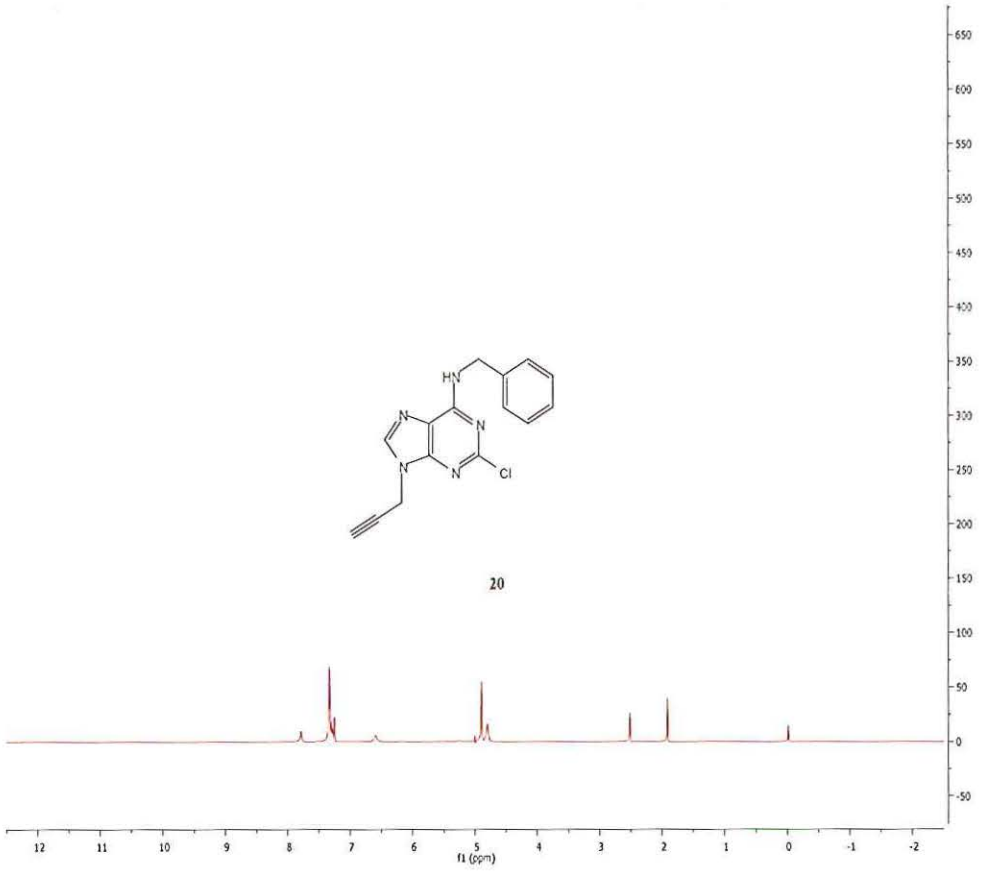

Figure 1.19. ^{1}H NMR (400MHz) spectra of 2.Chloro-6-benzylamino-9-(2-propynyl)purine (20)

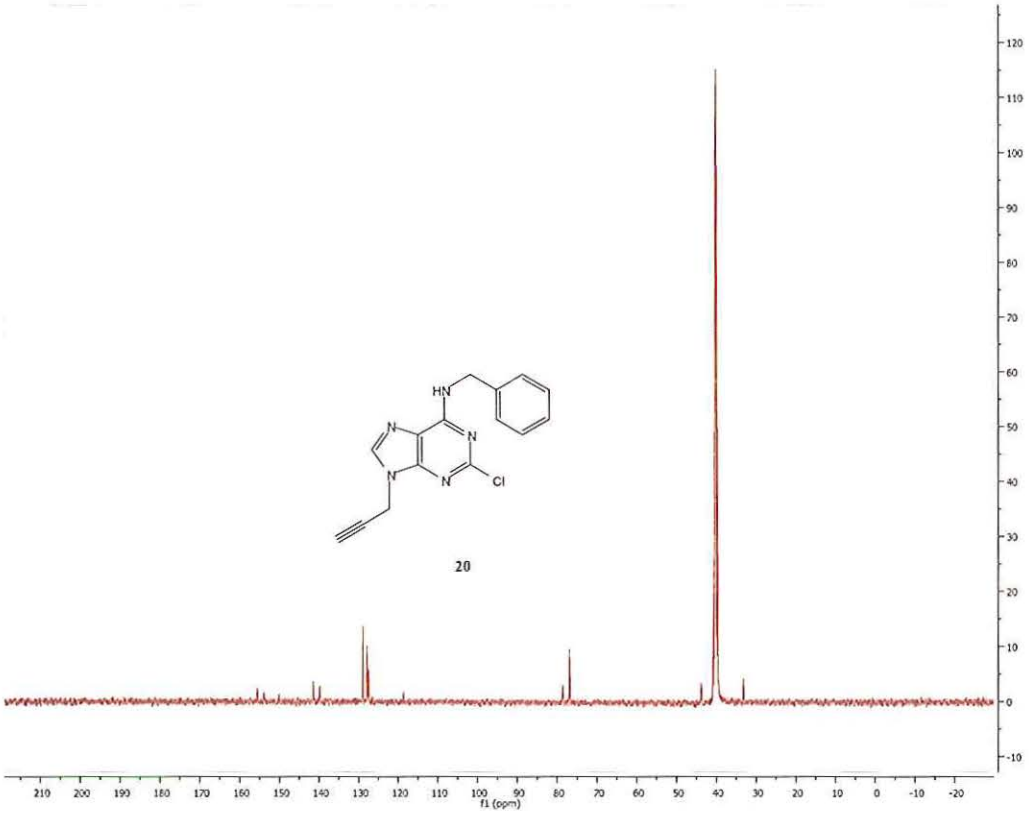

Figure 1.20. ^{13}C NMR (100MHz) spectra of 2-Chloro-6-benzylamino-9-(2-propynyl)purine (20)

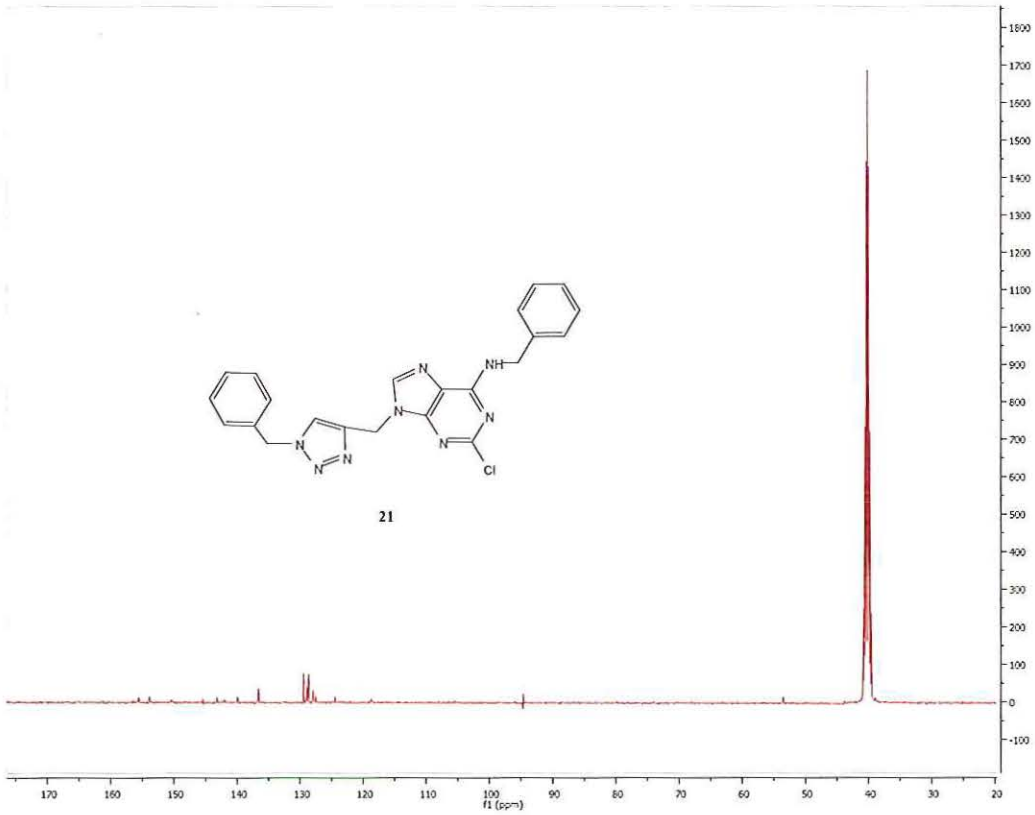

Figure 1.21. ^{13}C NMR (100MHz) spectra of 2-Chloro-6-benzylamino-9-(1-benzyl-1H-1,2,3.triazol-4.yl-methyl)purine (21).

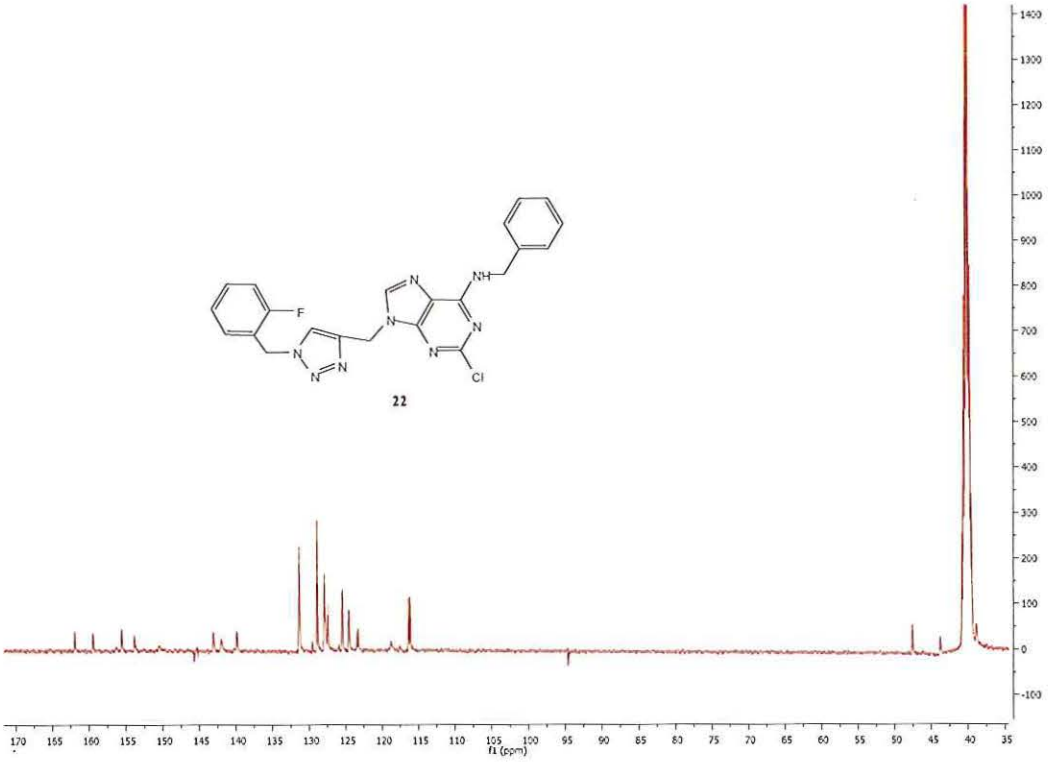

Figure 1.22. ^{13}C NMR (100MHz) spectra of 2-Chloro-6-benzylamino-9-[1-(2-fluorobenzyl)-1H-1,2,3.triazol-4.yl-methyl]purine (22).

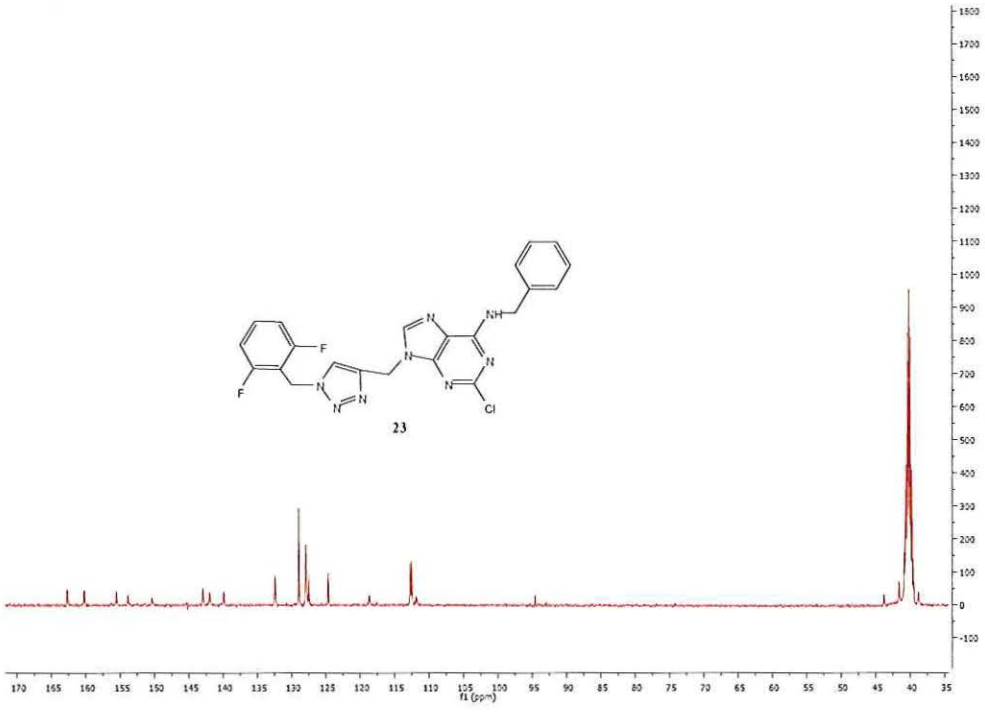

Figure 1.23. ^{13}C NMR (100MHz) spectra of 2.Chloro-6-benzylamino-9-[1-(2,6-difluorobenzyl)-1H-1,2,3.triazol-4-yl-methyl]purine (23).

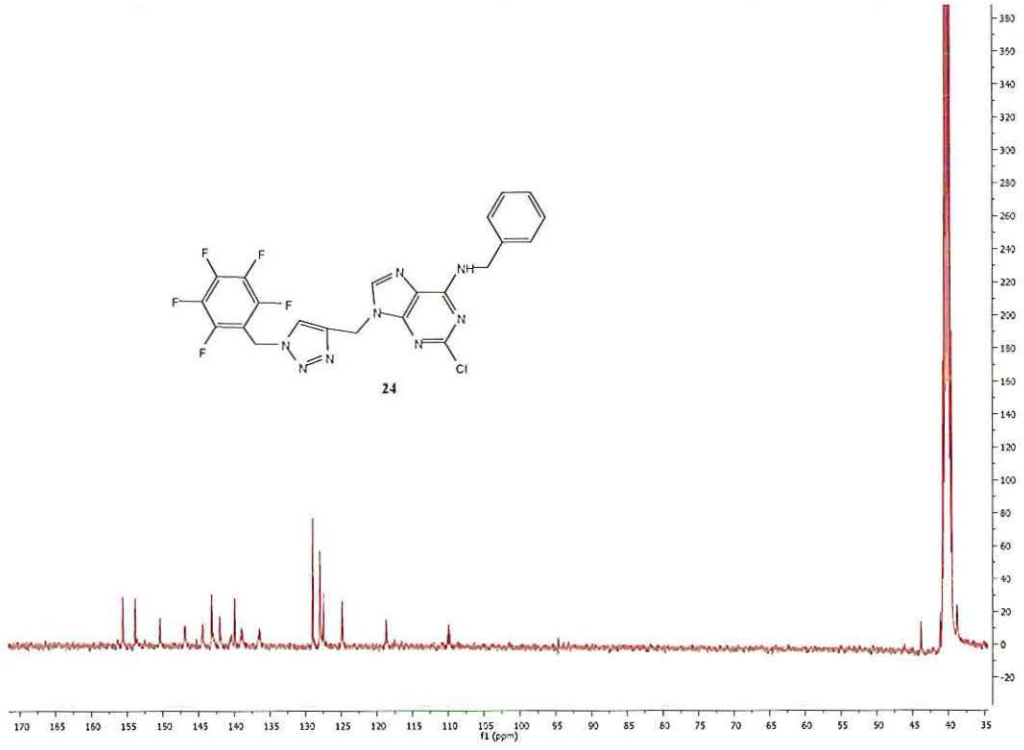

Figure 1.24. ^{13}C NMR (100MHz) spectra of 2.Chloro-6-benzylamino-9-[1-(pentafluorobenzyl)-1H-1,2,3-triazol-4-yl-methyl]purine (24)

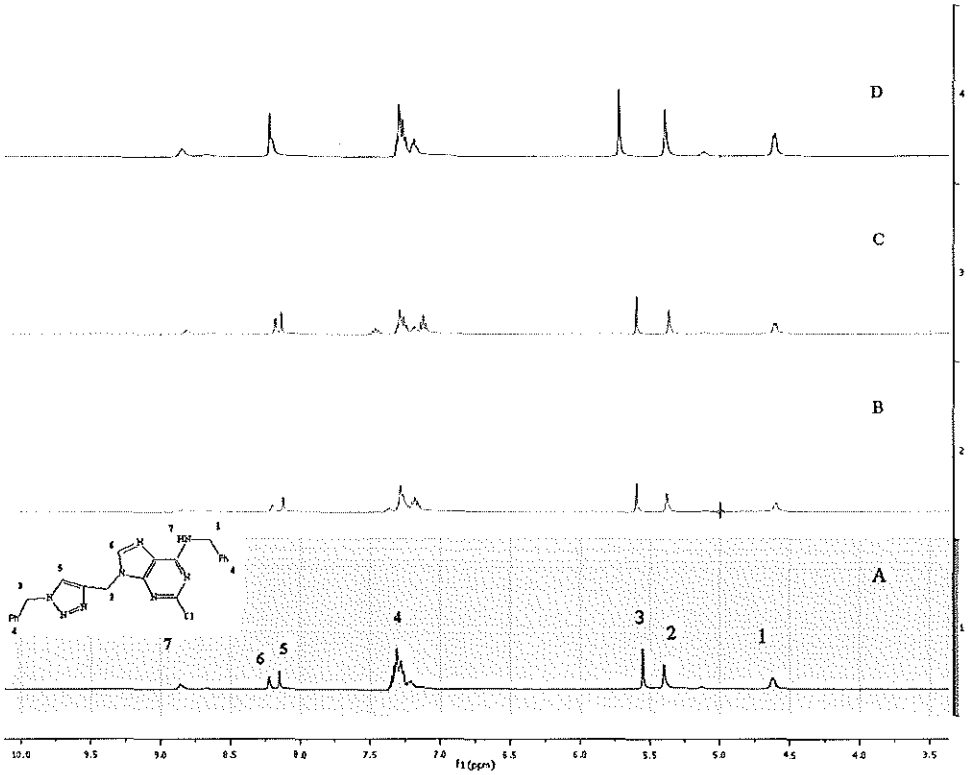

Figure 1.25. ^{1}H NMR (400MHz) spectra of compounds 21(A), 22(B), 23(C) and 24(D)

1.3 REFERENCES

[1] A. McShea, A. F. Wahl, M. A. Smith, Re-entry into the cell cycle: a mechanism for neurodegeneration in Alzheimer disease, *Med. Hypotheses* **1999**, *52*, 525.

[2] M. Z. Smith, Z. Nagy, M. M. Esiri, Cell cycle-related protein expression in vascular dementia and Alzheimer's disease, *Neurosci. Lett.* **1999**, *271*, 45.

[3] J. P. Lopes, M. Blurton-Jones, T. R. Yamasaki, P. Agostinho, F. M. La Ferla, Activation of Cell Cycle Proteins in Transgenic Mice in Response to Neuronal Loss but not Amyloid-beta and Tau Pathology, *Journal of Alzheimer's Disease* **2009**, *16*, 541.

[4] C. J. Sherr, G1 phase progression: cycling on cue, *Cell (Cambridge, Mass.)* **1994**, *79*, 551.

[5] X. Grana, E. P. Reddy, Cell cycle control in mammalian cells: role of cyclins, cyclin dependent kinases (CDKs), growth suppressor genes and cyclin-dependent kinase inhibitors (CKIs), *Oncogene* **1995**, *11*, 211.

[6] W. Meikrantz, R. Schlegel, Apoptosis and the cell cycle, *J. Cell. Biochem.* **1995**, *58*, 160.

[7] S. Cicero, K. Herrup, Cyclin-dependent kinase 5 is essential for neuronal cell cycle arrest and differentiation, *J. Neurosci.* **2005**, *25*, 9658.

[8] T. Ohshima, J. M. Ward, C.-G. Huh, G. Longenecker, Veeranna, H. C. Pant, R. O. Brady, L. J. Martin, A. B. Kulkarni, Targeted disruption of the cyclin-dependent kinase 5 gene results in abnormal corticogenesis, neuronal pathology and perinatal death, *Proc. Natl. Acad. Sci. U. S. A.* **1996**, *93*, 11173.

[9] E. C. Gilmore, T. Ohshima, A. M. Goffinet, A. B. Kulkarni, K. Herrup, Cyclin-dependent kinase 5-deficient mice demonstrate novel developmental arrest in cerebral cortex, *J. Neurosci.* **1998**, *18*, 6370.

[10] J. Ko, S. Humbert, R. T. Bronson, S. Takahashi, A. B. Kulkarni, E. Li, L.-H. Tsai, p35 and p39 are essential for cyclin-dependent kinase 5 function during neurodevelopment, *J. Neurosci.* **2001**, *21*, 6758.

[11] M. Nikolic, M. M. Chou, W. Lu, B. J. Mayer, L.-H. Tsai, The p35/Cdk5 kinase is a neuron-specific Rac effector that inhibits Pak1 activity, *Nature (London)* **1998**, *395*, 194.

[12] W. Xiong, R. Pestell, M. R. Rosner, Role of cyclins in neuronal differentiation of immortalized hippocampal cells, *Mol. Cell. Biol.* **1997**, *17*, 6585.

[13] J. A. Bibb, G. L. Snyder, A. Nishi, Z. Yan, L. Meijer, A. A. Fienberg, U. H. Tsai, Y. T. Kwon, J.-A. Girault, A. J. Czernik, R. L. Huganir, H. C. Hemmings, Jr., A. C. Nairn, P. Greengard, Phosphorylation of DARPP-32 by Cdk5 modulates dopamine signalling in neurons, *Nature (London)* **1999**, *402*, 669.

[14] K. Tomizawa, J. Ohta, M. Matsushita, A. Moriwaki, S.-T. Li, K. Takei, H. Matsui, Cdk5/p35 regulates neurotransmitter release through phosphorylation and downregulation of P/Q-type voltage-dependent calcium channel activity, *J. Neurosci.* **2002**, *22*, 2590.

[15] J. J. Pei, I. Grundke-Iqbal, K. Iqbal, N. Bogdanovic, B. Winblad, R. F. Cowburn, Accumulation of cyclin-dependent kinase 5 (cdk5) in neurons with early stages of Alzheimer's disease neurofibrillary degeneration, *Brain research* **1998**, *797*, 267.

[16] K.-H. Chang, Y. de Pablo, H.-p. Lee, H.-g. Lee, A. Smith Mark, K. Shah, Cdk5 is a major regulator of p38 cascade: relevance to neurotoxicity in Alzheimer's disease, *J Neurochem* **2010**, *113*, 1221.

[17] B. Ikiz, S. Przedborski, A sequel to the tale of p25/Cdk5 in neurodegeneration, *Neuron* **2008**, *60*, 731.

[18] B. Shelton Shirley, V. W. Johnson Gail, Cyclin-dependent kinase-5 in neurodegeneration, *J Neurochem* **2004**, *88*, 1313.

[19] U. Namgung, B.-H. Choi, S. Park, J.-U. Lee, H.-S. Seo, B.-C. Suh, K.-T. Kim, Activation of cyclin-dependent kinase 5 is involved in axonal regeneration, *Mol. Cell. Neurosci.* **2004**, *25*, 422.

[20] N. H. Varvel, K. Bhaskar, A. R. Patil, S. W. Pimplikar, K. Herrup, B. T. Lamb, Abeta oligomers induce neuronal cell cycle events in Alzheimer's disease, *J. Neurosci.* **2008**, *28*, 10786.

[21] J. P. Lopes, C. R. Oliveira, P. Agostinho, Neurodegeneration in an Abeta -induced model of Alzheimer's disease: the role of Cdk5, *Aging Cell* **2010**, *9*, 64.

[22] A. Giovanni, F. Wirtz-Brugger, E. Keramaris, R. Slack, D. S. Park, Involvement of cell cycle elements, cyclin-dependent kinases, pRb, and E2F x DP, in B-amyloid-induced neuronal death, *J Biol Chem* **1999**, *274*, 19011.

[23] K. I. Seyb, S. Ansar, G. Li, J. Bean, M. L. Michaelis, R. T. Dobrowsky, P35/cyclin-dependent kinase 5 is required for protection against beta -amyloid-induced cell death but not tau phosphorylation by ceramide, *J. Mol. Neurosci.* **2007**, *31*, 23.

[24] A. Tandon, H. Yu, L. Wang, E. Rogaeva, C. Sato, M. A. Chishti, T. Kawarai, H. Hasegawa, F. Chen, P. Davies, P. E. Fraser, D. Westaway, P. H. St George-Hyslop, Brain levels of CDK5 activator p25 are not increased in Alzheimer's or other neurodegenerative diseases with neurofibrillary tangles, *J. Neurochem.* **2003**, *86*, 572.

[25] J. Lew, L. Zhang, CDK5: an historical perspective, *Trends Cell Cycle Res.* **2008**, 277.

[26] M.-s. Lee, Y. T. Kwon, M. Li, J. Peng, R. M. Friedlander, L.-H. Tsai, Neurotoxicity induces cleavage of p35 to p25 by calpain, *Nature (London)* **2000**, *405*, 360.

[27] C. Cruz Jonathan, D. Kim, Y. Moy Lily, M. Dobbin Matthew, X. Sun, T. Bronson Roderick, L.-H. Tsai, p25/cyclin-dependent kinase 5 induces production and intraneuronal accumulation of amyloid beta in vivo, *J Neurosci* **2006**, *26*, 10536.

[28] Y. Tong, Y. Xu, K. Scearce-Levie, L. J. Ptacek, Y.-H. Fu, COL25A1 triggers and promotes Alzheimer's disease-like pathology in vivo, *Neurogenetics* **2010**, *11*, 41.

[29] A. Alvarez, R. Toro, A. Caceres, R. B. Maccioni, Inhibition of tau phosphorylating protein kinase cdk5 prevents beta-amyloid-induced neuronal death, *FEBS Lett* **1999**, *459*, 421.

[30] J. Ryder, Y. Su, F. Liu, B. Li, Y. Zhou, B. Ni, Divergent roles of GSK3 and CDK5 in APP processing, *Biochem. Biophys. Res. Commun.* **2003**, *312*, 922.

[31] A. McShea, P. L. Harris, K. R. Webster, A. F. Wahl, M. A. Smith, Abnormal expression of the cell cycle regulators P16 and CDK4 in Alzheimer's disease, *Am J Pathol* **1997**, *150*, 1933.

[32] Z. Nagy, M. M. Esiri, A. D. Smith, Expression of cell division markers in the hippocampus in Alzheimer's disease and other neurodegenerative conditions, *Acta Neuropathol* **1997**, *93*, 294.

[33] T. W. Smith, C. F. Lippa, Ki-67 immunoreactivity in Alzheimer's disease and other neurodegenerative disorders, *J. Neuropathol. Exp. Neurol.* **1995**, *54*, 297.

[34] Y. Yang, D. S. Geldmacher, K. Herrup, DNA replication precedes neuronal cell death in Alzheimer's disease, *J. Neurosci.* **2001**, *21*, 2661.

[35] D. J. Bonda, T. A. Evans, C. Santocanale, J. C. Llosa, J. Vina, V. P. Bajic, R. J. Castellani, S. L. Siedlak, G. Perry, M. A. Smith, H.-g. Lee, Evidence for the progression through S-phase in the ectopic cell cycle re-entry of neurons in Alzheimer disease, *Aging* **2009**, *1*, 382.

[36] J. Woods, M. Snape, M. A. Smith, The cell cycle hypothesis of Alzheimer's disease: Suggestions for drug development, *Biochim. Biophys. Acta, Mol. Basis Dis.* **2007**, *1772*, 503.

[37] S. R. D'Mello, P. C. Chin, Treating neurodegenerative conditions through the understanding of neuronal apoptosis, *Curr. Drug Targets CNS Neurol. Disord.* **2005**, *4*, 3.

[38] E. A. Monaco, III, M. L. Vallano, Role of protein kinases in neurodegenerative disease: cyclin-dependent kinases in Alzheimer's disease, *Frontiers in Bioscience* **2005**, *10*, 143.

[39] A. Beauchard, H. Laborie, H. Rouillard, O. Lozach, Y. Ferandin, R. Le Guevel, C. Guguen-Guillouzo, L. Meijer, T. Besson, V. Thiery, Synthesis and kinase inhibitory activity of novel substituted indigoids, *Bioorg. Med. Chem.* **2009**, *17*, 6257.

[40] R. Akue-Gedu, E. Debiton, Y. Ferandin, L. Meijer, M. Prudhomme, F. Anizon, P. Moreau, Synthesis and biological activities of aminopyrimidyl-indoles structurally related to meridianins, *Bioorg. Med. Chem.* **2009**, *17*, 4420.

[41] U. Jacquemard, N. Dias, A. Lansiaux, C. Bailly, C. Loge, J.-M. Robert, O. Lozach, L. Meijer, J.-Y. Merour, S. Routier, Synthesis of 3,5-bis(2-indolyl)pyridine and 3-[(2-indolyl)-5-phenyl]pyridine derivatives as CDK inhibitors and cytotoxic agents, *Bioorg. Med. Chem.* **2008**, *16*, 4932.

[42] A. Beauchard, Y. Ferandin, S. Frere, O. Lozach, M. Blairvacq, L. Meijer, V. Thiery, T. Besson, Synthesis of novel 5-substituted indirubins as protein kinases inhibitors, *Bioorg. Med. Chem.* **2006**, *14*, 6434.

[43] Q. Wang, D. M. Walsh, M. J. Rowan, D. J. Selkoe, R. Anwyl, Block of long-term potentiation by naturally secreted and synthetic amyloid beta -peptide in hippocampal slices is mediated via activation of the kinases c-Jun N-terminal kinase, cyclin-dependent kinase 5, and p38 mitogen-activated protein kinase as well as metabotropic glutamate receptor type 5, *J. Neurosci.* **2004**, *24*, 3370.

[44] C. J. Helal, Z. Kang, J. C. Lucas, T. Gant, M. K. Ahlijanian, J. B. Schachter, K. E. G. Richter, J. M. Cook, F. S. Menniti, K. Kelly, S. Mente, J. Pandit, N. Hosea, Potent and cellularly active 4-aminoimidazole inhibitors of cyclin-dependent kinase 5/p25 for the treatment of Alzheimer's disease, *Bioorg. Med. Chem. Lett.* **2009**, *19*, 5703.

[45] B. Apsel, J. A. Blair, B. Gonzalez, T. M. Nazif, M. E. Feldman, B. Aizenstein, R. Hoffman, R. L. Williams, K. M. Shokat, Z. A. Knight, Targeted polypharmacology: discovery of dual inhibitors of tyrosine and phosphoinositide kinases, *Nat. Chem. Biol.* **2008**, *4*, 691.

[46] P. Pevarello, M. Villa, Cyclin-dependent kinase inhibitors: a survey of the recent patent literature, *Expert Opin. Ther. Pat.* **2005**, *15*, 675.

[47] W. Zhong, H. Liu, M. R. Kaller, C. Henley, E. Magal, T. Nguyen, T. D. Osslund, D. Powers, R. M. Rzasa, H.-L. Wang, W. Wang, X. Xiong, J. Zhang, M. H. Norman, Design and synthesis of quinolin-2(1H)-one derivatives as potent CDK5 inhibitors, *Bioorg. Med. Chem. Lett.* **2007**, *17*, 5384.

[48] K. Bettayeb, H. Sallam, Y. Ferandin, F. Popowycz, G. Fournet, M. Hassan, A. Echalier, P. Bernard, J. Endicott, B. Joseph, L. Meijer, N-&-N, a new class of cell death-inducing kinase inhibitors derived from the purine roscovitine, *Mol. Cancer Ther.* **2008**, *7*, 2713.

[49] N. Oumata, K. Bettayeb, Y. Ferandin, L. Demange, A. Lopez-Giral, M.-L. Goddard, V. Myrianthopoulos, E. Mikros, M. Flajolet, P. Greengard, L. Meijer, H. Galons, Roscovitine-Derived, Dual-Specificity Inhibitors of Cyclin-Dependent Kinases and Casein Kinases 1, *J. Med. Chem.* **2008**, *51*, 5229.

[50] L. Vandromme, S. Piguel, O. Lozach, L. Meijer, M. Legraverend, D. S. Grierson, Suzuki-type Pd(0) coupling reactions in the synthesis of 2-arylpurines as Cdk inhibitors, *Bioorg. Med. Chem. Lett.* **2006**, *16*, 3144.

[51] N. Giocanti, R. Sadri, M. Legraverend, O. Ludwig, E. Bisagni, S. Leclerc, L. Meijer, V. Favaudon, In vitro evaluation of a novel 2,6,9-trisubstituted purine acting as a cyclin-dependent kinase inhibitor, *Ann. N. Y. Acad. Sci.* **1999**, *886*, 180.

[52] M. Legraverend, O. Ludwig, E. Bisagni, S. Leclerc, L. Meijer, N. Giocanti, R. Sadri, V. Favaudon, Synthesis and in vitro evaluation of novel 2,6,9-trisubstituted purines acting as cyclin-dependent kinase inhibitors, *Bioorg. Med. Chem.* **1999**, *7*, 1281.

[53] L. Meijer, A. Borgne, O. Mulner, J. P. J. Chong, J. J. Blow, N. Inagaki, M. Inagaki, J. G. Delcros, J. P. Moulinoux, Biochemical and cellular effects of roscovitine, a potent and selective inhibitor of the cyclin-dependent kinases cdc2, cdk2, and cdk5, *Eur. J. Biochem.* **1997**, *243*, 527.

[54] Veeranna, K. T. Shetty, N. Amin, P. Grant, R. W. Albers, H. C. Pant, Inhibition of neuronal cyclin-dependent kinase-5 by staurosporine and purine analogs is independent of activation by Munc-18, *Neurochem. Res.* **1996**, *21*, 629.

[55] L. Vandromme, M. Legraverend, S. Kreimerman, O. Lozach, L. Meijer, S. Grierson David, A Pd(0) based cross-coupling approach to the synthesis of 2-amidopurines and their evaluation as CDK inhibitors, *Bioorg. Med. Chem.* **2007**, *15*, 130.

[56] P. G. Wyatt, A. J. Woodhead, V. Berdini, J. A. Boulstridge, M. G. Carr, D. M. Cross, D. J. Davis, L. A. Devine, T. R. Early, R. E. Feltell, E. J. Lewis, R. L. McMenamin, E. F. Navarro, M. A. O'Brien, M. O'Reilly, M. Reule, G. Saxty, L. C. A. Seavers, D.-M. Smith, M. S. Squires, G. Trewartha, M. T. Walker, A. J. A. Woolford, Identification of N-(4-Piperidinyl)-4-(2,6-dichlorobenzoylamino)-1H-pyrazole-3-carboxamide (AT7519), a Novel Cyclin Dependent Kinase Inhibitor Using Fragment-Based X-Ray Crystallography and Structure Based Drug Design, *J. Med. Chem.* **2008**, *51*, 4986.

[57] M. Pallas, A. M. Canudas, E. Verdaguer, C. Allgaier, S. Garcia de Arriba, D. Alvira, F. X. Sureda, A. Camins, Inhibitors of cyclin-dependent kinases: Potential drugs for the treatment of neurodegenerative disorders?, *Current Medicinal Chemistry Central Nervous System Agents* **2005**, *5*, 101.

[58] S. R. D'Mello, E. Biehl, (University of Texas System, USA; Southern Methodist University). Application: US US, **2009**, pp. 16pp

[59] K. Johnson, L. Liu, N. Majdzadeh, C. Chavez, P. C. Chin, B. Morrison, L. Wang, J. Park, P. Chugh, H.-M. Chen, S. R. D'Mello, Inhibition of neuronal apoptosis by the cyclin-dependent kinase inhibitor GW8510: Identification of 3' substituted indolones as a scaffold for the development of neuroprotective drugs, *J. Neurochem.* **2005**, *93*, 538.

[60] W. Zhong, H. Liu, M. R. Kaller, C. Henley, E. Magal, T. Nguyen, T. D. Osslund, D. Powers, R. M. Rzasa, H.-L. Wang, W. Wang, X. Xiong, J. Zhang, M. H. Norman, Design and synthesis of quinolin-2(1H)-one derivatives as potent CDK5 inhibitors, *Bioorg. Med. Chem. Lett.* **2007**, *17*, 5384.

[61] R. M. Rzasa, M. R. Kaller, G. Liu, E. Magal, T. T. Nguyen, T. D. Osslund, D. Powers, V. J. Santora, V. N. Viswanadhan, H.-L. Wang, X. Xiong, W. Zhong, M. H. Norman, Structure-activity relationships of 3,4-dihydro-1H-quinazolin-2-one derivatives as potential CDK5 inhibitors, *Bioorg. Med. Chem.* **2007**, *15*, 6574.

[62] C. J. Helal, Z. Kang, J. C. Lucas, T. Gant, M. K. Ahlijanian, J. B. Schachter, K. E. G. Richter, J. M. Cook, F. S. Menniti, K. Kelly, S. Mente, J. Pandit, N. Hosea, Potent and cellularly active 4-aminoimidazole inhibitors of cyclin-dependent kinase 5/p25 for the treatment of Alzheimer's disease, *Bioorg. Med. Chem. Lett.* **2009**, *19*, 5703.

[63] S. Leclerc, M. Garnier, R. Hoessel, D. Marko, J. A. Bibb, G. L. Snyder, P. Greengard, J. Biernat, Y. Z. Wu, E. M. Mandelkow, G. Eisenbrand, L. Meijer, Indirubins inhibit glycogen synthase kinase-3 beta and CDK5/p25, two protein kinases involved in abnormal tau phosphorylation in Alzheimer's disease. A property common to most cyclin-dependent kinase inhibitors?, *J Biol Chem* **2001**, *276*, 251.

[64] M. R. Kaller, W. Zhong, C. Henley, E. Magal, T. Nguyen, D. Powers, R. M. Rzasa, W. Wang, X. Xiong, M. H. Norman, Design and synthesis of 6-oxo-1,6-dihydropyridines as CDK5 inhibitors, *Bioorg. Med. Chem. Lett.* **2009**, *19*, 6591.

[65] P. M. Fischer, A. Gianella-Borradori, Recent progress in the discovery and development of cyclin-dependent kinase inhibitors, *Expert Opin. Invest. Drugs* **2005**, *14*, 457.

[66] M. Mapelli, L. Massimiliano, C. Crovace, M. A. Seeliger, L.-H. Tsai, L. Meijer, A. Musacchio, Mechanism of CDK5/p25 binding by CDK inhibitors, *J. Med. Chem.* **2005**, *48*, 671.

[67] D. Alvira, M. Tajes, E. Verdaguer, S. Garcia de Arriba, C. Allgaier, C. Matute, R. Trullas, A. Jimenez, M. Pallas, A. Camins, Inhibition of cyclin-dependent kinases is neuroprotective in 1-methyl-4-phenylpyridinium-induced apoptosis in neurons, *Neuroscience (San Diego, CA, U. S.)* **2007**, *146*, 350.

[68] R. R. Rosato, J. A. Almenara, S. S. Kolla, S. C. Maggio, S. Coe, M. S. Gimenez, P. Dent, S. Grant, Mechanism and functional role of XIAP and Mcl-1 down-regulation in flavopiridol/vorinostat antileukemic interactions, *Molecular Cancer Therapeutics* **2007**, *6*, 692.

[69] E. W. Newcomb, M. A. Ali, T. Schnee, L. Lan, Y. Lukyanov, M. Fowkes, D. C. Miller, D. Zagzag, Flavopiridol downregulates hypoxia-mediated hypoxia-inducible factor-1alpha expression in human glioma cells by a proteasome-independent pathway: implications for in vivo therapy, *Neuro-Oncology (Durham, NC, United States)* **2005**, *7*, 225.

[70] Z.-T. Zhang, X.-B. Cao, N. Xiong, H.-C. Wang, J.-h. Huang, S.-G. Sun, Z.-H. Liang, T. Wang, DNA polymerase-beta is required for 1-methyl-4-phenylpyridinium-induced apoptotic death in neurons, *Apoptosis* **2010**, *15*, 105.

[71] E. G. Jorda, E. Verdaguer, A. M. Canudas, A. Jimenez, A. Bruna, C. Caelles, R. Bravo, E. Escubedo, D. Pubill, J. Camarasa, M. Pallas, A. Camins, Neuroprotective action of flavopiridol, a cyclin-dependent kinase inhibitor, in colchicine-induced apoptosis, *Neuropharmacology* **2003**, *45*, 672.

[72] Y. Wang, G. White Michael, C. Akay, A. Chodroff Rebecca, J. Robinson, A. Lindl Kathryn, A. Dichter Marc, Y. Qian, Z. Mao, L. Kolson Dennis, L. Jordan-Sciutto Kelly, Activation of cyclin-dependent kinase 5 by calpains contributes to human immunodeficiency virus-induced neurotoxicity, *J Neurochem* **2007**, *103*, 439.

[73] B. Menn, S. Bach, T. L. Blevins, M. Campbell, L. Meijer, S. Timsit, Delayed treatment with systemic (S)-roscovitine provides neuroprotection and inhibits in vivo CDK5 activity increase in animal stroke models, *PLoS One* **2010**, *5*, No pp given.

[74] M. Kitagawa, H. Higashi, I. S. Takahashi, T. Okabe, H. Ogino, Y. Taya, S. Hishimura, A. Okuyama, A cyclin-dependent kinase inhibitor, butyrolactone I, inhibits phosphorylation of RB protein and cell cycle progression, *Oncogene* **1994**, *9*, 2549.

[75] A. Fischer, F. Sananbenesi, C. Schrick, J. Spiess, J. Radulovic, Regulation of contextual fear conditioning by baseline and inducible septo-hippocampal cyclin-dependent kinase 5, *Neuropharmacology* **2003**, *44*, 1089.

[76] P. C. Chin, L. Liu, B. E. Morrison, A. Siddiq, R. R. Ratan, T. Bottiglieri, S. R. D'Mello, The c-Raf inhibitor GW5074 provides neuroprotection in vitro and in an animal model of neurodegeneration through a MEK-ERK and Akt-independent mechanism, *J. Neurochem.* **2004**, *90*, 595.

[77] H. N. Bramson, J. Corona, S. T. Davis, S. H. Dickerson, M. Edelstein, S. V. Frye, R. T. Gampe, Jr., P. A. Harris, A. Hassell, W. D. Holmes, R. N. Hunter, K. E. Lackey, B. Lovejoy, M. J. Luzzio, V. Montana, W. J. Rocque, D. Rusnak, L. Shewchuk, J. M. Veal, D. H. Walker, L. F. Kuyper, Oxindole-Based Inhibitors of Cyclin-Dependent Kinase 2 (CDK2): Design, Synthesis, Enzymatic Activities, and X-ray Crystallographic Analysis, *J. Med. Chem.* **2001**, *44*, 4339.

[78] L. Wang, H. Ankati, S. K. Akubathini, M. Balderamos, C. A. Storey, A. V. Patel, V. Price, D. Kretzschmar, E. R. Biehl, S. R. D'Mello, Identification of novel 1,4-benzoxazine compounds that are protective in tissue culture and in vivo models of neurodegeneration, *J. Neurosci. Res.* **2010**, *88*, 1970.

[79] Y. Ding, A. Qiao, G.-H. Fan, Indirubin-3'-monoxime rescues spatial memory deficits and attenuates beta -amyloid-associated neuropathology in a mouse model of Alzheimer's disease, *Neurobiol. Dis.* **2010**, *39*, 156.

[80] S. Zhang, Y. Zhang, L. Xu, X. Lin, J. Lu, Q. Di, J. Shi, J. Xu, Indirubin-3'-monoxime inhibits beta -amyloid-induced neurotoxicity in neuroblastoma SH-SY5Y cells, *Neurosci. Lett.* **2009**, *450*, 142.

[81] Y.-H. Hsiao, P.-S. Chen, S.-H. Yeh, C.-H. Lin, P.-W. Gean, N-acetylcysteine prevents beta -amyloid toxicity by a stimulatory effect on p35/cyclin-dependent kinase 5 activity in cultured cortical neurons, *J. Neurosci. Res.* **2008**, *86*, 2685.

[82] M. Chioua, A. Samadi, E. Soriano, O. Lozach, L. Meijer, J. Marco-Contelles, Synthesis and biological evaluation of 3,6-diamino-1H-pyrazolo[3,4-b]pyridine derivatives as protein kinase inhibitors, *Bioorg. Med. Chem. Lett.* **2009**, *19*, 4566.

[83] R. M. Rzasa, M. R. Kaller, G. Liu, E. Magal, T. T. Nguyen, T. D. Osslund, D. Powers, V. J. Santora, V. N. Viswanadhan, H.-L. Wang, X. Xiong, W. Zhong, M. H. Norman, Structure-activity relationships of 3,4-dihydro-1H-quinazolin-2-one derivatives as potential CDK5 inhibitors, *Bioorg. Med. Chem.* **2007**, *15*, 6574.

[84] C. Tarricone, R. Dhavan, J. Peng, L. B. Areces, L.-H. Tsai, A. Musacchio, Structure and regulation of the CDK5-p25nck5a complex, *Mol. Cell* **2001**, *8*, 657.

[85] M. Mapelli, A. Musacchio, The Structural Perspective on CDK5, *Neurosignals* **2003**, *12*, 164.

[86] N. P. Pavletich, Mechanisms of Cyclin-dependent Kinase Regulation: Structures of Cdks, their Cyclin Activators, and Cip and INK4 Inhibitors, *J. Mol. Biol.* **1999**, *287*, 821.

[87] S.-i. Hisanaga, T. Saito, The Regulation of Cyclin-Dependent Kinase 5 Activity through the Metabolism of p35 or p39 Cdk5 Activator, *Neurosignals* **2003**, *12*, 221.

[88] O. Buzko, K. M. Shokat, A kinase sequence database: sequence alignments and family assignment, *Bioinformatics* **2002**, *18*, 1274.

[89] G. M. Rubin, M. D. Yandell, J. R. Wortman, G. L. Gabor, G. L. G. Miklos, C. R. Nelson, I. K. Hariharan, M. E. Fortini, P. W. Li, R. Apweiler, W. Fleischmann, M. Cherry, S. Henikoff, M. P. Skupski, S. Misra, M. Ashburner, E. Birney, M. S. Boguski, T. Brody, P. Brokstein, S. E. Celniker, S. A. Chervitz, D. Coates, A. Cravchik, A. Gabrielian, R. F. Galle, W. M. Gelbart, R. A. George, L. S. B. Goldstein, F. Gong, P. Guan, N. L. Harris, B. A. Hay, R. A. Hoskins, J. Li, Z. Li, R. O. Hynes, S. J. M. Jones, P. M. Kuehl, B. Lemaitre, J. T. Littleton, D. K. Morrison, C. Mungall, P. H. O'Farrell, O. K. Pickeralt, C. Shue, L. B. Vosshall, J. Zhang, Q. Zhao, X. H. Zheng, F. Zhong, W. Zhong, R. Gibbs, J. C. Venter, M. D. Adams, S. Lewis, Comparative genomics of the eukaryotes, *Science (Washington, D. C.)* **2000**, *287*, 2204.

[90] G. Manning, D. B. Whyte, R. Martinez, T. Hunter, S. Sudarsanam, The Protein Kinase Complement of the Human Genome, *Science (Washington, DC, U. S.)* **2002**, *298*, 1912.

[91] M. Huse, J. Kuriyan, The conformational plasticity of protein kinases, *Cell (Cambridge, MA, U. S.)* **2002**, *109*, 275.

[92] L. N. Johnson, M. E. M. Noble, D. J. Owen, Active and inactive protein kinases: structural basis for regulation, *Cell (Cambridge, Mass.)* **1996**, *85*, 149.

[93] S. Hanks, T. Hunter, Protein kinases 6. The eukaryotic protein kinase superfamily: kinase (catalytic) domain structure and classification, *FASEB J.* **1995**, *9*, 576.

[94] P. D. Jeffrey, A. A. Russo, K. Polyak, E. Gibbs, J. Hurwitz, J. Massague, N. P. Pavletich, Mechanism of CDK activation revealed by the structure of a cyclin A-CDK2 complex, *Nature (London)* **1995**, *376*, 313.

[95] J. A. Endicott, M. E. M. Noble, J. A. Tucker, Cyclin-dependent kinases: inhibition and substrate recognition, *Curr. Opin. Struct. Biol.* **1999**, *9*, 738.

[96] D. O. Morgan, Principles of CDK regulation, *Nature (London)* **1995**, *374*, 131.

[97] A. J. Obaya, J. M. Sedivy, Regulation of cyclin-Cdk activity in mammalian cells, *Cell. Mol. Life Sci.* **2002**, *59*, 126.

[98] J. Lew, Q.-Q. Huang, Z. Qi, R. J. Winkfein, R. Aebersold, T. Hunt, J. H. Wang, A brain-specific activator of cyclin-dependent kinase 5, *Nature (London)* **1994**, *371*, 423.

[99] L.-H. Tsai, I. Delalle, V. S. Caviness, Jr., T. Chae, E. Harlow, P35 is a neural-specific regulatory subunit of cyclin-dependent kinase 5, *Nature (London)* **1994**, *371*, 419.

[100] T. Uchida, K. Ishiguro, J. Ohnuma, M. Takamatsu, S. Yonekura, K. Imahori, Precursor of cdk5 activator, the 23 kDa subunit of tau protein kinase II: its sequence and developmental change in brain, *FEBS Lett.* **1994**, *355*, 35.

[101] Z. Qi, Q.-Q. Huang, K.-Y. Lee, J. Lew, J. H. Wang, Reconstitution of neuronal Cdc2-like kinase from bacteria-expressed Cdk5 and an active fragment of the brain-specific activator. Kinase activation in the absence of Cdk5 phosphorylation, *J. Biol. Chem.* **1995**, *270*, 10847.

[102] M. Nishizawa, Y. Kanaya, A. Toh-E, Mouse cyclin-dependent kinase (Cdk) 5 is a functional homologue of a yeast Cdk, Pho85 kinase, *J. Biol. Chem.* **1999**, *274*, 33859.

[103] I. Bártová, M. Otyepka, Z. Kříž, J. Koča, Activation and inhibition of cyclin-dependent kinase-2 by phosphorylation; a molecular dynamics study reveals the functional importance of the glycine-rich loop, *Protein Science* **2004**, *13*, 1449.

[104] N. S. Gray, Exploiting chemical libraries, structure, and genomics in the search for kinase inhibitors, *Science* **1998**, *281*, 533.

[105] W. F. De Azevedo, S. Leclerc, L. Meijer, L. Havlicek, M. Strnad, S. H. Kim, Inhibition of cyclin-dependent kinases by purine analogs. Crystal structure of human cdk2 complexed with roscovitine, *Eur. J. Biochem.* **1997**, *243*, 518.

[106] W. F. De Azevedo, S. Leclerc, L. Meijer, L. Havlicek, M. Strnad, S.-H. Kim, Inhibition of cyclin-dependent kinases by purine analogues, *Eur. J. Biochem.* **1997**, *243*, 518.

[107] M. Mapelli, L. Massimiliano, C. Crovace, A. Seeliger Markus, L.-H. Tsai, L. Meijer, A. Musacchio, Mechanism of CDK5/p25 binding by CDK inhibitors, *J Med Chem* **2005**, *48*, 671.

[108] L. I. Rebhun, D. White, G. Sander, N. Ivy, Cleavage inhibition in marine eggs by puromycin and 6-dimethylaminopurine, *Experimental cell research* **1973**, *77*, 312.

[109] L. Meijer, P. Pondaven, Cyclic activation of histone H1 kinase during sea urchin egg mitotic divisions, *Experimental cell research* **1988**, *174*, 116.

[110] I. Neant, P. Guerrier, 6-Dimethylaminopurine blocks starfish oocyte maturation by inhibiting a relevant protein kinase activity, *Experimental cell research* **1988**, *176*, 68.

[111] V. Rialet, L. Meijer, A new screening test for antimitotic compounds using the universal M phase-specific protein kinase, p34cdc2/cyclin Bcdd13, affinity-immobilized on p13suc1-coated microtitration plates, *Anticancer Research* **1991**, *11*, 1581.

[112] J. Vesely, L. Havlicek, M. Strnad, J. J. Blow, A. Donella-Deana, L. Pinna, D. S. Letham, J. Kato, L. Detivaud, S. Leclerc, et al., Inhibition of cyclin-dependent kinases by purine analogues, *European journal of biochemistry / FEBS* **1994**, *224*, 771.

[113] S. R. Schow, R. L. Mackman, C. L. Blum, E. Brooks, A. G. Horsma, A. Joly, S. S. Kerwar, G. Lee, D. Shiffman, M. G. Nelson, X. Wang, M. M. Wick, X. Zhang, R. T. Lum, Synthesis and activity of 2,6,9-trisubstituted purines, *Bioorganic & Medicinal Chemistry Letters* **1997**, *7*, 2697.

[114] M. Legraverend, O. Ludwig, E. Bisagni, S. Leclerc, L. Meijer, N. Giocanti, R. Sadri, V. Favaudon, Synthesis and in vitro evaluation of novel 2,6,9-trisubstituted purines acting as cyclin-dependent kinase inhibitors, *Bioorganic & Medicinal Chemistry* **1999**, *7*, 1281.

[115] P. Imbach, H.-G. Capraro, P. Furet, H. Mett, T. Meyer, J. Zimmermann, 2,6,9-Trisubstituted purines: optimization towards highly potent and selective CDK1 inhibitors, *Bioorganic & Medicinal Chemistry Letters* **1999**, *9*, 91.

[116] N. S. Gray, L. Wodicka, A.-M. W. H. Thunnissen, T. C. Norman, S. Kwon, F. H. Espinoza, D. O. Morgan, G. Barnes, S. LeClerc, L. Meijer, S.-H. Kim, D. J. Lockhart, P. G. Schultz, Exploiting chemical libraries, structure, and genomics in the search for kinase inhibitors, *Science (Washington, D. C.)* **1998**, *281*, 533.

[117] F.-Y. Wei, K. Tomizawa, Cyclin-dependent kinase 5 (Cdk5): a potential therapeutic target for the treatment of neurodegenerative diseases and diabetes mellitus, *Mini - Reviews in Medicinal Chemistry* **2007**, *7*, 1070.

[118] U. Schulze-Gahmen, J. Brandsen, H. D. Jones, D. O. Morgan, L. Meijer, Multiple modes of ligand recognition: crystal structures of cyclin-dependent protein kinase 2 in complex with ATP and two inhibitors, olomoucine and isopentenyladenine, *Proteins Struct., Funct., Genet.* **1995**, *22*, 378.

[119] Y.-T. Chang, N. S. Gray, G. R. Rosania, D. P. Sutherlin, S. Kwon, T. C. Norman, R. Sarohia, M. Leost, L. Meijer, P. G. Schultz, Synthesis and application of functionally diverse 2,6,9-trisubstituted purine libraries as CDK inhibitors, *Chemistry & Biology* **1999**, *6*, 361.

[120] W. F. de Azevedo, Jr., H.-J. Mueller-Dieckmann, U. Schulze-Gahmen, P. J. Worland, E. Sausville, S.-H. Kim, Structural basis for specificity and potency of a flavonoid inhibitor of human CDK2, a cell cycle kinase, *Proc. Natl. Acad. Sci. U. S. A.* **1996**, *93*, 2735.

[121] N. Oumata, K. Bettayeb, Y. Ferandin, L. Demange, A. Lopez-Giral, M.-L. Goddard, V. Myrianthopoulos, E. Mikros, M. Flajolet, P. Greengard, L. Meijer, H. Galons, Roscovitine-Derived, Dual-Specificity Inhibitors of Cyclin-Dependent Kinases and Casein Kinases 1, *Journal of Medicinal Chemistry* **2008**, *51*, 5229.

[122] M. A. Fabian, W. H. Biggs, D. K. Treiber, C. E. Atteridge, M. D. Azimioara, M. G. Benedetti, T. A. Carter, P. Ciceri, P. T. Edeen, M. Floyd, J. M. Ford, M. Galvin, J. L. Gerlach, R. M. Grotzfeld, S. Herrgard, D. E. Insko, M. A. Insko, A. G. Lai, J.-M. Lelias, S. A. Mehta, Z. V. Milanov, A. M. Velasco, L. M. Wodicka, H. K. Patel, P. P. Zarrinkar, D. J. Lockhart, A small molecule-kinase interaction map for clinical kinase inhibitors, *Nature Biotechnology* **2005**, *23*, 329.

[123] J. Moravec, V. Krystof, J. Hanus, L. Havlicek, D. Moravcova, K. Fuksova, M. Kuzma, R. Lenobel, M. Otyepka, M. Strnad, 2,6,8,9-Tetrasubstituted Purines as New CDK1 Inhibitors, *Bioorganic & Medicinal Chemistry Letters* **2003**, *13*, 2993.

[124] M. Medina, J. Avila, Glycogen synthase kinase-3 (GSK-3) inhibitors for the treatment of Alzheimer's disease, *Curr. Pharm. Des.* **2010**, *16*, 2790.

[125] J. P. Lopes, C. R. Oliveira, P. Agostinho, Cell cycle re-entry in Alzheimer's disease: a major neuropathological characteristic?, *Curr. Alzheimer Res.* **2009**, *6*, 205.

[126] T. A. Evans, A. K. Raina, A. Delacourte, O. Aprelikova, H.-g. Lee, X. Zhu, G. Perry, M. A. Smith, BRCA1 may modulate neuronal cell cycle re-entry in Alzheimer disease, *Int. J. Med. Sci.* **2007**, *4*, 140.

[127] L. A. Previll, M. E. Crosby, R. J. Castellani, R. Bowser, G. Perry, M. A. Smith, X. Zhu, Increased Expression of p130 in Alzheimer Disease, *Neurochem. Res.* **2007**, *32*, 639.

[128] A. McShea, H.-G. Lee, R. B. Petersen, G. Casadesus, I. Vincent, N. J. Linford, J.-O. Funk, R. A. Shapiro, M. A. Smith, Neuronal cell cycle re-entry mediates Alzheimer disease-type changes, *Biochim. Biophys. Acta, Mol. Basis Dis.* **2007**, *1772*, 467.

[129] A. Evans Teresa, K. Raina Arun, A. Delacourte, O. Aprelikova, H.-g. Lee, X. Zhu, G. Perry, A. Smith Mark, BRCA1 may modulate neuronal cell cycle re-entry in Alzheimer disease, *Int. J. Med. Sci.* **2007**, *4*, 140.

[130] A. McShea, H.-g. Lee, B. Petersen Robert, G. Casadesus, I. Vincent, J. Linford Nancy, J.-O. Funk, A. Shapiro Robert, A. Smith Mark, Neuronal cell cycle re-entry mediates Alzheimer disease-type changes, *Biochim. Biophys. Acta* **2007**, *1772*, 467.

[131] J. Kanungo, Y.-l. Zheng, N. D. Amin, H. C. Pant, Targeting Cdk5 Activity in Neuronal Degeneration and Regeneration, *Cell. Mol. Neurobiol.* **2009**, *29*, 1073.

[132] K. Muller, C. Faeh, F. Diederich, Fluorine in pharmaceuticals: looking beyond intuition, *Science (New York, N.Y.)* **2007**, *317*, 1881.

[133] W. K. Hagmann, The Many Roles for Fluorine in Medicinal Chemistry, *J. Med. Chem.* **2008**, *51*, 4359.

[134] I. Ojima, Editor, *Fluorine In Medicinal Chemistry And Chemical Biology*, Wiley, New York, **2009**.

[135] F. Rizzolio, T. Tuccinardi, I. Caligiuri, C. Lucchetti, A. Giordano, CDK inhibitors: from the bench to clinical trials, *Curr. Drug Targets, 11*, 279.

[136] T. Hara, M. Omura-Minamisawa, Y. Kang, C. Cheng, T. Inoue, Flavopiridol Potentiates the Cytotoxic Effects of Radiation in Radioresistant Tumor Cells in Which p53 is Mutated or Bcl-2 is Overexpressed, *Int. J. Radiat. Oncol., Biol., Phys.* **2008**, *71*, 1485.

[137] K. C. Bible, S. H. Kaufmann, Flavopiridol: a cytotoxic flavone that induces cell death in noncycling A549 human lung carcinoma cells, *Cancer Res.* **1996**, *56*, 4856.

[138] C. Spiteri, J. E. Moses, Copper-Catalyzed Azide-Alkyne Cycloaddition: Regioselective Synthesis of 1,4,5-Trisubstituted 1,2,3-Triazoles, *Angew. Chem., Int. Ed.*, *49*, 31.

[139] G. C. Tron, T. Pirali, R. A. Billington, P. L. Canonico, G. Sorba, A. A. Genazzani, Click chemistry reactions in medicinal chemistry: applications of the 1,3-dipolar cycloaddition between azides and alkynes, *Med. Res. Rev.* **2008**, *28*, 278.

[140] A. Camins, E. Verdaguer, J. Folch, M. Canudas Anna, M. Pallas, The role of CDK5/P25 formation/inhibition in neurodegeneration, *Drug News Perspect* **2006**, *19*, 453.

[141] G. D. Cuny, Kinase inhibitors as potential therapeutics for acute and chronic neurodegenerative conditions, *Curr. Pharm. Des.* **2009**, *15*, 3919.

[142] N. Oumata, Y. Ferandin, L. Meijer, H. Galons, Practical Synthesis of Roscovitine and CR8, *Org. Process Res. Dev.* **2009**, *13*, 641.

[143] F. Amblard, J. H. Cho, R. F. Schinazi, Cu(I)-Catalyzed Huisgen Azide-Alkyne 1,3-Dipolar Cycloaddition Reaction in Nucleoside, Nucleotide, and Oligonucleotide Chemistry, *Chem. Rev.* **2009**, *109*, 4207.

[144] A. DerHovanessian, P. R. Rablen, A. Jain, Ab Initio and Density Functional Calculations of 19F NMR Chemical Shifts for Models of Carbonic Anhydrase Inhibitors, *J. Phys. Chem. A* **2000**, *104*, 6056.

[145] W. L. Klein, Abeta toxicity in Alzheimer's disease: globular oligomers (ADDLs) as new vaccine and drug targets, *Neurochem Int* **2002**, *41*, 345.

[146] N. Gogolla, I. Galimberti, V. DePaola, P. Caroni, Preparation of organotypic hippocampal slice cultures for long-term live imaging, *Nat Protoc* **2006**, *1*, 1165.

[147] Y. H. Chong, Y. J. Shin, E. O. Lee, R. Kayed, C. G. Glabe, A. J. Tenner, ERK1/2 activation mediates Abeta oligomer-induced neurotoxicity via caspase-3 activation and tau cleavage in rat organotypic hippocampal slice cultures, *J Biol Chem* **2006**, *281*, 20315.

2. NMR STUDIES OF TRANSITION METAL ION BINDING TO HISTIDINE, GLUTAMIC ACID AND ASPARTIC ACID: THE POTENTIAL METAL ION BINDING SITES OF AMYLOID-β PEPTIDE.

2.1 INTRODUCTION

2.1.1 Role of Metal Ions in Aβ Toxicity. Transition metal ions, mainly Fe(III), Cu(II), and Zn(II), are localized in amyloid-β (Aβ) plaques and neurofibrillary tangles in Alzheimer's disease (AD).[1-6] The oxidative stress arising as a result of the metal ion binding to the Aβ peptide is still debatable, although more recently a unified hypothesis involving oxidative damage through mitotic insults and metal ion induced oxidative stress on Aβ and neurofibrillary tangles is gaining much attention.[7-8] At low concentrations of the transition metal ions, the Aβ shows antioxidant activity due to the sequestration of the metal ions from the surrounding tissue environments, whereas at relatively higher concentrations, the metal ions serve as active sites for the Fenton-Haber-Weiss reaction, which results in onset of oxidative stress.[9-11] The highly redox active Cu(II) and Fe(II) are thus not only responsible for the formation of Aβ aggregates, but also in subsequent overproduction of reactive oxygen species (when bound to Aβ peptide) which have deleterious physiological consequences. Highly redox active Fe(III) and Cu(II), as Aβ complexes, are involved in the neurotoxicity, while the relatively less Fenton-active Zn(II) may be neuroprotective or neurotoxic depending on the concentration levels. [4, 6, 12] Many reports have suggested that low concentrations of Zinc(II) stabilize Aβ in the oligomeric form, restricting further polymerization into the fibrillary form.[13-14] This may in fact be detrimental as the oligomeric forms of Aβ have

been shown to be neurotoxic and the fibrillary forms relatively less harmful. While circulating levels of Zn(II) may be appear too low for such interactions, synaptic activity produces pulses of free Zn(II) release.[14] The immediate formation of Zn(II)-Aβ oligomer complexes may also directly affect synapse activity within the brain, as they bind directly to synapses, colocalize with synaptic markers, interfere with synaptic function, and correlate with synaptic loss.[15] Although Zn(II) ions play a crucial role in AD, its relatively binding efficiency compared to Cu(II) and Fe(III) has not been clearly demonstrated to date. A variety of metal-ion chelators such as clioquine and desferrioxamine are currently introduced as therapeutics in AD on the assumption that the transition metal ions released from the Aβ plaques play a key role in the oxidative stress in AD. [16-17]

2.1.2 NMR Characterization of Metal Ion Binding Site of Aβ. Recent ^{1}H nuclear magnetic resonance (NMR) and electron spin resonance (ESR) studies show that histidine residues of Aβ bind to Zn(II) through the imidazole nitrogens of His6, His13, and His14 residues of Aβ. [2, 9] X-ray absorption fine structure spectroscopy of histidine-Zn(II) complex shows the binding of Zn(II) mainly through the imidazole nitrogen(N1) and the amino group. [18]The hydrophilic region of $A\beta_{1.28}$ has three histidine residues (H6, 13, 14) which are mostly responsible for the strong metal ion binding, although other carboxylate side chain amino acids, aspartic acid and glutamic acid and the hydroxyl group of tyrosine may exert some binding affinity.[2, 13, 19-24] Recent studies using site specific N-15 and C-13 labeling show histidine as the major ligand for Cu(II) ion.[25] Further, the ^{1}H NMR spectra of uniformly ^{15}N-labeled $A\beta_{1.40}$ show upfield shifts for the

side chain imidazole-C2 hydrogens of histidines (H6, H13, and H14), reflecting presumably rapid conformational changes for the $A\beta_{1.40}$ peptide during metal ion binding.[26] Thus the mode of binding of Zn(II), Fe(III), and Cu(II) to $A\beta_{1.40}$ could not be established through the use of either the smaller peptide fragments ($A\beta_{1.16}$, $A\beta_{1.28}$) or $A\beta_{1.40}$ peptide itself.

As far as we are aware there are no systematic studies of the relative strengths of the Zn, Fe and Cu ion binding to the Aβ peptide. NMR methods are ideally suited for direct estimation of binding strengths. However, the paramagnetic nature of the Fe(II), Fe(III), and Cu(II) causes appreciable line broadening at the concentrations required for determining their binding stoichiometry. Zn(II) is diamagnetic and in the absence of fast intermolecular exchange would give reliable NMR data for its complexes. Metal ions that bind stronger than Zn(II) are expected to show deshielded absorptions for hydrogens near the coordination site. Further, peak broadening due to the added paramagnetic Fe(III), Fe(II) or Cu(II) species indicate their displacement of Zn(II) ions from the Zn(II)-complex. Thus using histidine (H), tyrosine (Y), aspartic acid (D), and glutamic acid (E), which are the potential metal ion binding centers in the hydrophilic region of Aβ, we have probed their relative binding efficiencies of Zn(II), Fe(III), Fe(II), and Cu(II) species.

2.2 METAL ION BINDING STUDIES OF HISTIDINE, GLUTAMIC ACID AND ASPARTIC ACID: RESULTS AND DISCUSSION

Aβ peptide binds transition metal ions, such as copper, zinc, and iron. At low concentrations of these metals, Aβ acts as antioxidant through removal of the metal ions from the surrounding cellular environments. On the other hand, when coordinated to larger amounts of the metal ions, it acts as pro-oxidant through Fenton reactions of the associated metal.[10] Although the nature of the metal ion complexation and its resultant effects on oxidative stress are currently under debate, it is important to know the relative binding strengths of the metal ions to Aβ. N-terminal domain, 1.28 (underlined on the sequence below), of Aβ is hydrophilic with potential metal ion coordinating amino acids, aspartic acid, glutamic acid, tyrosine and histidine as shown below.

1 DAEFRHDSGY EVHHQKLVFF AEDVGSNKGA IIGLMVGGVV IA 42

The remarkably high affinity of Cu(II) to Aβ, as shown by fluorescence titration methods, indicates that Cu(II) is central to the neurotoxicity.[27] A recent study, involving selective N-15 and C-13 labeling of glutamic acid and alanine, respectively, shows that H6, H13, H14, and carbonyl oxygen of A2 bind to Cu(II) in a square planar structure.[25] Further, it was found by these site specific labeling studies that Y10 hydroxyl is not a key ligand at physiological pH range.[25] On the other hand, other studies show the importance of glutamic acid and aspartic acid residues in the coordination of metal ions.[28]

From the above discussion, it is evident that histidine residues in Aβ are the major binding sites for the metal ions, and in order to understand the relative binding efficiencies of Cu(II), Zn(II) and Fe(II) to Aβ we have used histidine as a model

aminoacid and estimated its metal ion binding strengths through NMR titrations. We have also compared the metal ion binding efficiencies of aspartic acid, glutamic acid and tyrosine by this method. Earlier NMR studies of Zn(II) complexation of Aβ or its hydrophilic fragments (1-28 or 1-16) revealed significant peak broadenings of histidine, aspartic acid, and glutamic acid residues, but there were no clear cut deshieldings of the NMR absorptions, presumably due to the rapid conformational changes of the peptides upon metal ion complexation.[19-20, 29] Therefore, we chose histidine as a model amino acid and compared its relative metal ion chelating efficiencies towards Zn(II), Fe(II), Fe(II)), and Cu(II) at physiological pH and ambient temperatures.

We have chosen Zn(II) ions initially for our NMR studies because it is diamagnetic; there will not be significant signal broadening in the measured range of concentrations required for the saturation of the binding sites. The ^{1}H NMR spectra for incremental addition of Zn(II) to histidine in phosphate buffer (D_2O) (Figure 2.1) shows deshielded absorptions for all the histidine protons.

Significantly large deshieldings were observed for δ^1H 7.49 (C2.imidazole H) implying strong coordination through N1.imidazole nitrogen. Both amino and carboxy groups may be involved in coordination, as the δ^1H at 3.74 and diastereotopic hydrogens at C3 (δ^1H 2.92) are also deshielded by relatively smaller extent.

Mol ratio plots of [Zn(II)]/[His] and chemical deshielding for δ^1H for C2.imidazole hydrogen (Figure 2.2) show a stoichiometry for Zn(II):His of 1:2, from the abrupt changes in the slope [30]. Based on this data we propose an octahedral structure (1) for Zn(II)-histidine complex (Scheme 1). Earlier x-ray structures for related Cu(II)-

histidine complexes were shown to involve equilibrating square pyramid and square planar structure with 2:1 histidine-Cu(II) stoichiometry.[31]

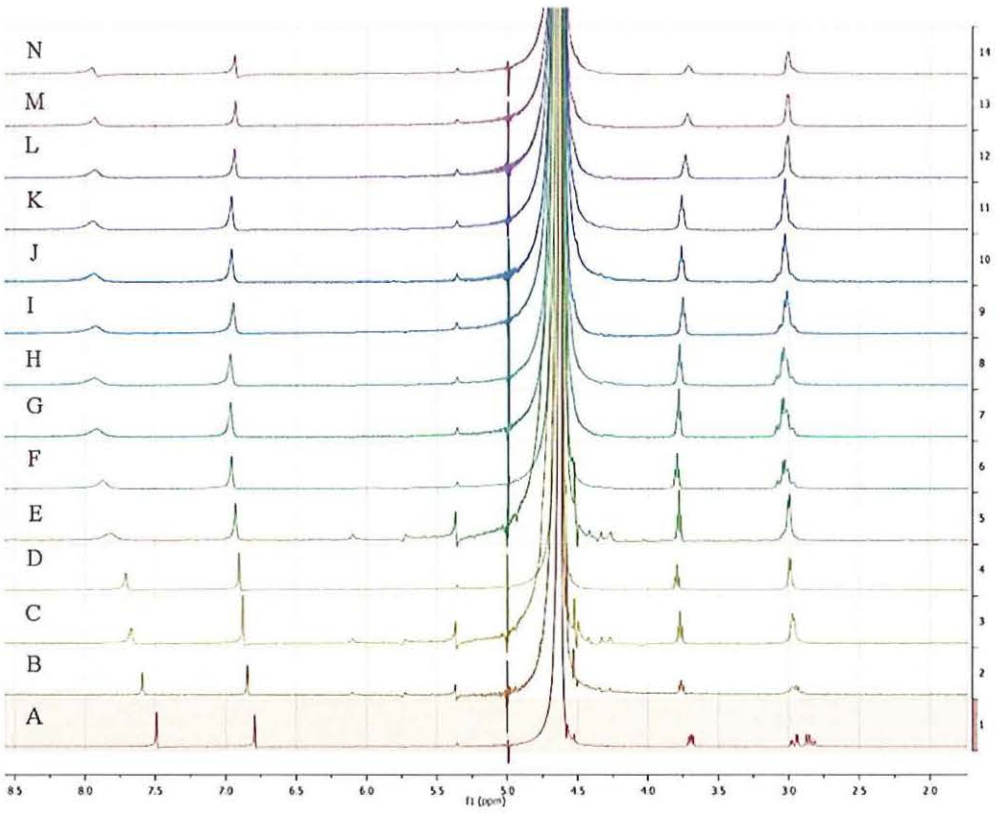

Figure 2.1. ^{1}H NMR titration of histidine with Zn(II) in D_2O (δ^1H (D_2O) = 4.63ppm) solution at 25 °C and at a pH of 7.45 ± 0.01. Spectrum A is for histidine dissolved in phosphate buffered D_2O (pH 7.45); spectra B to N are for incremental additions of Zn (II) to histidine solution (A); in each of these later solutions the [Zn(II)] / [histidine] ratios are as follows: B, 0.05; C, 0.10; D, 0.15; E, 0.2; F, 0.31; G, 0.52; H, 0.73; I, 1.04; J, 1.25; K, 1.41; L, 1.99; M, 3.91; N, 5.75. The absorption at δ^1H 7.49 corresponding to imidazole-2H was relatively most deshielded indicating strong binding of histidine through imidazole-N3. From the spectral changes it is evident that other binding sites of histidine are the amino and carboxyl groups.

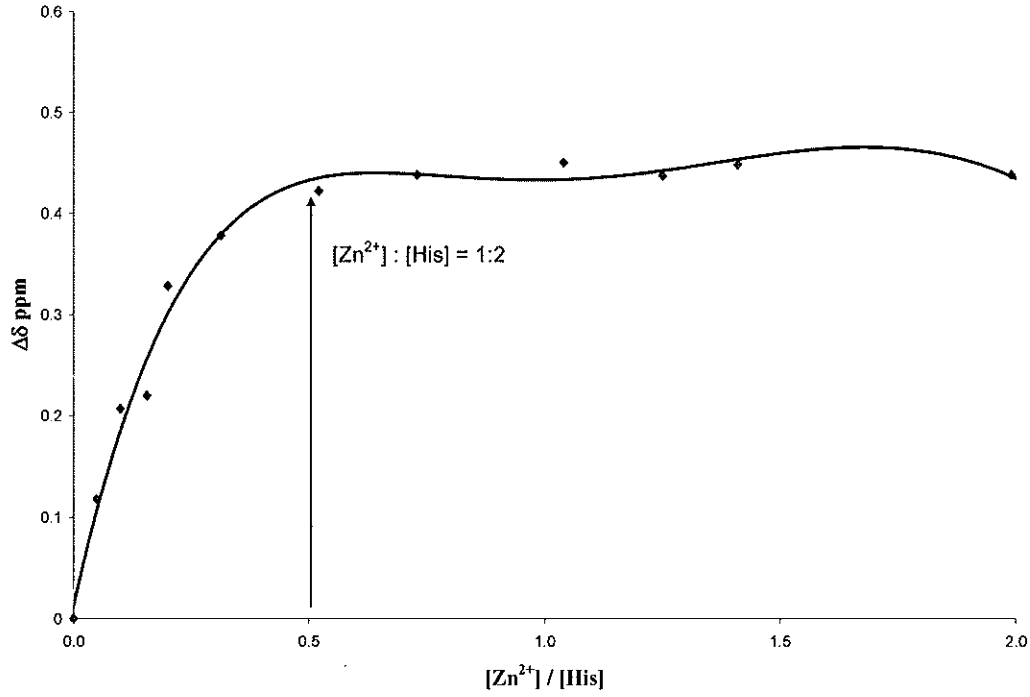

Figure 2.2. Mol ratio plot for the incremental addition of Zn(II) to histidine. The concentration of histidine is kept constant at 92 mM and Zn(II) concentration was varied from 0 to 6 molar equivalents. The stoichiometry of Zn(II) to histidine was found to be 1:2 as indicated by the abrupt changes in slope of the curve.

Incremental addition of Zn(II) (0 to 1 equiv.) to glutamic acid (50 mM) and aspartic acid (40 mM) solutions in phosphate buffer (D_2O) showed no chemical shift variations, implying non-binding of these amino acids with Zn(II).These data are not in agreement with the NMR studies of Zn(II) complexation with human and rat $A\beta_{1.28}$ by Gaggelli and coworkers' who reported chemical shift variations for the aspartic acid (D1) and glutamic acid (E11) upon Zn(II) complexation.[19]The conformational changes of Aβ induced by Zn(II) may explain the discrepancies as we have used the individual amino acids in our studies. Zirah and coworkers' TOCSY NMR studies of Zn(II)

complexation of $A\beta_{1.16}$ showed no chemical shift variations but based on the line broadening of the peaks they have inferred the coordination of H6, H13, H14, E11 residues to Zn(II).[20] Our observation of the significant downfield shifts of histidine-C2.imidazole hydrogens confirm the involvement of histidine residues in the Zn(II) ion binding (Scheme 2.1). These observations imply the major role of histidine residues in the binding to Zn(II) ions, also in accordance with the recent experimental observations on Aβ peptide.[13]

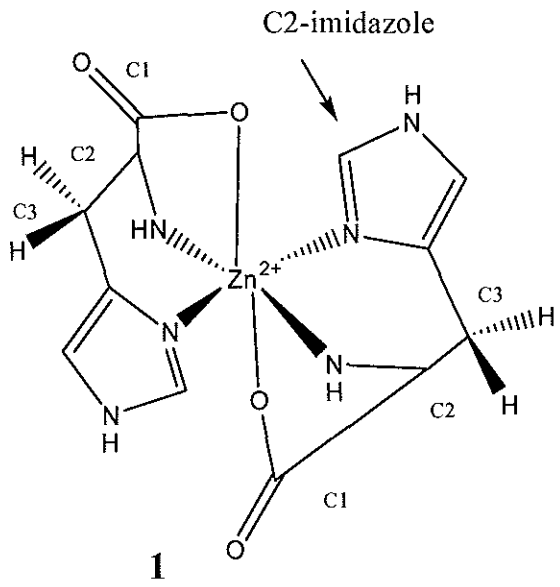

1

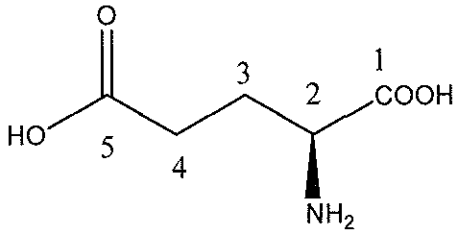

Glutamic acid (E)

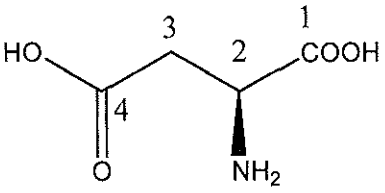

Aspartic acid (D)

Scheme 2.1. Structures of the proposed octahedral His-Zn(II) complex (1), glutamic acid (E), and aspartic acid (D); the carbons are numbered in accordance with the descriptions in the text.

2.2.1 Relative Binding Efficiencies of Fe(III), Cu(II) and Zn(II). In order to investigate the relative binding efficiencies of iron and copper ions, in separate experiments we have titrated the Zn(II)-histidine complex solutions (phosphate buffer, pH 7.4) with Fe(III) and Cu(II) salts. Upon addition of 0.1 mol equivalents of Cu (II) to Zn(II)-histidine (0.5:1 molar ratio) solution, the absorptions at δ^1H 7.9 and 6.9 have slightly shifted downfield (0.12 ppm and 0.1ppm respectively) and are significantly broadened due to the paramagnetic nature of the Cu(II) species (Figure 2.3). The peak broadening, as well as slight deshielding effect at this concentration level, show that Cu(II) is relatively more efficient than Zn(II) in binding to histidine.

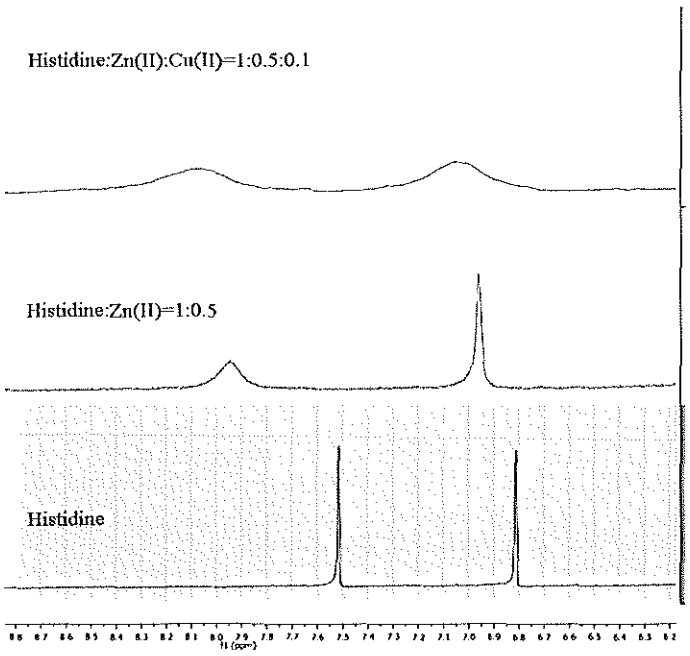

Figure 2.3. Partial ^{1}H NMR spectra of histidine-Zn(II)/Cu(II). Titration of Cu(II) solution to Zn(II)-histidine solution resulted in significant line broadening even at 8.3 mM range (0.1 mol eq of Cu(II)) due to its paramagnetic character. The sight deshielding and line broadening indicate competing replacement of Zn (II) by Cu(II) from its complex.

Similarly, addition of Fe(III) to Zn(II)-histidine in phosphate buffer (pH 7.4) shows significantly deshielded peaks (Figure 2.4), which indicates much stronger binding efficiency of Fe(III) to histidine as compared to Zn(II). In accordance with this evidence, addition of 0.5 mol equivalents of Fe(III) to 92 mM solution of pure histidine in phosphate buffer (pH 7.4) resulted in deshielding of the peak at δ^1H 7.5 to 8.5 ($\Delta\delta = 1$; Figure 2.4).

Under similar conditions, the Zn(II) complex showed relatively smaller chemical shift difference of ($\Delta\delta = 0.5$). The observed significant deshielding for Fe(III) complexes supports the greater binding affinity of Fe(III) to histidine as compared to Zn(II). In a control experiment, reverse addition of Zn(II) to a solution of histidine-Fe(III) resulted in no changes in the ^{1}H NMR chemical shifts, further confirming the relatively higher binding efficiency of Fe(III) over that of Zn(II).

In a separate experiment we have also titrated Cu(II) chloride and Fe(II) sulfate to histidine solution (phosphate buffer, pH 7.4). Due to the high paramagnetic nature of the Cu(II) species we were able to obtain NMR spectra for solutions up to 0.1 mol equivalents of Cu(II). Even at this relatively low concentration of Cu(II), the imidazole-C2.H and imidazole-C5-H of histidine were significantly deshielded by 0.57 and 0.27 ppm, respectively.

Addition of 0.1 mol equivalents of Fe(II) to histidine solution resulted in downfield shift of the imidazole-C2.H and imidazole-C5-H by 0.22 and 0.15 ppm, respectively.Under similar conditions titration of Fe(III) chloride with histidine solution shifted the imidazole-C2.H and imidazole-C5-H of histidine downfield by 0.45 and 0.15 ppm, respectively (Figure 2.5).

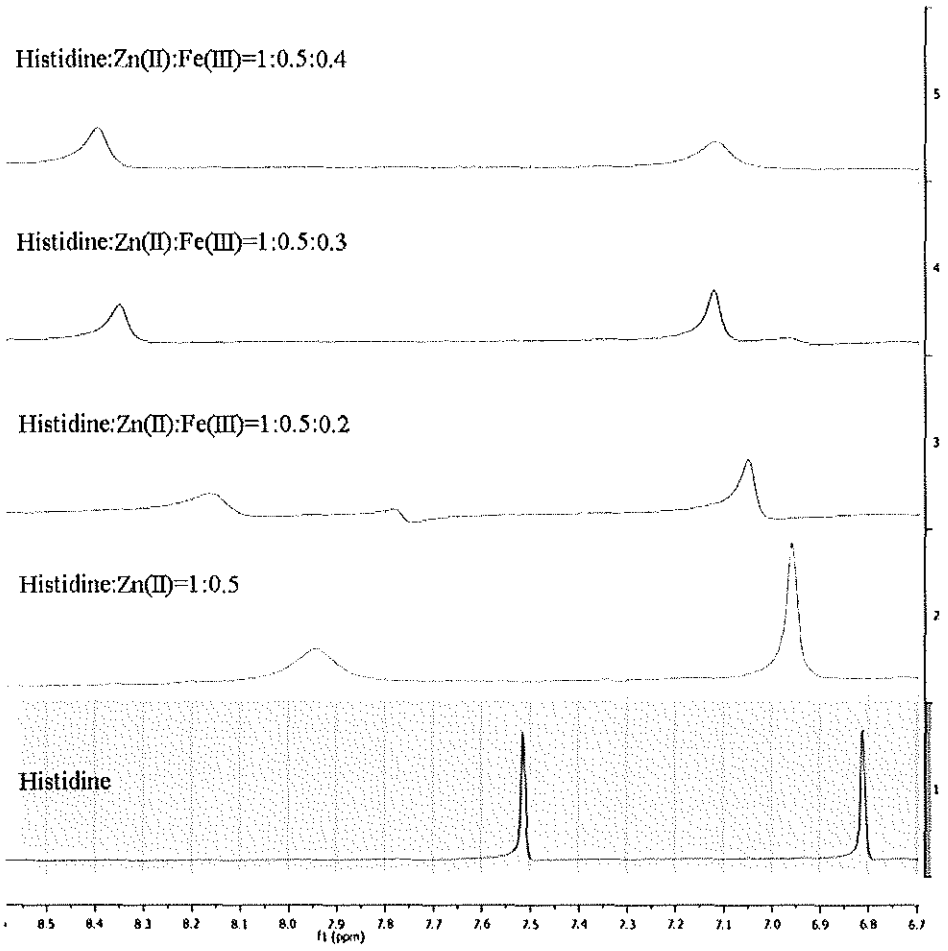

Figure 2.4. Partial ^{1}H NMR spectra of histidine-Zn(II)/Fe(III). As Fe(III) was added to a Zn(II)/histidine solution the absorptions for the imidazole protons were broadened and were shifted to downfield indicating relatively stronger binding affinity of Fe(III) over Zn(II).

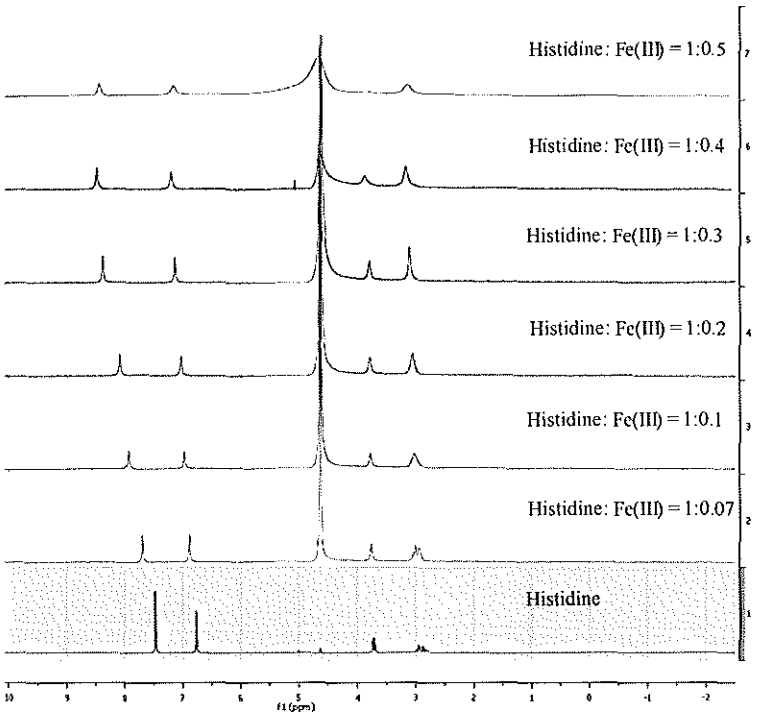

Figure 2.5. ^{1}H NMR spectra of histidine/Fe (III). Addition of 0.5 mol equivalents of Fe(III) to histidine resulted in significantly downfield shifts for the imidazole hydrogens as compared to similar titration with Zn(II) under similar conditions. The relatively much deshielded absorptions indicate higher binding efficiency for Fe(III) as compared to Zn(II). Maximum concentration of Fe(III), which could be used for these NMR binding studies was 0.5 mol equivalents due the broadening of the peaks.

Titrations of Zn(II) with histidine under same conditions resulted in downfield shifts for C2. and C5- imidazole hydrogens by 0.2 ppm and 0.1 ppm, respectively. From the observed deshielding of the C2.imidazole hydrogen in the above experiments, the relative binding efficiencies of the metal ions to histidine is in the following order: Cu(II) > Fe(III) > Fe(II) > Zn(II). Overall, these results indicate superior complexing ability of iron and copper ions over zinc ions.

2.2.2 Relative Metal Ion Binding Efficiencies of Glu, Asp and Tyr.

The hydrophilic region of $A\beta_{1.28}$ contains, in addition to histidine, other potentially metal ion coordinating amino acids, Glu(3,11,22), Asp(1,7,23), and Tyr(10). In order to evaluate their relative metal ion binding efficiencies we have performed similar proton NMR titration studies for these amino acids. Metal ion complexation to the side chain carboxyl groups of these amino acids would be expected to deshield the hydrogens on its neighboring carbons (C4 and C3 for E and D, respectively). Upon addition of Fe(III) (0.3 equivalents) to buffered glutamic acid (50mM) and aspartic acid (40mM) solutions in D_2O, the C4.protons of glutamic acid and C3 protons of aspartic acid were deshielded by 0.05 ppm and 0.07 ppm, respectively (Figure 2.6). Under comparable conditions (i.e., histidine: Fe(III) = 1 : 0.3) histidine-C2.imidazole hydrogens were deshielded by 1 ppm, showing relatively much greater coordinating ability of histidine groups.

Thus, the relative binding efficiencies of glutamic acid and aspartic in Aβ are insignificant as compared to that of histidine. These findings are in accordance with recent hyperfine sublevel correlation spectroscopy studies of site specifically N-15 and C-13 labeled Aβ peptide which show complexation mainly by histidine residues.[25]

The results on tyrosine are not conclusive due to its relative insolubility in water, but overall there are no significant chemical shift variations for tyrosine in the presence of Fe(III), also in accordance with the recent ^1H NMR studies of $A\beta_{1.40}$ peptide.[26]

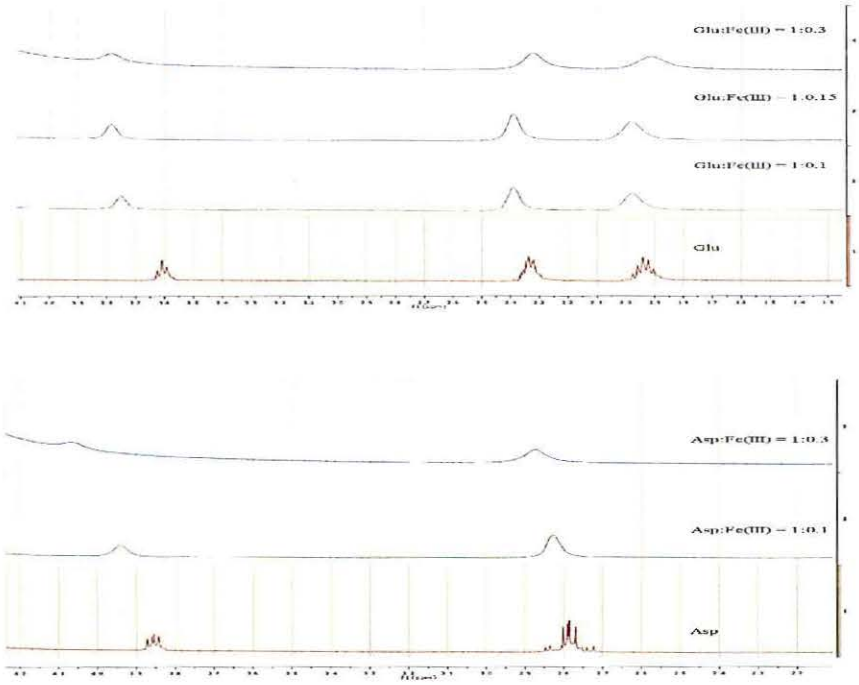

Figure 2.6. ^{1}H NMR spectra of glutamic acid/Fe(III) (top) and aspartic acid/Fe(III) (bottom). Addition of up to 0.3 mol equivalents of Fe(III) to glutamic acid and aspartic acid resulted in relatively minor deshielding of the chemical shifts, as compared to histidine, showing relatively weak binding affinity of these amino acids with Fe(III).

2.2.3 Conclusion. As a model to the metal ion binding to Aβ peptide, we have investigated the relative binding efficiencies of Fe(III), Cu(II), and Zn(II) to histidine, tyrosine, aspartic acid and glutamic acid using ^{1}H NMR titration experiments. From the observed deshielding of the chemical shifts it is evident that histidine is the major binding site for the metal ions. We have found a stoichiometry of Zn:histidine of 1:2, suggesting an octahedral structure to the complex. From NMR titration experiments it can be concluded that the Fe(III)/Fe(II) and Cu(II) bind relatively more strongly than Zn(II) to histidine.

2.3 EXPERIMENTAL SECTION

2.3.1 Materials and Methods. Zinc(II) nitrate hexahydrate (>98% pure), Iron(III) chloride hexahydrate (ACS reagent; >97% pure), Iron(II) sulfate heptahydrate, (>99% pure), Copper(II) Chloride dihydrate (>99.99% disodium hydrogen phosphate heptahydrate ($Na_2HPO_4,7H_2O$) (>99.99%), sodium dihydrogen phosphate monohydrate ($NaH_2PO_4.H_2O$) (>98%), L-Aspartic acid (>98%), L-Glutamic acid (99%), L-Tyrosine (>98%) were obtained from Aldrich and used as received. L-Histidine (>98% pure) was obtained from Alfa Aesar. Deuterium oxide (Cambridge Isotope laborotories, Inc.) used in NMR experiments had an isotopic purity of >99.9% .

^1H NMR spectra (at 399.7MHz) were obtained on a Varian Inova 400 MHz spectrometer in D_2O solutions at 25 °C. pH of the solutions was measured using a Accumet excel XL15 pH meter.

2.3.2 Buffer Preparations. A 10 mM stock solution of the phosphate buffer was prepared by dissolving the monobasic $NaH_2PO_4.H_2O$ (0.0312 g) and the dibasic $Na_2HPO_4,7H_2O$ (0.2075 g) in distilled water (100 mL). pH of the buffer solution was adjusted to 7.45±0.01 by titrating with concentrated hydrochloric acid solution, using the pH meter.

2.3.3 NMR Titrations. A series of solutions of Zinc(II) nitrate in histidine were prepared by adding appropriate amounts of $Zn(NO_3)_2$ hexahydrate (0 to 53 mM in D_2O) to histidine (92 mM in D_2O) so that the resulting solutions had Zn^{2+}/His mol ratio

varying from 0:1 to 6:1. Each of these solutions was buffered to pH 7.4 by adding 0.1 mL of the buffer stock solution, and transferred into 5 mm NMR tubes. The ^{1}H NMR spectra of these solutions were recorded at 400 MHz at 25 °C. The stoichiometry of the metal complexes was determined through linear least squares plots of changes in chemical shifts ($\Delta\delta$) versus $[Zn^{2+}]$/[His] from the abrupt changes in the slope.

The comparative binding efficiencies of Fe(III), Fe(II), Cu(II), and Zn(II) were determined as follows: incremental amounts of Fe(III) (0 to 0.5 mol equivalents), Fe(II) (0 to 0.1 mol equivalents) and Cu(II) (0 to 0.1 equivalents) salts were added to the 5 mm NMR tubes containing solutions of Zn(II) and histidine in D_2O (mol ratio of Zn(II):histidine = 0.5; initial concentration of histidine = 92 mM) and the spectra were recorded at 25 °C. The NMR peaks gradually broadened and disappeared into baseline as the concentrations of the salts increased. Similar titration experiments were carried out for aspartic acid (40 mM), glutamic acid (50 mM). Due to limited solubility the NMR experiments with tyrosine were done at much smaller concentrations (< 9 mM) and there were no noticeable chemical shift changes under these conditions.

2.4 REFERENCES

[1] J. Ryu, K. Girigoswami, C. Ha, S. H. Ku, C. B. Park, Influence of Multiple Metal Ions on beta -Amyloid Aggregation and Dissociation on a Solid Surface, *Biochem.* 2008, *47*, 5328.

[2] C. D. Syme, J. H. Viles, Solution 1H NMR investigation of Zn2+ and Cd2+ binding to amyloid-beta peptide (A.beta) of Alzheimer's disease, *Biochim. Biophys. Acta, Proteins Proteomics* 2006, *1764*, 246.

[3] C. Ha, J. Ryu, C. B. Park, Metal Ions Differentially Influence the Aggregation and Deposition of Alzheimer's beta -Amyloid on a Solid Template, *Biochem.* 2007, *46*, 6118.

[4] G. M. Bishop, S. R. Robinson, The amyloid paradox: Amyloid-beta -metal complexes can be neurotoxic and neuroprotective, *Brain Pathol.* 2004, *14*, 448.

[5] C. S. Atwood, R. C. Scarpa, X. Huang, R. D. Moir, W. D. Jones, D. P. Fairlie, R. E. Tanzi, A. I. Bush, Characterization of copper interactions with Alzheimer amyloid beta peptides: identification of an attomolar-affinity copper binding site on amyloid beta 1.42, *J. Neurochem.* 2000, *75*, 1219.

[6] X. Huang, M. P. Cuajungco, C. S. Atwood, R. D. Moir, R. E. Tanzi, A. I. Bush, Alzheimer's disease, beta -amyloid protein and zinc, *J. Nutr.* 2000, *130*, 1488S.

[7] X. Zhu, G. Perry, M. A. Smith, Two hits and you're out? A novel mechanistic hypothesis of Alzheimer disease, *Adv. Behav. Biol.* 2008, *57*, 191.

[8] K. J. Barnham, C. C. Curtain, A. I. Bush, Free radicals, metal ions, and Aβ aggregation and neurotoxicity, *Protein Rev.* 2007, *6*, 31.

[9] M. Nakamura, N. Shishido, A. Nunomura, M. A. Smith, G. Perry, Y. Hayashi, K. Nakayama, T. Hayashi, Three Histidine Residues of Amyloid-beta Peptide Control the Redox Activity of Copper and Iron, *Biochem.* 2007, *46*, 12737.

[10] V. P. Reddy, X. Zhu, G. Perry, M. A. Smith, Oxidative Stress in Diabetes and Alzheimer's Disease, *J. Alzheimer's Dis.* 2009, *16*, 763.

[11] C. S. Atwood, G. Perry, H. Zeng, Y. Kato, W. D. Jones, K.-Q. Ling, X. Huang, R. D. Moir, D. Wang, L. M. Sayre, M. A. Smith, S. G. Chen, A. I. Bush, Copper Mediates Dityrosine Cross-Linking of Alzheimer's Amyloid-beta, *Biochem.* 2004, *43*, 560.

[12] M. P. Cuajungco, K. Y. Faget, Zinc takes the center stage: its paradoxical role in Alzheimer's disease, *Brain Res. Rev.* 2003, *41*, 44.

[13] J. Danielsson, R. Pierattelli, L. Banci, A. Graeslund, High-resolution NMR studies of the zinc-binding site of the Alzheimer's amyloid beta -peptide, *Febs J.* 2007, *274*, 46.

[14] D. Noy, I. Solomonov, O. Sinkevich, T. Arad, K. Kjaer, I. Sagi, Zinc-amyloid beta interactions on a millisecond time-scale stabilize non-fibrillar Alzheimer-related species, *J. Am. Chem. Soc.* 2008, *130*, 1376.

[15] A. Deshpande, H. Kawai, R. Metherate, C. G. Glabe, J. Busciglio, A role for synaptic zinc in activity-dependent Abeta oligomer formation and accumulation at excitatory synapses, *J. Neurosci.* 2009, *29*, 4004.

[16] A. I. Bush, R. E. Tanzi, Therapeutics for Alzheimer's disease based on the metal hypothesis, *Neurotherapeutics* 2008, *5*, 421.

[17] C. Koppenal, A. E. Finefrock, A. I. Bush, P. M. Doraiswamy, Copper, iron and zinc as therapeutic targets in Alzheimer's disease, *Res. Pract. Alzheimer's Dis.* 2004, *9*, 250.

[18] E. F. Aziz, W. Eberhardt, S. Eisebitt, Effect of cysteine vs. histidine on the electronic structure of Zn2+ upon complex formation, *Z. Phys. Chem. (Muenchen, Ger.)* 2008, *222*, 727.

[19] E. Gaggelli, A. Janicka-Klos, E. Jankowska, H. Kozlowski, C. Migliorini, E. Molteni, D. Valensin, G. Valensin, E. Wieczerzak, NMR Studies of the Zn^{2+} Interactions with Rat and Human beta -Amyloid (1.28) Peptides in Water-Micelle Environment, *J. Phys. Chem. B* 2008, *112*, 100.

[20] S. Zirah, S. A. Kozin, A. K. Mazur, A. Blond, M. Cheminant, I. Segalas-Milazzo, P. Debey, S. Rebuffat, Structural Changes of Region 1.16 of the Alzheimer Disease Amyloid beta -Peptide upon Zinc Binding and in Vitro Aging, *J. Biol. Chem.* 2006, *281*, 2151.

[21] Y. Mekmouche, Y. Coppel, K. Hochgrafe, L. Guilloreau, C. Talmard, H. Mazarguil, P. Faller, Characterization of the ZnII binding to the peptide amyloid-beta 1.16 linked to Alzheimer's disease, *ChemBioChem.* 2005, *6*, 1663.

[22] V. Minicozzi, F. Stellato, M. Comai, M. Dalla Serra, C. Potrich, W. Meyer-Klaucke, S. Morante, Identifying the Minimal Copper- and Zinc-binding Site Sequence in Amyloid-beta Peptides, *J. Biol. Chem.* 2008, *283*, 10784.

[23] C. C. Curtain, F. Ali, I. Volitakis, R. A. Cherny, R. S. Norton, K. Beyreuther, C. J. Barrow, C. L. Masters, A. I. Bush, K. J. Barnham, Alzheimer's disease amyloid-beta binds copper and zinc to generate an allosterically ordered membrane-penetrating structure containing superoxide dismutase-like subunits, *J. Biol. Chem.* 2001, *276*, 20466.

[24] C. D. Syme, R. C. Nadal, S. E. J. Rigby, J. H. Viles, Copper Binding to the Amyloid-beta (Abeta) Peptide Associated with Alzheimer's Disease: Folding, coordination Geometry, pH Dependence, Stoichiometry, and Affinity of Abeta - (1.28): Insights from a Range of Complementary Spectroscopic Techniques, *J. Biol. Chem.* 2004, *279*, 18169.

[25] S. C. Drew, C. L. Masters, K. J. Barnham, Alanine-2 Carbonyl is an Oxygen Ligand in Cu2+ Coordination of Alzheimer's Disease Amyloid-beta Peptide - Relevance to N-Terminally Truncated Forms, *J. Am. Chem. Soc.* 2009, *131*, 8760.

[26] L. Hou, M. G. Zagorski, NMR Reveals Anomalous Copper(II) Binding to the Amyloid Abeta Peptide of Alzheimer's Disease, *J. Am. Chem. Soc.* 2006, *128*, 9260.

[27] J. Sarell Claire, D. Syme Christopher, E. J. Rigby Stephen, H. Viles John, Copper(II) binding to amyloid-beta fibrils of Alzheimer's disease reveals a picomolar affinity: stoichiometry and coordination geometry are independent of Aβ oligomeric form, *Biochem.* 2009, *48*, 4388.

[28] V. A. Streltsov, S. J. Titmuss, V. C. Epa, K. J. Barnham, C. L. Masters, J. N. Varghese, The structure of the amyloid-beta peptide high-affinity copper II binding site in Alzheimer disease, *Biophys. J.* 2008, *95*, 3447.

[29] Q.-F. Ma, J. Hu, W.-H. Wu, H.-D. Liu, J.-T. Du, Y. Fu, Y.-W. Wu, P. Lei, Y.-F. Zhao, Y.-M. Li, Characterization of copper binding to the peptide amyloid-beta (1.16) associated with Alzheimer's disease, *Biopolymers* 2006, *83*, 20.

[30] K. A. Connors, *Binding Constants: The Measurements of Molecular Complex Stability*, 1987.

[31] P. Deschamps, P. P. Kulkarni, B. Sarkar, X-ray Structure of Physiological Copper(II)-Bis(L-histidinato) Complex, *Inorg. Chem.* 2004, *43*, 3338.

3. METAL ION BINDING STUDIES OF PEPTIDE MIMETICS AND AMINO ACIDS

3.1 METAL ION BINDING STUDIES OF CARNOSINE AND HISTIDINE : BIOLOGICALLY RELEVANT ANTIOXIDANTS.

3.1.1 Introduction. Age-related diseases including Parkinson disease and Alzheimer's disease are characteristically associated with transition metal ion catalyzed oxidative damage to lipids, proteins and nucleic acids. Transition metal ion catalyzed lipid peroxidation, through Fenton reactions, leads to the formation of a variety of toxic byproducts such as *trans*-4.hydroxy-2.nonenal (HNE) and trans-4.oxo-2.nonenal (ONE).[32-34] The latter toxicants can potentially deplete intracellular levels of glutathione and related cellular antioxidants. Biologically interesting antioxidants based on histidine and its derived dipepides, and related analogues, play a major role in chelating transition metal ions (Figure 3.1).[35-37]

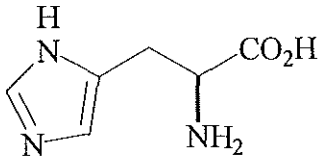

Histidine

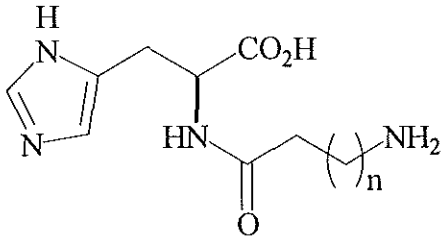

Carnosine (n = 1)
Homocarnosine (n = 2)

Figure 3.1. Structures of Histidine and carnosine.

Further, they can exert their antioxidant properties through reaction with secondary toxicants such a HNE and acrolein, thus attenuating their deleterious activities. Histidine and its derivatives, in particular, carnosine (β-alanyl-L-histidine), is also postulated to be effective in trapping the Fenton reaction derived reactive oxygen species (ROS). Carnosine is also known to be antiglycating agent as it can trap the advanced glycation end products (AGEs) resulting from the Maillard reactions of protein amino groups with reactive carbonyl compounds.[38-40]

Histidine-derived naturally occurring antioxidants such as carnosine and its analogues, anserine and carcinine are known to be a superior *in vivo* antioxidant as compared to histidine, although the precise mechanism of its antioxidant activity remains to be established.[41-48] The antioxidants effects of histidine and its derivatives may be ascribed to 1) transition metal ion chelation, 2) trapping of ROS, 3) through reaction with cellular toxicants such as HNE, and suppressing the formation of AGEs.[39, 49] Chelation of transition metal ions also helps in attenuating the production of ROS. It would thus be interesting to explore whether, indeed, transition metal ion chelation play a major role in the antioxidant properties of histidine and its derived peptides. The binding constants of amino acids and peptides are dependent on the pH values of their corresponding solutions. There have been reports of the binding constants of histidine and carnosine, although a close comparison for these two compounds could not be achieved as they are measured under varied experimental conditions.[35-37, 42] With that goal, we have now estimated the comparative binding constants of Cu(II) ions by histidine and carnosine at close to physiological pH range under similar experimental conditions.

3.1.2 Results and Discussion. We have measured the binding constants of histidine and carnosine with Cu(II) ions in order to determine their relative metal ion chelating abilities in aqueous solutions maintained at pH 7.84 ± 0.18, which is in the range of biological pH. We have adopted the continuous variation method, as described by Karikari and coworkers, for the measurement of binding constants.[50-51] The relative volumes of the Cu(II) solution and the antioxidants are shown in (Table 3.1).

Table 3.1. Relative volumes of the stock solutions of Cu^{2+} and antioxidants, and the resulting absorbances in the continuous variation method.

Volume (mL) of Cu(II) solution (2.00 x 10^{-2} M)	Volume (mL) of His/ Carnosine solutions. (2.00 x 10^{-2} M)	Absorbance (carnosine/ Cu^{2+} at 800 nm)	Absorbance (histidine/ Cu^{2+} at 810 nm)
2.5	0	0.261	0.234
2	0.5	0.232	0.218
1.5	1	0.197	0.210
1	1.5	0.147	0.161
0.5	2	0.062	0.093
0	2.5	0.001	0.004

Thus the total volume of each of the solutions is kept constant at 2.5 mL, and the sum of the moles of the Cu(II) and the antioxidant for each of these solutions was also constant (5 x 10^{-5} moles), as required for the continuous variation method. The absorption at 800 nm, for the Cu(II) species, was shifted to lower wavelengths upon successive additions of the aliquots of the antioxidants, histidine and carnosine. The absorption maxima for the complexed species were observed between 350 to 1000 nm (Figure 3.2 and 3.3).

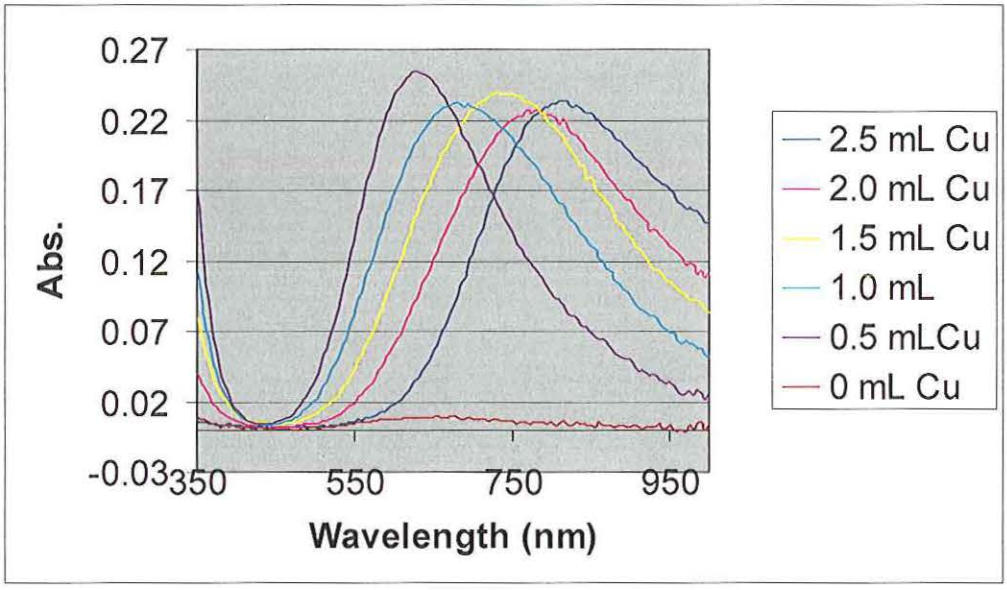

Figure 3.2. UV/vis absorbance of L-Histidine-Cu(II) complex

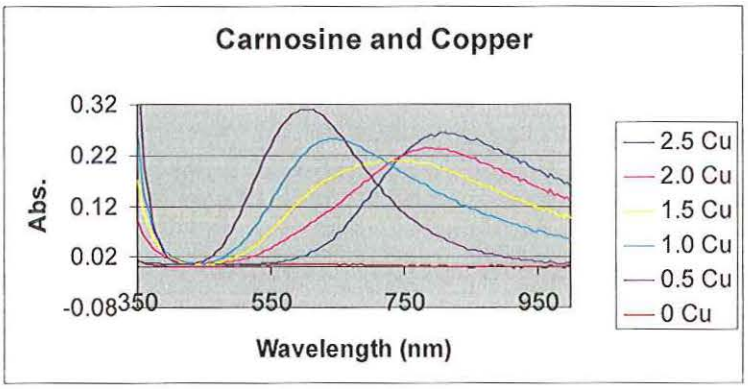

Figure 3.3. UV/vis absorbance of L-Carnosine-Cu(II) complex

The absorbances at a fixed wavelength (800 nm in case of carnosine and 810 nm in case of histidine) were then recorded at different mole fractions (represented as X in Figures 3.4 and 3.5) of Cu(II), and the changes in absorbance of the Cu(II) ion complexes as compared to the uncomplexed Cu(II) species were calculated from these spectra.

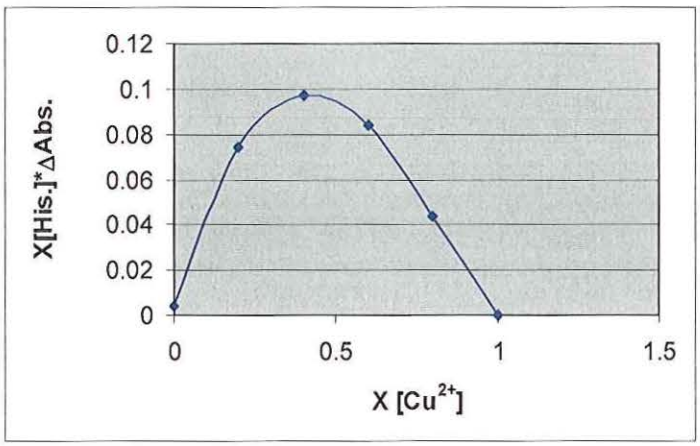

Figure 3.4. Job's plot for L-Histidine-Cu(II) complex

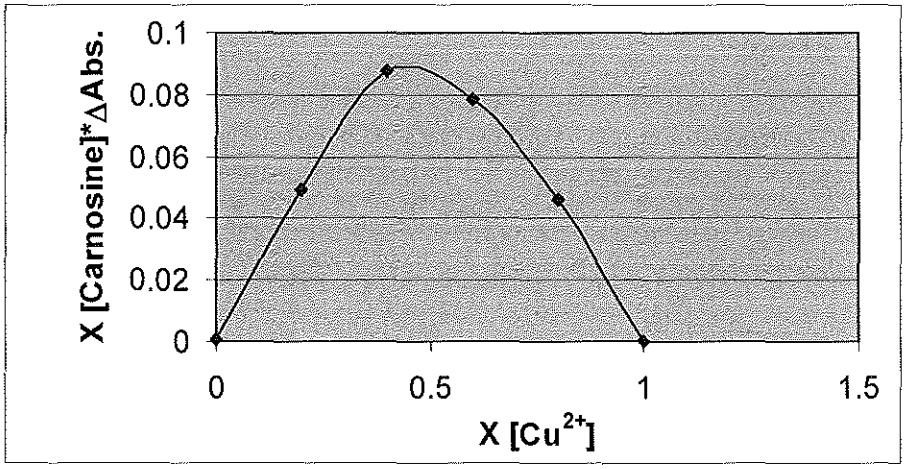

Figure 3.5. Job's plot for L-Carnosine-Cu(II) complex

From this data, JOB's plots were constructed which showed a 1:1 complexation of Cu(II) for both histidine and carnosine. Thus, the plots involving Cu(II) mole fraction versus the change in absorbance multiplied by the mole fraction of the substrates showed parabolic curves in both cases.[50] These plots show a maximum at 0.5 mole fraction of Cu(II) indicating their 1:1 complex formation with Cu(II) ions (Figures 3. 4 and 3. 5).

The binding constants (K_a) were estimated from the UV/vis spectral data using Benesi-Hildebrand plots, involving plots of the inverse of Cu(II) chloride concentrations against the inverse of changes in their respective absorbances ($1/\Delta A$ vs $1/[Cu^{2+}]$) (Figure 3.6 and 3.7).[50] The following equation (1) was used to calculate the binding constants from these plots:

$$\frac{1}{\Delta A} = \frac{1}{K_a \Delta A[Cu]} + \frac{1}{\Delta A} \qquad (1)$$

Where $\frac{1}{K_a \Delta A}$ is the slope obtained from the Benesi-Hildebrand graph and $\frac{1}{\Delta A}$ is the y-intercept. The binding constants of histidine and carnosine using the above procedure were found to be 71.14 M^{-1} and 1.1 M^{-1}, respectively.

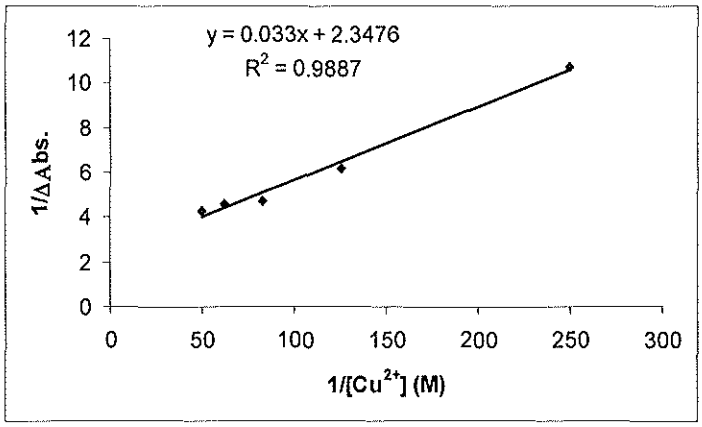

Figure 3.6. Benesi-Hildebrand plot for L-Histidine-Cu(II) complex

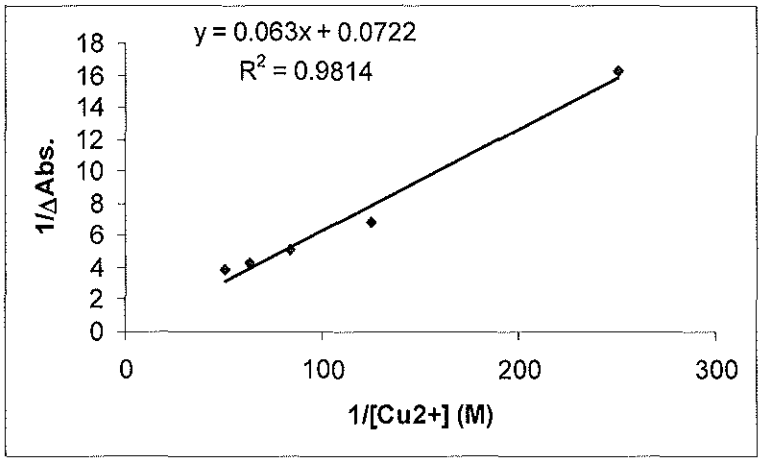

Figure 3.7. Benesi-Hildebrand plot for L-Carnosine-Cu(II) complex

At first glance it is intriguing that the Cu(II) ion binding constant of carnosine is remarkably smaller than that of histidine. If metal ion chelation is the major factor in the antioxidant effect of carnosine, we would have expected to obtain its superior Cu(II) binding constant as compared to that of histidine. However, there are other mechanisms of antioxidant effects, which include the sequestering of ROS, and removal of intracellularly formed lipid-peroxidation derived toxicants such as HNE and acrolein.[39] Products derived from the latter reaction pathway for histidine and carnosine have been characterized by electrospray ionization mass spectroscopic techniques.[32, 52-53] It was also suggested that among other mechanisms, carnosine may play an important role in suppressing Alzheimer's disease through its ability to react with protein carbonyls and by suppressing the reactivity of glycated proteins.[40] In accordance with our interpretation, recently, Rizzarelli and coworkers have shown that Cu(II) complexes of homocarnosine are good scavengers of hydroxyl radicals, yet the complexation of Cu(II) is not detrimental to the superior hydroxyl radical scavenging properties of uncomplexed homocarnosine by itself.[54]

In conclusion, we have shown that carnosine has a relatively lower binding constant with Cu(II) ions as compared to that of histidine, which implies that the superior antioxidant properties of carnosine may be attributed to other factors such as its efficient trapping of ROS and sequestration of lipid-peroxide derived toxicants such as HNE. However, transition metal ion chelation may be partly responsible for the antioxidant behavior of histidine and its derivatives as they have significant metal ion binding constants. Further experiments on the effect of pH and structural modifications of

carnosine/histidine on the transition metal ion binding are currently in progress in our laboratory.

3.1.3 Experimental Sections. *Reagents and stock solutions:* L-Histidine (>98%) and $CuCl_2 \cdot 2H_2O$were obtained fromAlfa, and l-carnosine (>99%) was obtained from Sigma Chemicals, and were used as received. A stock solution of the Cu(II) chloride solution (2.00×10^{-2} M) was prepared by dissolving $CuCl_2 \cdot H_2O$ (0.178 g) in distilledwater (50 mL),immediately prior to use. The 2.00×10^{-2}M stock solutions of L-histidine (0.155 g in 50mL H2O; pH 7.71) and L-carnosine (0.225 g in 50mL H_2O; pH 7.97) were prepared immediately prior to use.

Instrumentation: A Cary-50 UV/vis spectrophotometer equipped with a 1cm path-length cell was used for the measurement of binding studies, and the spectra were recorded in the range of 350–1000 nm. The micropipettes used were capable of delivering 1mL solutions, having adjustable ranges between 100 and 1000 μL.

General methods for the determination of binding constants and stoichiometry of complexation: A continuous variation method (or Job's method) was employed for the investigations of the stoichiometry of the L-histidine– Cu(II) complex. Aliquots were successively added to the cuvette accordingly as shown in Table 1. The successive UV/vis spectra are recorded from 350 to 1000 nm, and sample solutions showed UV/vis absorbance in the range of 0.02–0.30. The molar ratios of the two components were varied, while maintaining the total volume in the cuvette at 2.5 mL. The UV/vis peaks were shifted to lower wavelength regions, upon successive additions of the aliquots of histidine or carnosine solutions. Changes in the relative absorption for each successive

addition of the histidine or carnosine multiplied by their respective mole fractions were plotted against the mole fraction of the Cu(II) chloride. These Job's plot resulted in parabolic curves which show a maximum at 0.5 mol fraction of Cu(II) chloride indicating 1:1 complex formation in both cases.

3.2 SYNTHESIS OF CYCLOPROPYL CONTAINING PEPTIDE MIMETICS

A variety of natural and synthetic cyclopropane containing compounds is known to possess biological activity ranging from enzyme inhibitors, insecticides, antimicrobial, antibacterial, antitumor to antiviral properties.[55-63] The biological activity of these compounds can be attributed to unique reactivity due to unusual bonding and inherent strain (27.5 kcal/mol), lipophilicity, and conformational restriction.[64] As a rigid yet chemically relatively stable structural unit, cyclopropane is smaller than isopropyl and less sterically demanding than germinal dimethyl. Because of these characteristics, cyclopropyl is being taken into consideration more and more in designing new pharmaceuticals. The introduction of a cyclopropyl or its replacement of an alicyclic chain or a larger alicyclic ring often showed beneficial effect to the bioactivity of the original targets. We have synthesized histidine derived cyclopropyl containing peptide mimetics (1.2) (Figure 3.8) and they were characterized using single X-ray crystallography and Nuclear magnetic resonance spectroscopy. Metal ion binding efficiencies of compounds 1 and 2 were estimated based on the chemical shift changes on addition of copper (II) to a solution of these compounds in deuterated methanol.

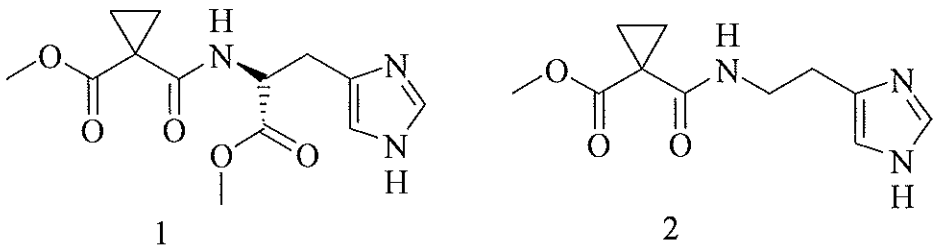

1 2

Figure 3.8 Structures of synthesized cyclopropyl derive peptide mimetics

3.2.1 Synthesis and Characterization. 1,2 deactivated cyclopropanes are generally prepared by the condensation reaction of 1,2.dihaloethane and dialkylmalonate using a base. Diethyl cyclopropane-1,1.dicarboxylate was first prepared by Perkin and coworkers by heating diethyl malonate and 1,2.dibromoethane in the presence of sodium ethoxide for 20h. The yield was only 29%. The disadvantage of this reaction is the separation of unreacted starting material dimethyl malonate and 1,2.dibromoethane from the product by distillation. Later on the reaction conditions were varied by researchers to get better yield.[65-74] All these reaction either gave poor yield or involved harsh reaction conditions.[69] For example, using 1, 2.dichloroethane, as an alternative to 1, 2.dibromoethane, resulted in the 50% byproduct tetraethylbutane-1,1,4,4.tetracarboxylate, which is formed in a competing intermolecular reaction. Later on potassium carbonate/dimethylformamide (DMF) was used as base instead of the sodium ethoxide.[75] Carrying out the reaction at room temperature for 22h gave product in 28% yield.[71] Phase transfer alkylation using potassium carbonate as a base and a mixture of water and benzene as solvents significantly improved the yield to 85%.[66] The main disadvantages here were the longer reaction time (20 h) and high temperature

(80 °C).Use of benzene is no longer allowed due to its carcengenicity. Klaus-Dieter synthesized of 1,1-diactivated cyclopropane in 83% yield from 1,2-dichloroethane and dimethylmalonate by heating the reaction to 115 °C in DMF.[73] Recently there was a report on cycloalkylation reactions of active methylene compds. In the presence of readily available imidazolium salts (ionic liqs.) as a phase transfer catalysts to afford the dimethyl 1,1-cyclopropanedicarboxylate[70] in 94% yield.

Our attempts to synthesize the dimethyl 1,1.cyclopropanedicarboxylate following reported literature procedures resulted in poor yield. We modified the procedure to improve the yield and reduce the reaction time. Initially the 1, 2-dibromoethane was reacted with dimethylmalonate in the presence potassium carbonate/DMSO at room temperature for 24 hrs. The analysis of crude product by GC/MS showed 40% of unreacted dimethylmalonate and 1,2-dibromoethane. Distillation of the product at low pressure gave the pure product in 10% yield. The distillation was not very effective in separating the starting compound. Most of the distillate contained a mixture of starting compound and product.

Use of sodium hydroxide instead of potassium carbonate as a base, resulted in the dicarboxylic acid derivative of cyclopropyl compound in low yield. We studied the reaction in several solvents. The reaction was faster when DMSO was used as a solvent may due to the higher acidity of diethylmalonate in DMSO. We varied the reaction conditions for complete conversion of the starting compounds. Heating the reaction to 100 °C didnot afford a complete conversion even after 24 hrs.

Addition of phase transfer catalyst benzyltriethylammonium chloride to the same reaction mixture also resulted in low yield and due to incompletion of reaction. Longer

reaction time also didnot facilitate the completion of reaction. However, when the same reaction was carried out in an ultrasonic bath, it was completed in 3hrs, in the absence of a phase transfer catalyst (Scheme 3.1). This improvement of the reaction gave the product in very high yield after extraction (80%). This is a very efficient method for the synthesis of 1,1-diactivated cyclopropyl compounds in high yield at a relatively shorter reaction time and less harsh conditions.

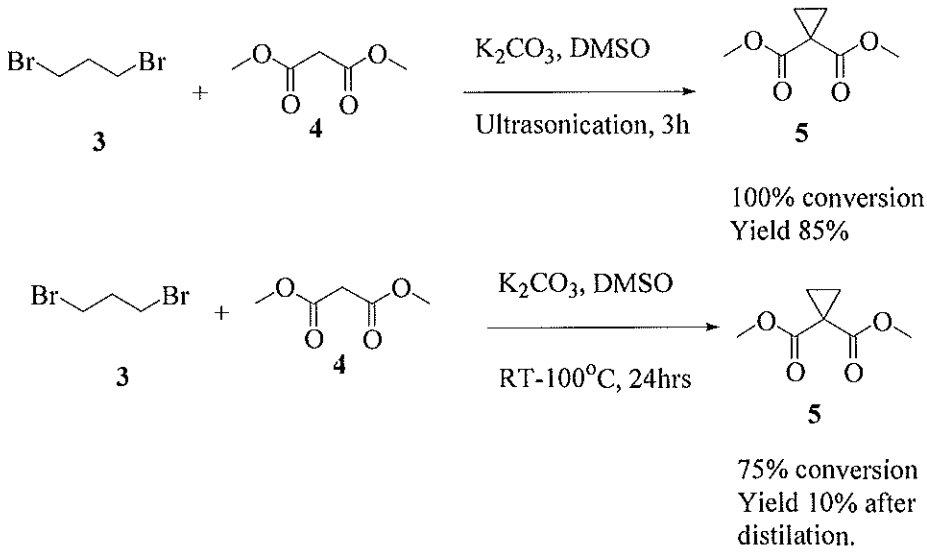

Scheme 3.1. Synthesis scheme for Dimethyl 1, 1-cyclopropanedicarboxylate.

The excess potassium carbonate and potassium bromide formed was simply filtered and washed with DMSO to remove any product sticking to the solid. Employment of DMSO as reaction solvent not only made the reaction faster, but also made the extraction easier. Extraction of the product from the reaction mixture was effected by freezing the reaction mixture to 0 °C. The DMSO (mp = 18.5 °C) solidifies at

0 °C. The product was extracted using ethyl ether at 0 °C. Any residual DMSO is removed by washing the ether solution with water. The product obtained was used without further purification for the next step. Selective saponification of one of the ester group was carried out by reacting stoichiometric amount of sodium hydroxide with Dimethyl 1, 1. cyclopropanedicarboxylate in methanol/water solution (Scheme 3.2).

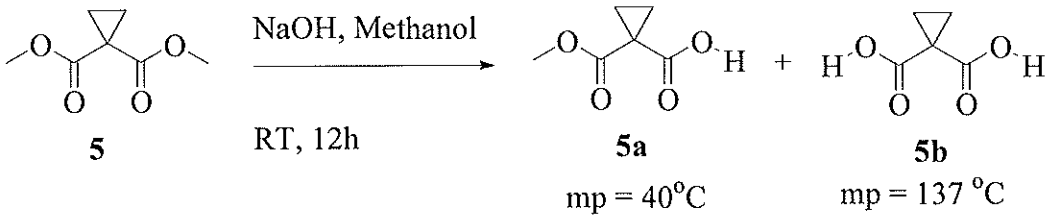

Scheme 3.2. Saponification reaction of Dimethyl 1, 1-cyclopropanedicarboxylate

The reaction yielded a 1:1 mixture of mono and dicarboxylic acid. These compounds were separated based on their solubility in dichloromethane. Monocarboxylic acid (5a) was readily soluble in dichloromethane, where as dicarboxylic acid was almost insoluble. The monocarboxylic acid has low melting point. It melted at 40 °C, where as dicarboxylic acid melted at 137 °C. The compound 5 obtained was used without purification for the next step. Compounds 1 and 2 were synthesized by coupling, compound 5a, with histidine or histamine using reported literature procedure (Scheme 3.3).[76]

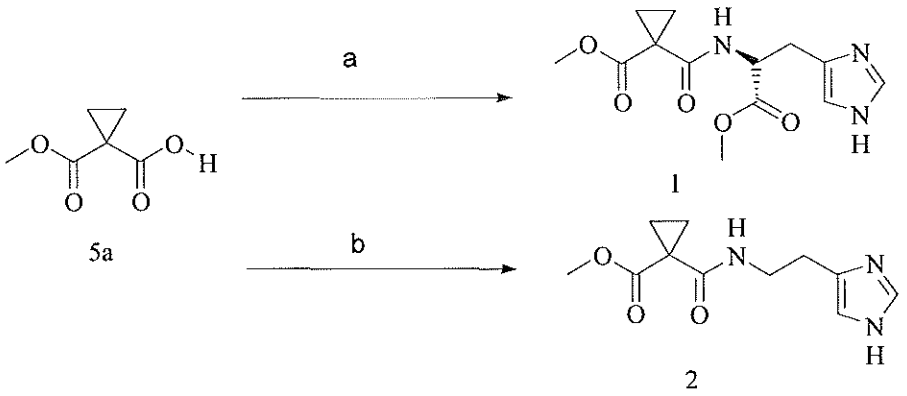

[a] Histidine/ EDCI/ dichloromethane/ water/ HOBt, triethylamine/; [b]Histamine/ EDCI/ dichloromethane/ water/ HOBt, triethylamine

Scheme 3.3. Synthesis scheme for cyclopropyl derived peptides.

The product obtained was extracted using ethyl acetate and purified by recrystalization from hot ethylacetate. The compounds were characterized using NMR spectroscopy and single X-ray crystallography. Compounds 1 and 2 readily gave X-ray quality crystal from hot ethyl acetate solution .The single crystal X-ray quality crystals were obtained by re-crystalization of the compounds 1 and 2 from hot ethylacetate solution.

Compound 1 crystallizes in $P2_12_12_1$ space group and compound 2 in $p2_1/c$. From the X-ray crystal structure the molecule 1 can complex to metal ions through ring nitrogen N1 and amide nitrogen N3 which will form a stable six membered ring. In the case of compound 2, it can bind to metal ions through O2 and N3 (Figure 3.9).

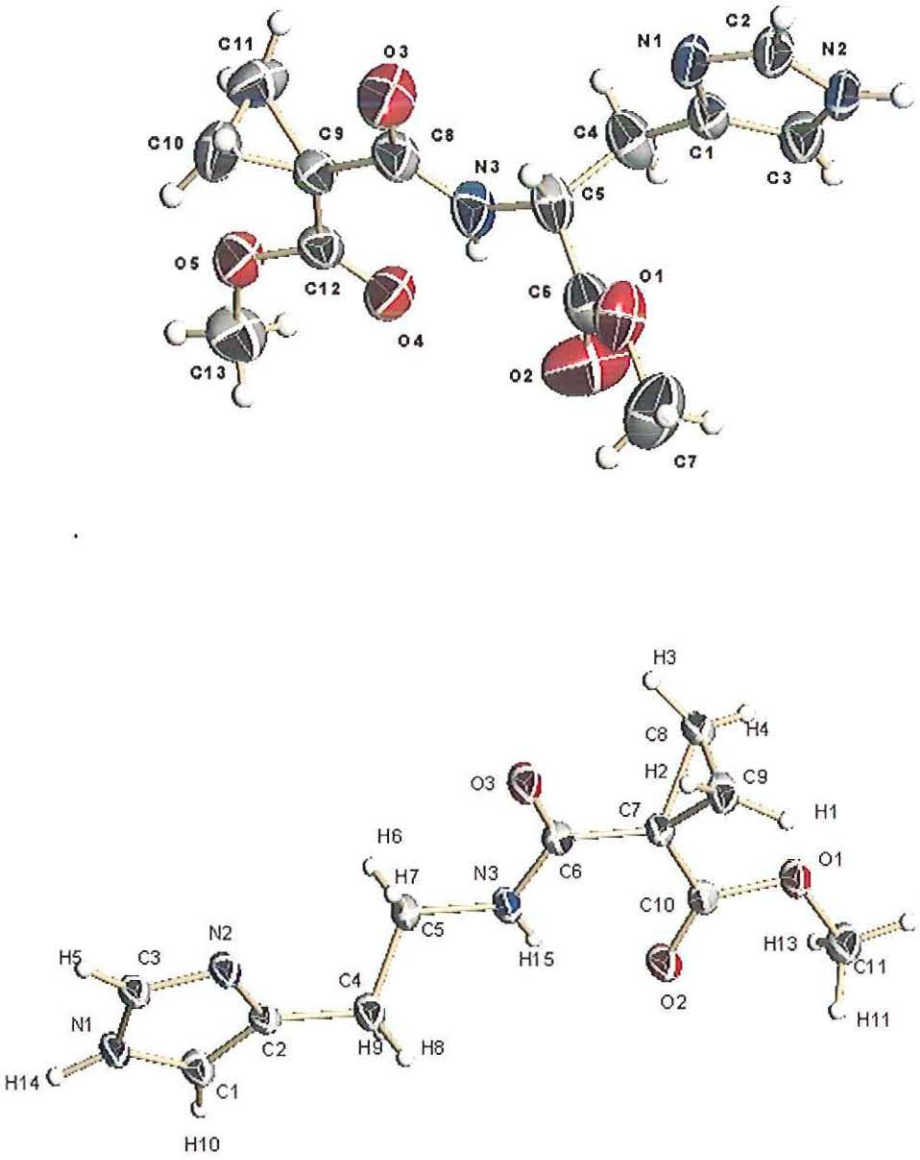

Figure 3.9. Single crystal X-ray structure of N-(α)-((1-mehoxycarbonyl)cyclopropylcarbonyl)histamine (2) (B) and N-(α)-((1-mehoxycarbonyl)cyclopropylcarbonyl)histidine (1) (A)

3.2.2 Metal Ion Binding Studies of Cyclopropyl-Derived Peptide Mimetics.

The metal ion binding efficiencies the compounds 1 and 2 were explored using ^{1}H NMR titration experiments. We selected Zn(II) for our studies, in order to avoid paramagnetic broadening of peaks , which is evident in the case of Cu(II) and Fe(III) metal ions. On addition of Zinc (II) nitrate to a solution of N-(α)-((1-mehoxycarbonyl)cyclopropylcarbonyl)histamine (or N-(α)-((1-Mehoxycarbonyl) cyclopropylcarbonyl) Histidine), the absorption at δ ^{1}H 7.5 corresponding to imidazole 2H and δ ^{1}H 6.7 corresponding to imidazole 5H shifted down filed and broadened (refer to Figure 3.10 for numbering) . The absorption at δ ^{1}H 7.5 was relatively most deshielded indicating strong binding of N-(α)-((1-mehoxycarbonyl)cyclopropylcarbonyl)histamine(N-(α)-((1-mehoxycarbonyl) cyclopropylcarbonyl)histidine) through imidazole N3.

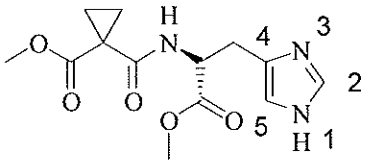

Figure 3.10. Structure of N-(α)-((1-mehoxycarbonyl)cyclopropylcarbonyl)histidine

When 0.2 equivalents of Zn^{2+} was added to the solution of N-(α)-((1-mehoxycarbonyl)cyclopropylcarbonyl)histamine, the peaks at δ 7.5 and δ 6.7 was shifted to δ 7.9 and δ 6.9. The peak at δ 2.76 corresponding to C6H was also broadened and

shifted downfield slightly (Figure 3.11 and Figure 3.12), indicating its proximity to binding site.

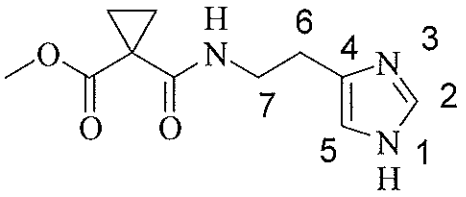

Figure 3.11. Structure of N-(α)-((1-mehoxycarbonyl)cyclopropylcarbonyl)histamine

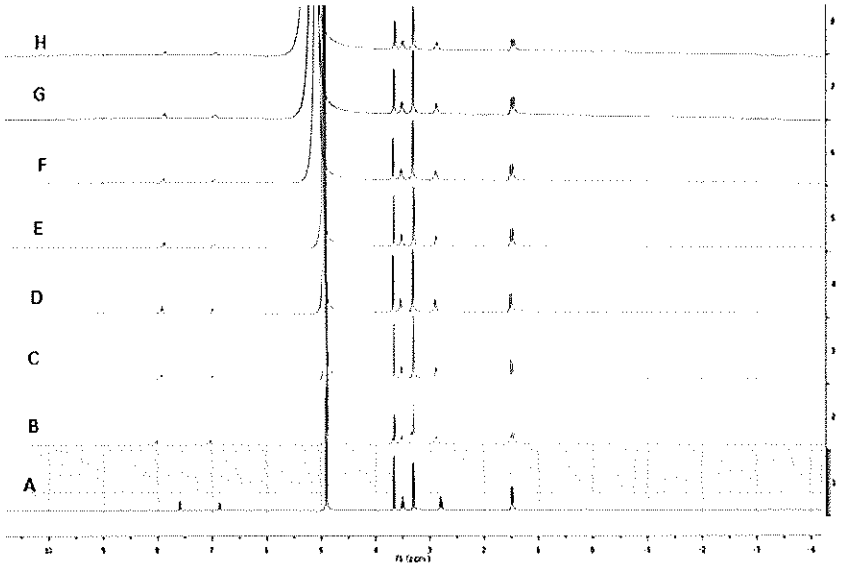

Figure 3.12. ^{1}H NMR titration of N-(α)-((1-mehoxycarbonyl)cyclopropylcarbonyl)histamine (N-(α)-((1-mehoxycarbonyl)cyclopropylcarbonyl)histamine) with Zn(II) in Methanol-*d*. Spectrum A is for N-(α)-((1-mehoxycarbonyl)cyclopropylcarbonyl)histamine in Methanol-*d* solution; spectra B-H are for incremental additions of Zn(II) to solution of 5 b (A). In each of these later solutions the [Zn(II)]/ [N-(α)-((1-mehoxycarbonyl)cyclopropylcarbonyl)histamine] ratios are as follows; B, 0.2; C, 0.4; D, 0.6; E, 1; F,2, G,4, H, 5

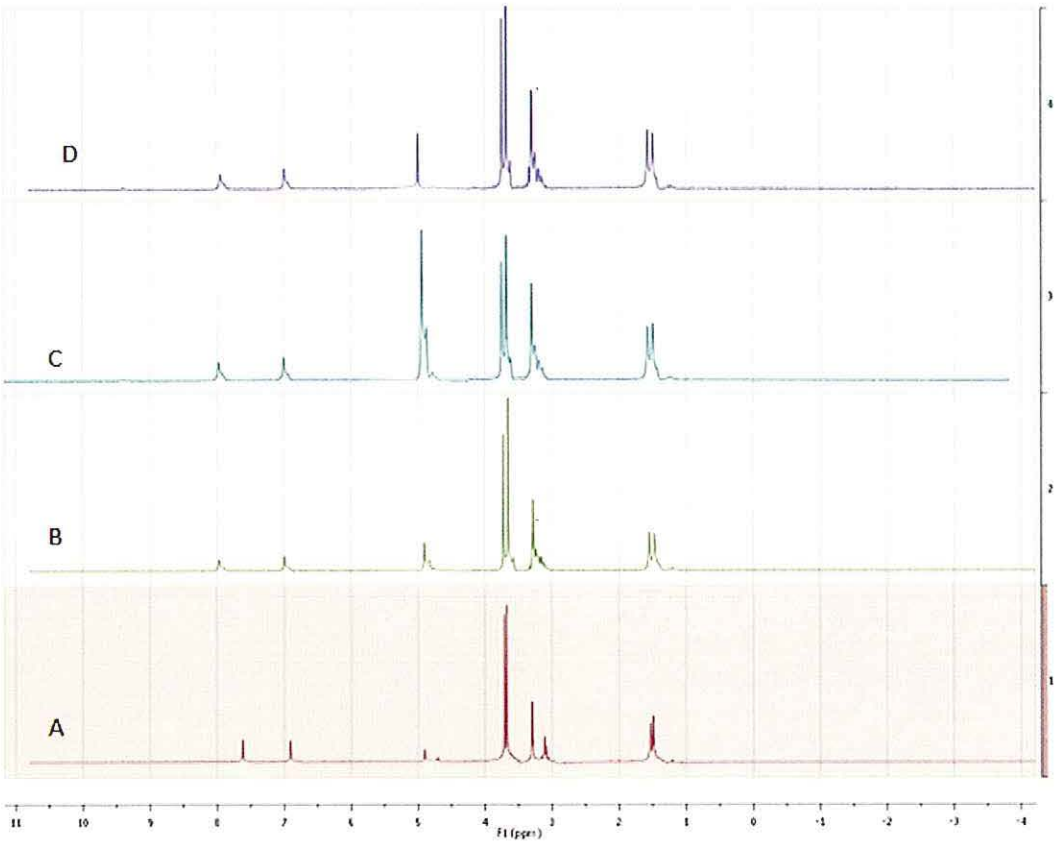

Figure 3.13. ^{1}H NMR titration of N-(α)-((1-mehoxycarbonyl)cyclopropylcarbonyl)histidine (N-(α)-((1-mehoxycarbonyl)cyclopropylcarbonyl)histidine) with Zn(II) in Methanol-*d*. Spectrum A is for N-(α)-((1-mehoxycarbonyl)cyclopropylcarbonyl)histidine in Methanol-*d* solution; spectra B-D are for incremental additions of Zn(II) to solution of N-(α)-((1-mehoxycarbonyl)cyclopropylcarbonyl)histidine (A). In each of these later solutions the [Zn(II)]/ [N-(α)-((1-mehoxycarbonyl)cyclopropylcarbonyl) histidine ratios are as follows; B, 0.2; C, 0.5; D, 2.

C7 H and cyclopropyl hydrogens are also broadened, but their chemical shift changes were negligible. There was no further change in chemical shift on increasing addition of Zinc (II) (up to 5 equivalents). Similarly on addition of 0.2 equivalents of Zn (II) solution to N-(α)-((1-mehoxycarbonyl)cyclopropylcarbonyl)histidine the peaks at δ 7.5 and δ 6.7 was shifted to δ 7.9 and δ 6.9 almost to the same extent as that of N-(α)-((1-mehoxycarbonyl) cyclopropylcarbonyl)histamine. Also the peak at 4.5 was shifted downfield and broadened further confirming the main binding site as N3.Further increase in concentration of zinc nitrate (up to 2 equivalents), gave no chemical shift variations. These results may indicate that compound 1 and 2 bind to metal ions at lower concentration and higher concentration of the salt reduced the binding affinity.

3.2.3 Conclusion. Cyclopropyl-derived peptide mimetics (1 and 2) were synthesized and characterized by NMR and single crystal X-ray crystallography.^{1}H NMR titrations of these compounds with Zn(II) ions show that at low concentration, they bind to metal ions and their main metal ion binding centre is N3 imidazole.

3.2.4 Experimental Section. *Materials and methods.* 1,2.dibromoethane (>98%), dimethylmalonate (>98%), Zinc (II) nitrate hexahydrate (>98% pure), potassium carbonate (anhydrous powder, >99.99% , dimethyl sulfoxide (Acs reagent, 99.99%), sodium hydroxide (Acs reagent, pellets, >99.99%), Methanol (Acs reagent , 99.8%), N-(3.Dimethylaminopropyl)-N′-ethylcarbodiimide hydrochloride (crystalline), 1.hydroxybenzotriazole hydrate (purum, >97%), Dichloromethane (Acs reagent , 99.5%) and Triethylamine (>99%) were obtained from sigma Aldrich and used as received.

Methanol-*d* (Cambridge Isotope laborotories, Inc.) used in NMR experiments had an isotopic purity of >99.9%. ^{1}H NMR spectra (at 399.7MHz) were obtained on a Varian Inova 400 MHz spectrometer in methanol-*d* solutions at 25 °C (Figure 3.14 to Figure 3.18).

NMR Titrations. A series of solutions of Zinc(II) nitrate incompouns 1(2) were prepared by adding appropriate amounts of $Zn(NO_3)_2$ hexahydrate (0 to 200 mM in methanol-*d*) to N-(α)-((1-mehoxycarbonyl)cyclopropylcarbonyl)histidine (42 mM methanol-d) so that the resulting solutions had [N-(α)-((1-mehoxycarbonyl)cyclopropylcarbonyl)histidine]/Zn^{2+} mol ratio varying from 1:0 to 1:5. Each of these solutions was transferred into 5 mm NMR tubes. The ^{1}H NMR spectra of these solutions were recorded at 400 MHz at 25 °C . The metal ion binding efficiencies of these compounds were determined from the chemical shift changes and peak broadening.

3.2.4.1 Synthesis procedure: *Synthesis of Cyclopropane-1,1-dicarboxylic acid dimethyl ester (3)*: To Dimethyl malonate 1(10.5g, 79.5 mmol) in DMSO (25mL) added K_2CO_3 (21.9g, 158.6mmol) and 1, 2.dibromoethane 2(15g, 187.86) respectively. Reaction was then heated in ultrasonic bath 3 h. Completion of reaction was checked by GC/MS.The reaction mixture was filtered and precipitate was washed with ether (100ML) to remove solid potassium carbonate and potassium bromide .The filtrate was frozen to 0 °C. The solid DMSO formed was removed by decanting the liquid at 0 °C. The melting point of the DMSO is 18.5 °C. The ether layer was washed with water was dried over anhydrous sodium sulfite. Concentration of ether solution in rotary evaporator

and high vacuum gave the product as a clear liquid (80%, 10g). EI/MS, 157, 127, 95, 68; ^{1}H δ $CDCl_3$: 3.7 (bs, 6H) 1.3 (bs, 4H) ; ^{13}C δ $CDCl_3$: 171.1, 52.8 (q, J_{C-H} = 146 Hz), 28.6 , 16.3 (t, J_{C-H} = 171 Hz)

Synthesis of Cyclopropane-1,1.dicarboxylic acid methyl ester (5a): To Dimethyl 1,1-cyclopropanedicarboxylate (7.2g, 45 mmol) dissolved in methanol (10 mL) , sodium hydroxide (1.82g, 45 mmol)dissolved in 10 mL of water was added at 0 °C slowly .The reaction was stirred at room temperature for 12hrs and completion of reaction was checked with GC/MS. The reaction mixture was washed with pentane at a pH of 7 to remove any starting material and excess methanol was removed under high pressure. The concentrated solution is acidified to pH 3 and transferred in to separatory funnel and extracted with ethyl acetate. Ethyl acetate solution is concentrated to obtain a 1:1 ratio of mono and dicarboxylic acid as crystalline solids, which melts at room temperature as shown by NMR. Two compounds were separated based on difference in solubility in dichloromethane. Compound 5a is extracted from the mixture by repeatedly washing with dichloromethane. Compound 5b was left as a solid. The dichloromethane solution was filtered and filtrate is concentrated and refrigerated to obtain 5a as crystalline solid (mp 40 °C). Total Yield was 88%.; ^{1}H δ methanol *–d*: 3.6 (bs,3H) 1.7–1.6 (m, 4H) ; ^{13}C δ methanol –d: 174.5, 171.7, 53.0 (quartet, J = 147 Hz), 25.6, 20.6 (t, J= 169 Hz); The solid left after washing with dichloromethane was dried to obtain 5b (mp 137 °C) . ^{1}H δ methanol –d: 1.4(bs, 4H); ^{13}C δ methanol –d:177, 25.7, 20.8 (t, J = 169 Hz).

Procedure A: Synthesis of N-(α)-((1-Mehoxycarbonyl) cyclopropylcarbonyl)histidine (1). In an RB flask, compound 4(1.0 g, 6.8 mmol), Histidine methylester dihydrochloride (1.6g, 6.8 mmol), N-methylmorpholin(2.0g, 20.4

mmol), EDC hydrochloride (1.3g, 6.8 mmol), and 1.hydroxytriazole (1.1g, 6.8 mmol) were dissolved in dichloromethane/water (5mL/5mL) solution and stirred for 12 hrs. The reaction mixture was extracted with dichloromethane and washed with water. The dichloromethane solution was dried using $MgSO_4$ and concentrated in a rotary evaporator to obtain compound 1 as white precipitate. Solid obtained was purified by recrystalization form hot ethyl acetate solution. Yield 15%. Decomposed on heating to 200 °C; ^{1}H NMR (400 MHz, Methanol-d) δ 7.45 (s, 1H), 6.75 (s, 1H), 4.55 (dd, 2H, J = 15Hz), 3.55 (s, 3H), 2.95 (m, 1H), 1.35 (m, 4H); ^{13}C NMR (100 MHz, $CDCl_3$) δ 173.5, 171.8, 169.0, 135.7, 133.4, 117.2, 53.0, 52.2, 29.9, 26.4, 20.4.

Synthesis of N-(α)-((1-Mehoxycarbonyl) cyclopropylcarbonyl)histamine (2): The compound 2 was synthesized following the procedure A. White crystalline solid (yield 20%); mp = 130 °C, ^{1}H NMR (400 MHz, Methanol-*d*) δ 7.56(s, 1H), 6.86(s, 1H), 3.64(s, 3H), 3.47(t, 2H, J = 8Hz) 2.76(t, 2H, J= 8Hz), 1.46 (m, 4H) ; ^{13}C NMR (100 MHz, Methanol-*d*) δ 174.2, 170.5, 136.1, 117.7, 52.8, 40.6, 27.7, 27.6, 19.0.

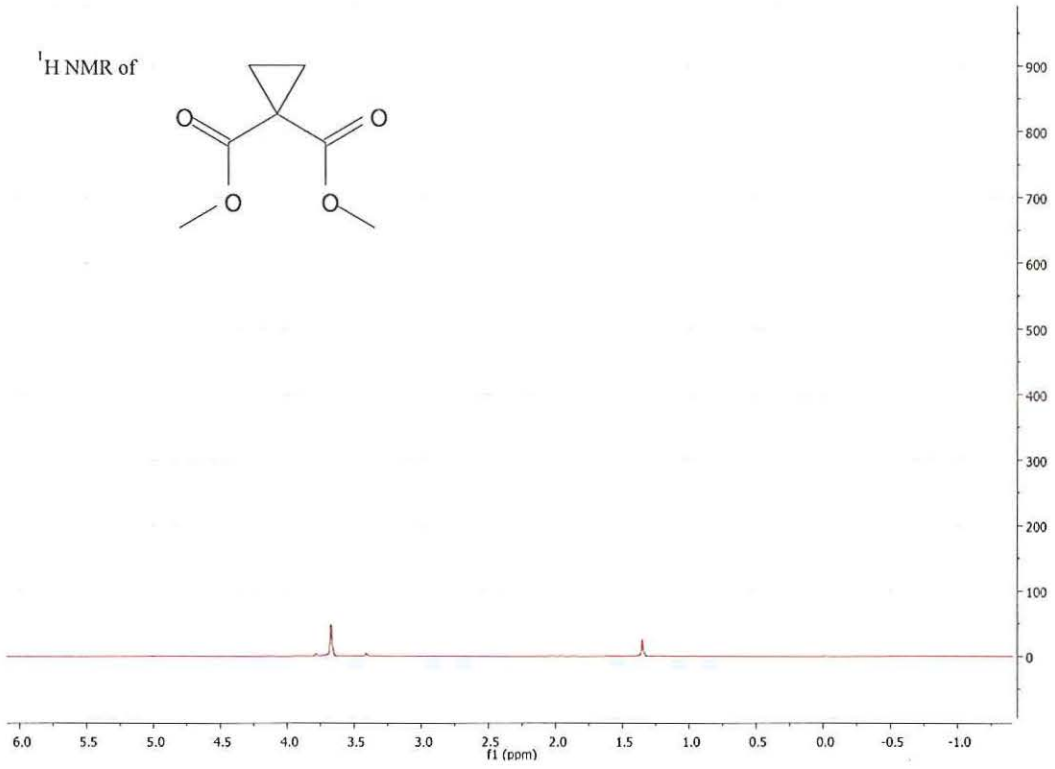

Figure 3.14 ^{1}H NMR (400MHz) spectrum of Dimethyl 1,1.cyclopropanedicarboxylate (5a)

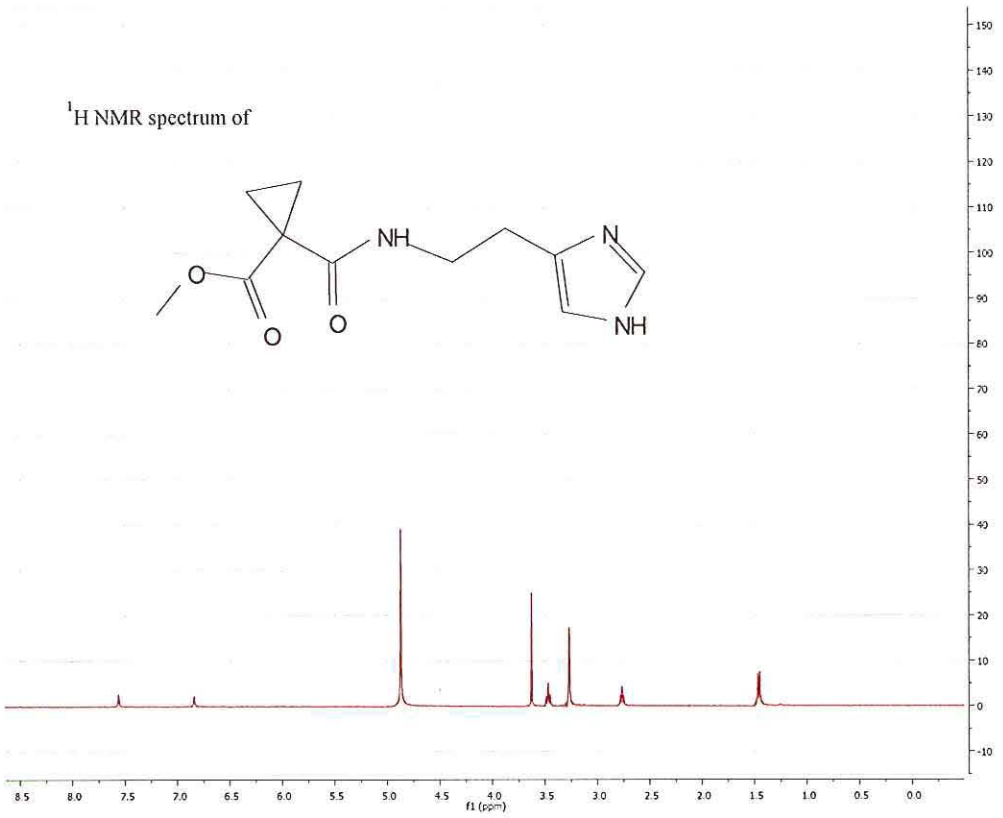

Figure 3.15. ^{1}H NMR (400MHz) spectrum of N-(α)-((1-mehoxycarbonyl)cyclopropylcarbonyl)histamine

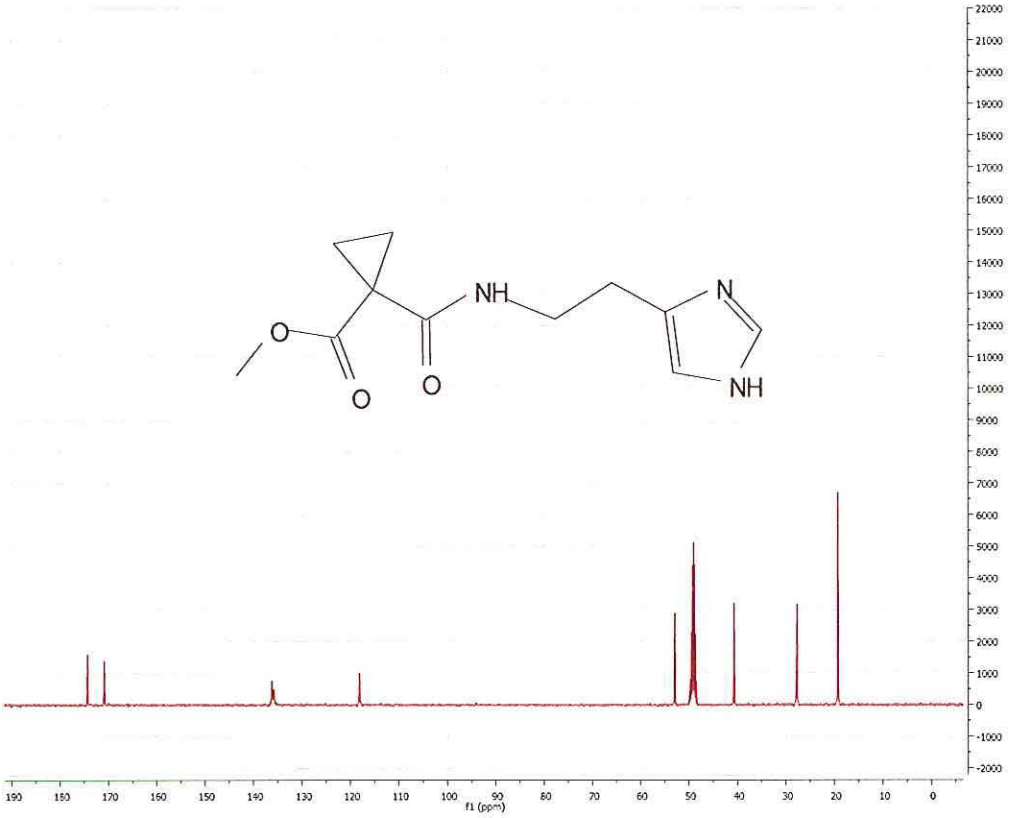

Figure 3.16. ^{13}C (100MHz) NMR spectrum of N-(α)-((1-mehoxycarbonyl)cyclopropylcarbonyl)histamine.

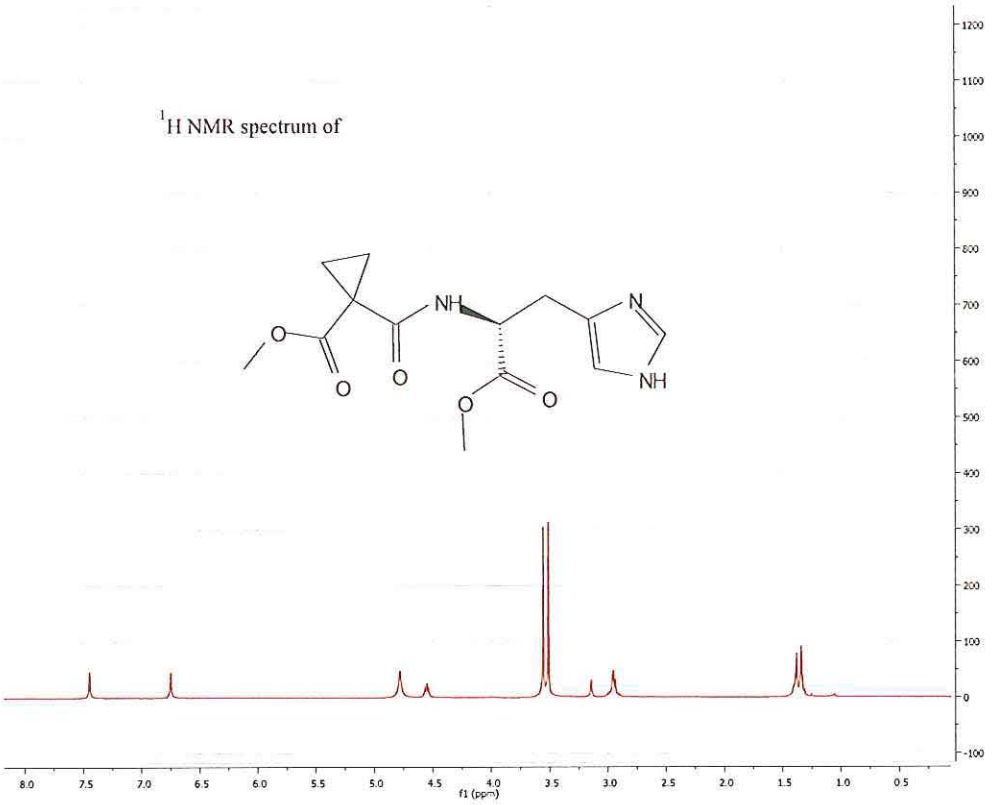

Figure 3.17. ^{1}H (400 MHz) NMR spectrum of N-(α)-((1-mehoxycarbonyl) cyclopropylcarbonyl)histidine

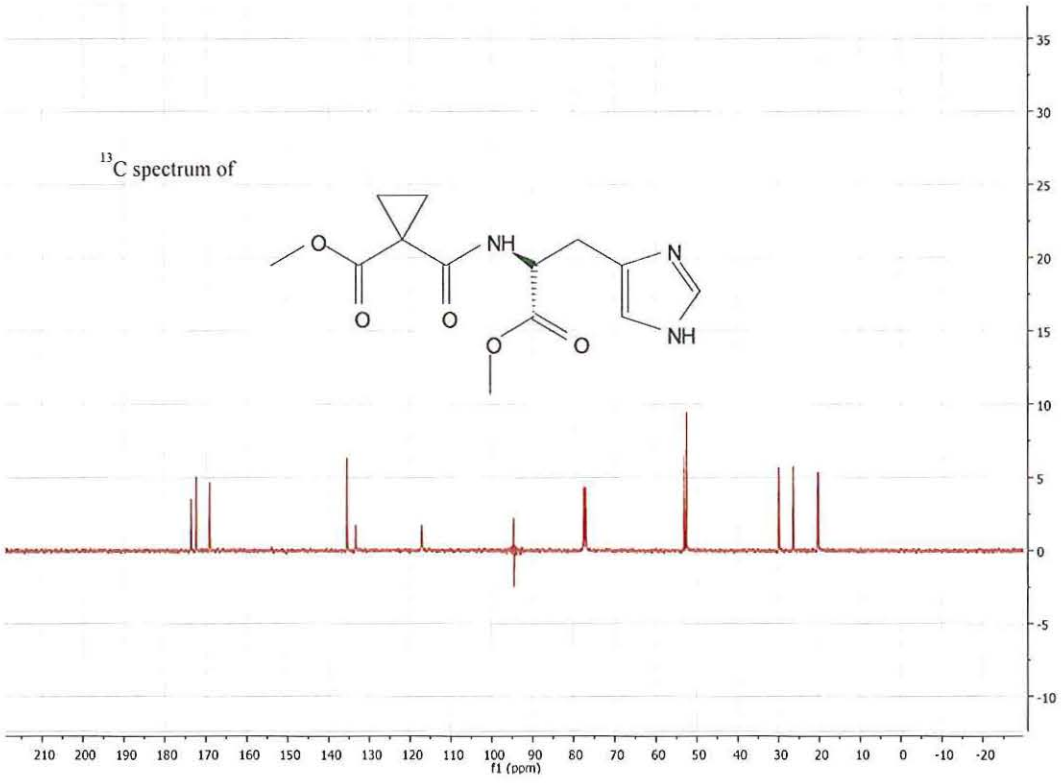

Figure 3.18. ^{13}C (100MHz) NMR spectrum of N-(α)-((1-mehoxycarbonyl) cyclopropylcarbonyl)histidine.

3.2.4.2 Single crystal X-ray crystallographic analysis. *Crystal Structure Analysis of compound 1:* Data collection: Bruker Instrument Service v2009, 3, 0, 0; cell refinement: *APEX2* v2009.3.0 (Bruker AXS); data reduction: *SAINT* V7.60A (Bruker AXS, 2008); program(s) used to solve structure: *SHELXS97* (Sheldrick, 2008); program(s) used to refine structure: *SHELXL97* (Sheldrick, 2008).

Table 3-2. Crystal data for compound 1

$C_{11}H_{15}N_3O_3$	$F(000) = 504$
$M_r = 237.26$	$D_x = 1.370$ Mg m^{-3}
Monoclinic, $P2_1/c$	Mo $K\alpha$ radiation, $\lambda = 0.71073$ Å
Hall symbol: -P 2ybc	Cell parameters from 123 reflections
$a = 10.2579$ (5) Å	$\theta = 2.9–28.1°$
$b = 9.3388$ (5) Å	$\mu = 0.10$ mm^{-1}
$c = 12.2079$ (5) Å	$T = 154$ K
$\beta = 100.466$ (1)°	Cut fragment, clear colourless
$V = 1150.02$ (10) Å^3	0.46 × 0.41 × 0.40 mm
$Z = 4$	

3.3 REFERENCES

[1] J. Ryu, K. Girigoswami, C. Ha, S. H. Ku, C. B. Park, Influence of Multiple Metal Ions on beta -Amyloid Aggregation and Dissociation on a Solid Surface, *Biochemistry* **2008**, *47*, 5328.

[2] C. D. Syme, J. H. Viles, Solution 1H NMR investigation of Zn2+ and Cd2+ binding to amyloid-beta peptide (A.beta) of Alzheimer's disease, *Biochim. Biophys. Acta, Proteins Proteomics* **2006**, *1764*, 246.

[3] C. Ha, J. Ryu, C. B. Park, Metal Ions Differentially Influence the Aggregation and Deposition of Alzheimer's beta -Amyloid on a Solid Template, *Biochemistry* **2007**, *46*, 6118.

[4] G. M. Bishop, S. R. Robinson, The amyloid paradox: Amyloid-beta -metal complexes can be neurotoxic and neuroprotective, *Brain Pathol.* **2004**, *14*, 448.

[5] C. S. Atwood, R. C. Scarpa, X. Huang, R. D. Moir, W. D. Jones, D. P. Fairlie, R. E. Tanzi, A. I. Bush, Characterization of copper interactions with Alzheimer amyloid beta peptides: identification of an attomolar-affinity copper binding site on amyloid beta 1-42, *J. Neurochem.* **2000**, *75*, 1219.

[6] X. Huang, M. P. Cuajungco, C. S. Atwood, R. D. Moir, R. E. Tanzi, A. I. Bush, Alzheimer's disease, beta -amyloid protein and zinc, *J. Nutr.* **2000**, *130*, 1488S.

[7] X. Zhu, G. Perry, M. A. Smith, Two hits and you're out? A novel mechanistic hypothesis of Alzheimer disease, *Adv. Behav. Biol.* **2008**, *57*, 191.

[8] K. J. Barnham, C. C. Curtain, A. I. Bush, Free radicals, metal ions, and Aβ aggregation and neurotoxicity, *Protein Rev.* **2007**, *6*, 31.

[9] M. Nakamura, N. Shishido, A. Nunomura, M. A. Smith, G. Perry, Y. Hayashi, K. Nakayama, T. Hayashi, Three Histidine Residues of Amyloid-beta Peptide Control the Redox Activity of Copper and Iron, *Biochemistry* **2007**, *46*, 12737.

[10] V. P. Reddy, X. Zhu, G. Perry, M. A. Smith, Oxidative Stress in Diabetes and Alzheimer's Disease, *J. Alzheimer's Dis.* **2009**, *16*, 763.

[11] C. S. Atwood, G. Perry, H. Zeng, Y. Kato, W. D. Jones, K.-Q. Ling, X. Huang, R. D. Moir, D. Wang, L. M. Sayre, M. A. Smith, S. G. Chen, A. I. Bush, Copper Mediates Dityrosine Cross-Linking of Alzheimer's Amyloid-beta, *Biochemistry* **2004**, *43*, 560.

[12] M. P. Cuajungco, K. Y. Faget, Zinc takes the center stage: its paradoxical role in Alzheimer's disease, *Brain Res. Rev.* **2003**, *41*, 44.

[13] J. Danielsson, R. Pierattelli, L. Banci, A. Graeslund, High-resolution NMR studies of the zinc-binding site of the Alzheimer's amyloid beta -peptide, *Febs J.* **2007**, *274*, 46.

[14] D. Noy, I. Solomonov, O. Sinkevich, T. Arad, K. Kjaer, I. Sagi, Zinc-amyloid beta interactions on a millisecond time-scale stabilize non-fibrillar Alzheimer-related species, *J. Am. Chem. Soc.* **2008**, *130*, 1376.

[15] A. Deshpande, H. Kawai, R. Metherate, C. G. Glabe, J. Busciglio, A role for synaptic zinc in activity-dependent Abeta oligomer formation and accumulation at excitatory synapses, *J. Neurosci.* **2009**, *29*, 4004.

[16] A. I. Bush, R. E. Tanzi, Therapeutics for Alzheimer's disease based on the metal hypothesis, *Neurotherapeutics* **2008**, *5*, 421.

[17] C. Koppenal, A. E. Finefrock, A. I. Bush, P. M. Doraiswamy, Copper, iron and zinc as therapeutic targets in Alzheimer's disease, *Res. Pract. Alzheimer's Dis.* **2004**, *9*, 250.

[18] E. F. Aziz, W. Eberhardt, S. Eisebitt, Effect of cysteine vs. histidine on the electronic structure of Zn2+ upon complex formation, *Z. Phys. Chem. (Muenchen, Ger.)* **2008**, *222*, 727.

[19] E. Gaggelli, A. Janicka-Klos, E. Jankowska, H. Kozlowski, C. Migliorini, E. Molteni, D. Valensin, G. Valensin, E. Wieczerzak, NMR Studies of the Zn^{2+} Interactions with Rat and Human beta -Amyloid (1-28) Peptides in Water-Micelle Environment, *J. Phys. Chem. B* **2008**, *112*, 100.

[20] S. Zirah, S. A. Kozin, A. K. Mazur, A. Blond, M. Cheminant, I. Segalas-Milazzo, P. Debey, S. Rebuffat, Structural Changes of Region 1-16 of the Alzheimer Disease Amyloid beta -Peptide upon Zinc Binding and in Vitro Aging, *J. Biol. Chem.* **2006**, *281*, 2151.

[21] Y. Mekmouche, Y. Coppel, K. Hochgrafe, L. Guilloreau, C. Talmard, H. Mazarguil, P. Faller, Characterization of the ZnII binding to the peptide amyloid-beta 1-16 linked to Alzheimer's disease, *ChemBioChem* **2005**, *6*, 1663.

[22] V. Minicozzi, F. Stellato, M. Comai, M. Dalla Serra, C. Potrich, W. Meyer-Klaucke, S. Morante, Identifying the Minimal Copper- and Zinc-binding Site Sequence in Amyloid-beta Peptides, *J. Biol. Chem.* **2008**, *283*, 10784.

[23] C. C. Curtain, F. Ali, I. Volitakis, R. A. Cherny, R. S. Norton, K. Beyreuther, C. J. Barrow, C. L. Masters, A. I. Bush, K. J. Barnham, Alzheimer's disease amyloid-beta binds copper and zinc to generate an allosterically ordered membrane-penetrating structure containing superoxide dismutase-like subunits, *J. Biol. Chem.* **2001**, *276*, 20466.

[24] C. D. Syme, R. C. Nadal, S. E. J. Rigby, J. H. Viles, Copper Binding to the Amyloid-beta (Abeta) Peptide Associated with Alzheimer's Disease: Folding, coordination Geometry, pH Dependence, Stoichiometry, and Affinity of Abeta -(1-28): Insights from a Range of Complementary Spectroscopic Techniques, *J. Biol. Chem.* **2004**, *279*, 18169.

[25] S. C. Drew, C. L. Masters, K. J. Barnham, Alanine-2 Carbonyl is an Oxygen Ligand in Cu2+ Coordination of Alzheimer's Disease Amyloid-beta Peptide - Relevance to N-Terminally Truncated Forms, *J. Am. Chem. Soc.* **2009**, *131*, 8760.

[26] L. Hou, M. G. Zagorski, NMR Reveals Anomalous Copper(II) Binding to the Amyloid Abeta Peptide of Alzheimer's Disease, *J. Am. Chem. Soc.* **2006**, *128*, 9260.

[27] J. Sarell Claire, D. Syme Christopher, E. J. Rigby Stephen, H. Viles John, Copper(II) binding to amyloid-beta fibrils of Alzheimer's disease reveals a picomolar affinity: stoichiometry and coordination geometry are independent of Aβ oligomeric form, *Biochemistry* **2009**, *48*, 4388.

[28] V. A. Streltsov, S. J. Titmuss, V. C. Epa, K. J. Barnham, C. L. Masters, J. N. Varghese, The structure of the amyloid-beta peptide high-affinity copper II binding site in Alzheimer disease, *Biophys. J.* **2008**, *95*, 3447.

[29] Q.-F. Ma, J. Hu, W.-H. Wu, H.-D. Liu, J.-T. Du, Y. Fu, Y.-W. Wu, P. Lei, Y.-F. Zhao, Y.-M. Li, Characterization of copper binding to the peptide amyloid-beta (1-16) associated with Alzheimer's disease, *Biopolymers* **2006**, *83*, 20.

[30] K. A. Connors, *Binding Constants: The Measurements of Molecular Complex Stability*, **1987**.

[31] P. Deschamps, P. P. Kulkarni, B. Sarkar, X-ray Structure of Physiological Copper(II)-Bis(L-histidinato) Complex, *Inorg. Chem.* **2004**, *43*, 3338.

[32] Y. Liu, G. Xu, L. M. Sayre, Carnosine Inhibits (E)-4-Hydroxy-2-nonenal-Induced Protein Cross-Linking: Structural Characterization of Carnosine-HNE Adducts, *Chem. Res. Toxicol.* **2003**, *16*, 1589.

[33] Z. Liu, P. E. Minkler, L. M. Sayre, Mass Spectroscopic Characterization of Protein Modification by 4-Hydroxy-2-(E)-nonenal and 4-Oxo-2-(E)-nonenal, *Chem. Res. Toxicol.* **2003**, *16*, 901.

[34] T. Wataya, A. Nunomura, M. A. Smith, S. L. Siedlak, P. L. R. Harris, S. Shimohama, L. I. Szweda, M. A. Kaminski, J. Avila, D. L. Price, D. W. Cleveland, L. M. Sayre, G. Perry, High molecular weight neurofilament proteins are physiological substrates of adduction by the lipid peroxidation product hydroxynonenal, *J. Biol. Chem.* **2002**, *277*, 4644.

[35] D. L. Price, P. M. Rhett, S. R. Thorpe, J. W. Baynes, Chelating activity of advanced glycation end-product inhibitors, *J. Biol. Chem.* **2001**, *276*, 48967.

[36] E. J. Baran, Metal complexes of carnosine, *Biochemistry (Moscow)* **2000**, *65*, 789.

[37] P. G. Daniele, E. Prenesti, G. Ostacoli, Ultraviolet-circular dichroism spectra for structural analysis of copper(II) complexes with aliphatic and aromatic ligands in aqueous solution, *J. Chem. Soc., Dalton Trans.* **1996**, 3269.

[38] V. P. Reddy, A. Beyaz, Inhibitors of the Maillard reaction and AGE breakers as therapeutics for multiple diseases, *Drug Discovery Today* **2006**, *11*, 646.

[39] V. P. Reddy, R. Garrett Matthew, G. Perry, A. Smith Mark, Carnosine: a versatile antioxidant and antiglycating agent, *Sci. Aging Knowledge Environ. : SAGE KE* **2005**, *18*, pe12.

[40] A. R. Hipkiss, Could Carnosine or Related Structures Suppress Alzheimer's Disease?, *J. Alzheimers Dis.* **2007**, *11*, 229.

[41] A. Guiotto, A. Calderan, P. Ruzza, G. Borin, Carnosine and carnosine-related antioxidants: A review, *Curr. Med. Chem.* **2005**, *12*, 2293.

[42] V. V. Mossine, T. P. Mawhinney, Na-(1-Deoxy-D-fructos-1-yl)-L-histidine (\"D-Fructose-L-histidine\"): a Potent Copper Chelator from Tomato Powder, *J. Agric. Food Chem.* **2007**, *55*, 10373.

[43] M.-S. S. Alhamdani, A.-H. A. M. Al-Kassir, F. K. H. Abbas, N. A. Jaleel, M. F. Al-Taee, Antiglycation and Antioxidant Effect of Carnosine against Glucose Degradation Products in Peritoneal Mesothelial Cells, *Nephron* **2007**, *107*, c26.

[44] L. Shao, Q.-h. Li, Z. Tan, L-Carnosine reduces telomere damage and shortening rate in cultured normal fibroblasts, *Biochem. Biophys. Res. Commun.* **2004**, *324*, 931.

[45] A. Boldyrev, E. Bulygina, T. Leinsoo, I. Petrushanko, S. Tsubone, H. Abe, Protection of neuronal cells against reactive oxygen species by carnosine and related compounds, *Comp. Biochem. Physiol., Part B: Biochem. Mol. Biol.* **2004**, *137B*, 81.

[46] A. Boldyrev, R. Song, D. Lawrence, D. O. Carpenter, Carnosine protects against excitotoxic cell death independently of effects on reactive oxygen species, *Neuroscience (Oxford)* **1999**, *94*, 571.

[47] A. A. Boldyrev, P. Johnson, Y. Wei, Y. Tan, D. O. Carpenter, Carnosine and taurine protect rat cerebellar granular cells from free radical damage, *Neurosci. Lett.* **1999**, *263*, 169.

[48] A. R. Pavlov, A. A. Revina, A. M. Dupin, A. A. Boldyrev, A. I. Yaropolov, The mechanism of interaction of carnosine with superoxide radicals in water solutions, *Biochim. Biophys. Acta* **1993**, *1157*, 304.

[49] M. A. Babizhayev, M.-C. Seguin, J. Gueyne, R. P. Evstigneeva, E. A. Ageyeva, G. A. Zheltukhina, L-Carnosine (b-alanyl-L-histidine) and carcinine (b-alanylhistamine) act as natural antioxidants with hydroxyl-radical-scavenging and lipid-peroxidase activities, *Biochem. J.* **1994**, *304*, 509.

[50] A. S. Karikari, B. D. Mather, T. E. Long, Association of Star-Shaped Poly(D,L-lactide)s Containing Nucleobase Multiple Hydrogen Bonding, *Biomacromolecules* **2007**, *8*, 302.

[51] H.-J. Schneider, A. K. Yatsimirsky, in *Principles and Methods in Supramolecular Chemistry*, John Wiley, New York, **2000**, pp. 148.

[52] G. Beretta, R. Artali, L. Regazzoni, M. Panigati, R. Maffei Facino, Glycyl-histidyl-lysine (GHK) Is a Quencher of a,b-4-Hydroxy-trans-2-nonenal: A Comparison with Carnosine. Insights into the Mechanism of Reaction by Electrospray Ionization Mass Spectrometry, 1H NMR, and Computational Techniques, *Chem. Res. Toxicol.* **2007**, *20*, 1309.

[53] P. Mineo, D. Vitalini, D. La Mendola, E. Rizzarelli, E. Scamporrino, G. Vecchio, Electrospray mass spectrometric studies of L-carnosine (b-alanyl-L-histidine) complexes with copper(II) or zinc ions in aqueous solution, *Rapid Commun. Mass Spectrom.* **2002**, *16*, 722.

[54] F. Bellia, D. La Mendola, G. Maccarrone, P. Mineo, D. Vitalini, E. Scamporrino, S. Sortino, G. Vecchio, E. Rizzarelli, Copper(II) complexes with b-cyclodextrin-homocarnosine conjugates and their antioxidant activity, *Inorg. Chim. Acta* **2007**, *360*, 945.

[55] T. Fujita, Structure-activity relations. 6. Structure-activity relations of monoamine oxidase inhibitors, *Journal of Medicinal Chemistry* **1973**, *16*, 923.

[56] D. M. Campoli-Richards, J. P. Monk, A. Price, P. Benfield, P. A. Todd, A. Ward, Ciprofloxacin. A review of its antibacterial activity, pharmacokinetic properties and therapeutic use, *Drugs* **1988**, *35*, 373.

[57] R. Wise, J. M. Andrews, L. J. Edwards, In vitro activity of Bay 09867, a new quinoline derivative, compared with those of other antimicrobial agents, *Antimicrobial Agents and Chemotherapy* **1983**, *23*, 559.

[58] E. Vilsmaier, T. Goerz, Diastereoselective syntheses of N-protected derivatives of 1alpha ,5alpha ,6beta -6-amino-3-azabicyclo[3.1.0]hexane. A route to trovafloxacin 6beta -diastereomer, *Synthesis* **1998**, 739.

[59] J. Salaun, Cyclopropane derivatives and their diverse biological activities, *Topics in Current Chemistry* **2000**, *207*, 1.

[60] P.-Y. Kuo, T.-L. Shie, Y.-S. Chen, J.-T. Lai, D.-Y. Yang, Enzyme inhibition potency enhancement by active site metal chelating and hydrogen bonding induced conformation-restricted cyclopropanecarbonyl derivatives, *Bioorganic & Medicinal Chemistry Letters* **2006**, *16*, 6024.

[61] M. Shaabanzadeh, F. Khabari, One-pot synthesis of new spiro[cyclopropane-1,3'-[3H]indol]-2'(1'H)-ones from 3-phenacylideneoxindoles, *Journal of Heterocyclic Chemistry* **2010**, *47*, 949.

[62] N. T. Pokhodylo, V. S. Matiichuk, N. D. Obushak, Methyl 3-cyclopropyl-3-oxopropanoate in the synthesis of heterocycles having a cyclopropyl substituent, *Russian Journal of Organic Chemistry* **2010**, *46*, 894.

[63] Y.-M. Shen, P.-C. Lv, W. Chen, P.-G. Liu, M.-Z. Zhang, H.-L. Zhu, Synthesis and antiproliferative activity of indolizine derivatives incorporating a cyclopropylcarbonyl group against Hep-G2 cancer cell line, *European Journal of Medicinal Chemistry* **2010**, *45*, 3184.

[64] S. Abele, P. Seiler, D. Seebach, Synthesis, crystal structures, and modeling of beta -oligopeptides consisting of 1-(aminomethyl)cyclopropanecarboxylic acid: ribbon-type arrangement of eight-membered H-bonded rings, *Helvetica Chimica Acta* **1999**, *82*, 1559.

[65] A. Harthun, M. Neumann, C. Theis, (Degussa-Huels A.-G., Germany). Application: US, **2001**, p. 8 pp.

[66] J. Heiszman, I. Bitter, K. Harsanyi, L. Toke, A facile synthesis of dialkyl cyclopropane-1,1-dicarboxylates and alkyl 1-cyanocyclopropanecarboxylates by phase-transfer alkylation, *Synthesis* **1987**, 738.

[67] U. Jegelka, C. Osterholt, D. Hille, (Degussa A.-G., Germany). Application: DE, **2001**, p. 6 pp.

[68] A. Krief, M. Trabelsi, Efficient syntheses of (d,l) and (d) selenomethionine, *Synth. Commun.* **1989**, *19*, 1203.

[69] J. Metz, C. Osterholt, (Huels A.-G., Germany). Application: DE, **1999**, p. 4 pp.

[70] S. Muthusamy, B. Gnanaprakasam, Imidazolium salts as phase transfer catalysts for the dialkylation and cycloalkylation of active methylene compounds, *Tetrahedron Lett.* **2005**, *46*, 635.

[71] H. Ogoshi, Y. Kikuchi, T. Yamaguchi, H. Toi, Y. Aoyama, Asymmetric induction in the nucleophilic cyclopropane ring cleavage reaction with vitamin B12s, *Organometallics* **1987**, *6*, 2175.

[72] F. Ojima, T. Osa, Perkin-Markovnikov type reaction initiated with electrogenerated superoxide ion, *Bull. Chem. Soc. Jpn.* **1989**, *62*, 3187.

[73] K.-D. Steffen, (Huels AG, Germany). Application: DE, **1995**, p. 5 pp.

[74] X. Zheng, M. A. Kerr, Synthesis and Cross-Coupling Reactions of 7-Azaindoles via a New Donor-Acceptor Cyclopropane, *Org. Lett.* **2006**, *8*, 3777.

[75] D. A. White, Alkylations with potassium carbonate in dimethylformamide, *Synth. Commun.* **1977**, *7*, 559.

[76] I. Grayson, Water-soluble carbodiimide - an efficient coupling agent for synthesis, *Spec. Chem.* **2000**, *20*, 86.

4. BORON BASED ANION RECEPTORS: SYNTHESIS, ANION BINDING STUDIES, AND *AB-INITIO* CALCULATIONS.

4.1 INTRODUCTION

A large number of boron based anion receptors have been developed to selectively bind fluoride ions.[1-2] Among the biologically important anions, fluoride anion has received much attention due to its established importance in preventing dental caries. Fluoride is also an important constituent of osteoporosis drugs. Regardless of the beneficial advantages, overdoses of fluoride results in dental and skeletal fluorosis. Further, fluoride ion receptors have major applications in lithium ion batteries. Lithium fluoride being a low molecular weight salt potentially imparts high power densities to lithium ion batteries. However, due to its insolubility in commonly used carbonate based electrolyte solvents, its application in lithium ion batteries are limited. Appropriate anion receptors would help dissociate lithium fluoride and increase its solubility. [3-4]

Anions are Lewis bases, which can interact with Lewis acidic species. Tri-coordinated boron compounds can bind anions covalently to form complexes. On complexation with the anions the hybridization of boron changes partially from sp^2 to sp^3. Compared to pure Columbic interaction which depends on the distance and size of the charge, Lewis acid base interaction depends on the properties of the interacting species. e.g, stereo electronic properties, symmetry of molecular orbitals, hard-soft property, back bonding ability etc.[2, 5]

The chemistry of boron-based anion receptors started when Shriver and Biallas[6] first reported the anion chelating ability of acyclic boron compounds in 1967. Shriver and

coworkers showed that bis(difluoroboryl)ethane 1 can chelate methoxide ions.[6] In a competition experiment they found that the complex formed by bidentate ligand is more stable than the monodentate ligand BF_3 (Scheme 4.1).

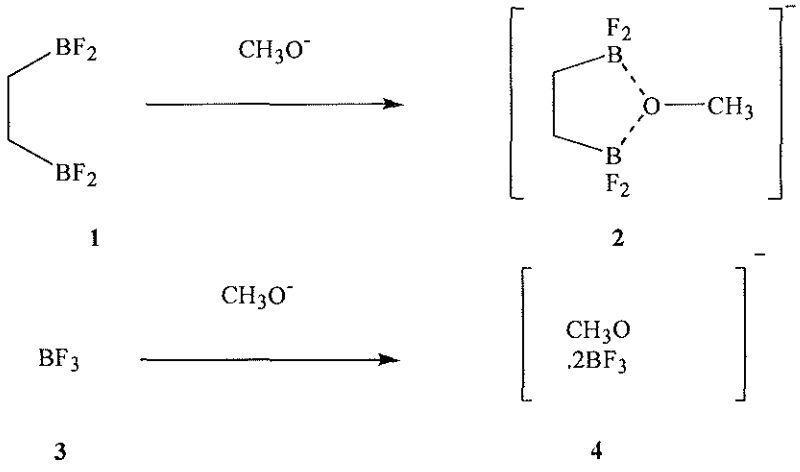

Scheme 4.1. Chelated complexes of bis(difluoroboryl)ethane.

In 1985 H.E. Katz[7-8] synthesized 'hydride sponges' which was a naphthalene derivative of bisdimethylborane 6 (Figure 4.1). In solution the compound was able to abstract proton from potassium hydrides and other borohydrides. The X-ray crystal structure of the complex 6 with KH showed that hydride is unsymmetrically bound between two boron atoms with an average B-H-B bond length of 1.3 A^0 (1.20 and 1.49A^0) and an angle of 140^0.

Compound 6 was able to abstract proton from compound 5 indicating that chelate effect stabilizes the complexes. These compounds were shown to complex fluoride ions and hydroxide ions. In 1987 same author synthesized naphthalene derivative of bis(dichloroborane) which was the first bidentate boron chloride chelate (8).[9] X-ray crystallography showed that chloride is chetaled by two boron atoms symmetrically with B-Cl bond length of 1.83 A^0 (Figure4.1).

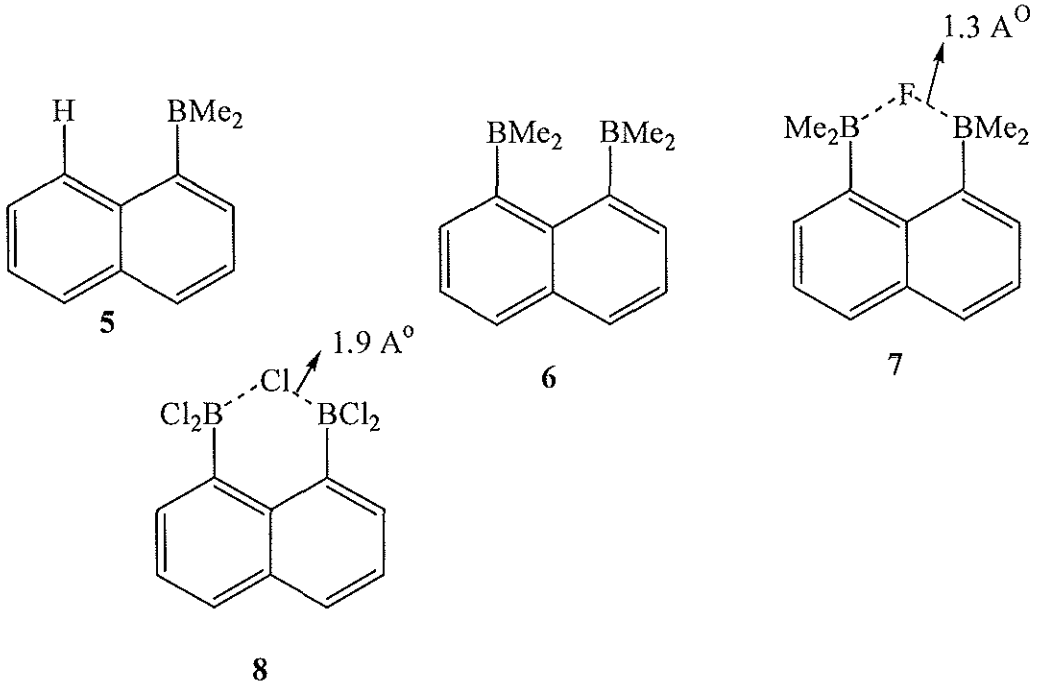

Figure 4.1. Naphthalene derived bidentate Lewis Acids for fluoride anion receptors.

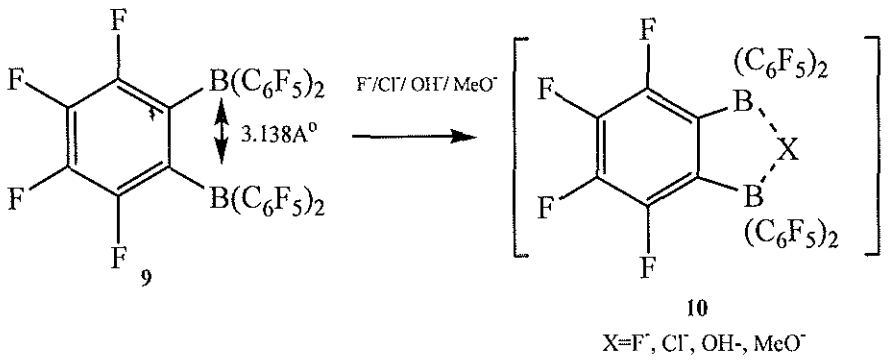

Scheme 4.2. Perfluorinated aryl derived diboranes complexe with fluoride, hydroxide, chloride and methoxide ions.

William and coworkers showed that perfluorinated aryl boranes(9) complexes with fluoride, hydroxide, chloride and methoxide ions.The anions are chelated between the boron atoms which are 3.13 A^0 apart[10](Scheme 4.2).Boron based bidentate, colorimetric and phosphorescent fluoride sensors have also been reported Compound 11, for example, originally yellow in color, upon complexation with fluoride becomes colorless.[11] The mercuriated analog of the latter compound 13 on the other hand gives phosphorescent fluoride adducts (Scheme 4.3).[12]

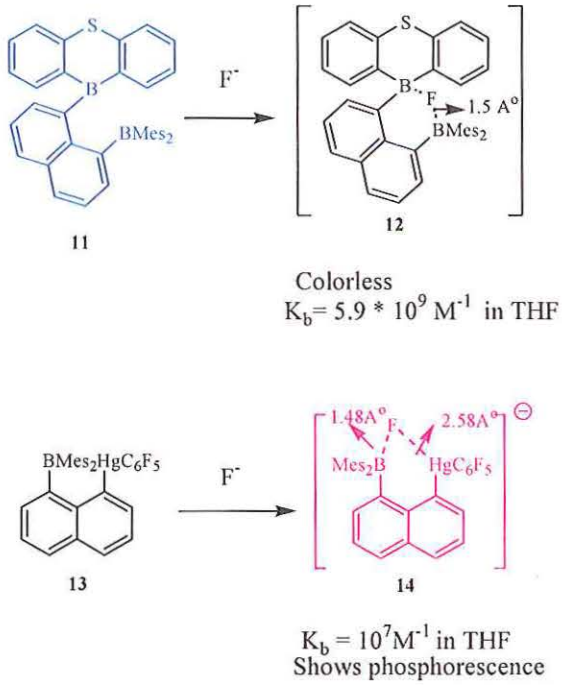

Scheme 4.3. Examples of bidentate Lewis acids as Colorimetric and Phosphorescent Fluoride Sensor.

All of these bidentate anion receptors for fluoride, as discussed above are limited to organic solvents. Due to the importance of detection of fluoride ions in water, Hudnall and coworkers developed cationic boranes, involving quaternary ammonium and phosphonium groups (15, 16 and 17) for fluoride anion binding in aqueous solutions (Figure 4.2). [12] However, their binding constants with fluoride are less than their related bidentate anion receptors. More importantly, compounds 15 and 17 are selective for fluoride anion, whereas para-substituted compound 16 is relatively more selective for cyanide anions.

These differences in their relative binding constants may be explained as due to the enhanced electrophilicity of the boron center when the electron withdrawing quaternary ammonium group is in the *ortho*-position. Fluoride anion, being hydrated in the aqueous solution, is relatively less nucleophilic than the cyanide and hence the increased electrophilicity is required for its binding. The relatively more bulky cyanide anion, on the other hand prefers the *para* substituted receptor, 16. In other words, the boron center in compound 16 is not sufficiently electrophilic for the fluoride anion binding.

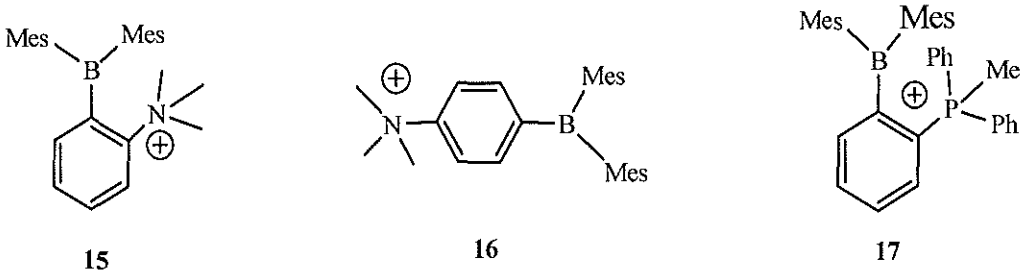

15 **16** **17**

Figure 4.2 Examples of boron based anion receptors for selective binding of fluoride ions and cyanide ions from water.

In addition to boron, mercury, tin and silicon derivatives, e.g., compounds 18, 19, and 20 have also been reported as anion receptors (Figure 4.3). [12] However, these anion receptors are not useful as selective fluoride anion receptors.

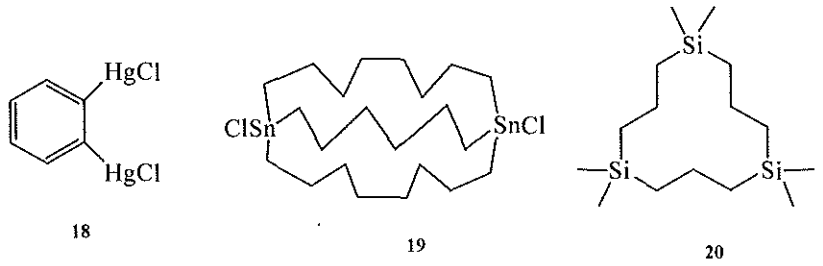

18 19 20

Figure 4.3 Other Lewis acid based receptors.

Anions are always accompanied by their counter cations. Therefore, one approach to synthesis of anion receptors is to synthesize dual ion receptors which are capable of binding both anions and cations, which increases the stability of the fluoride complexes. Very few Lewis acid based ditopic anion receptors, such as crown ether derived boronates (e.g., 21) are reported to date. [12] Compound 21 binds to potassium fluoride more efficiently as compared to related boron derived anion receptors lacking the crown ether substituent (Scheme 4.4). Crown ether moiety in compound 21 selectively binds to K^+ and the boron binds to the fluoride anion giving the ditopic complex 22(Scheme 4.4).

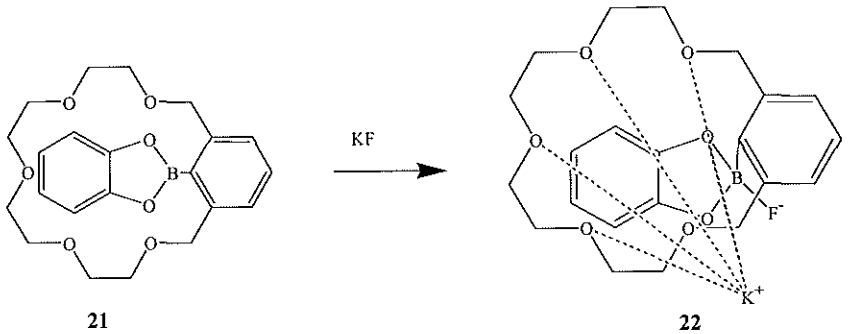

21 22

Scheme 4.4. Ditopic anion receptors.

4.2 SYNTHESIS AND FLUORIDE ANION BINDING STUDIES OF BORANE BASED ANION RECEPTORS

4.2.1 Introduction. Boranes are Lewis acidic compounds which can bind to nucleophilic anions. Previous studies as discussed above had shown that Lewis acidic boron center is a selective binding site for fluoride ions presumably due to hard acid-base type interaction. The binding affinity of boron center can be fine tuned by the electronic effects of substituents at the boron centre. Towards this goal, we have synthesized fluorinated borane based anion receptors (Figure 4.4), and their binding affinities with various anions were studied using multinuclear NMR, UV-Vis and mass spectroscopy.

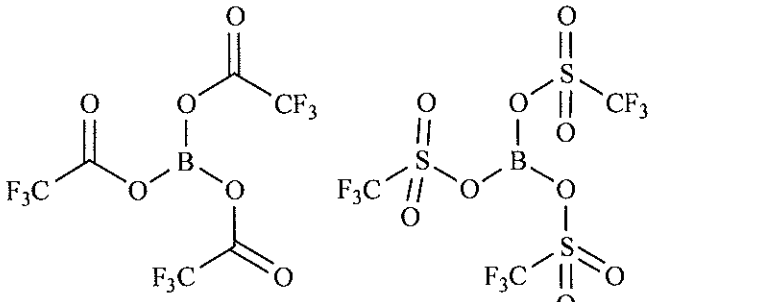

Figure 4.4. Structures of BTTA and B $(OTf)_3$

4.2.2 Synthesis and Fluoride Ion Binding Studies of Boron Tris(trifate). Boron tris(triflate) was synthesized using reported procedures(Scheme 4.5).[13] Boron tribromide was reacted with triflic acid at 0 °C under inert atmosphere. A white precipitate was formed which was filtered under inert atmosphere and dried under high vacuum overnight to remove the hydrogen bromide produced.

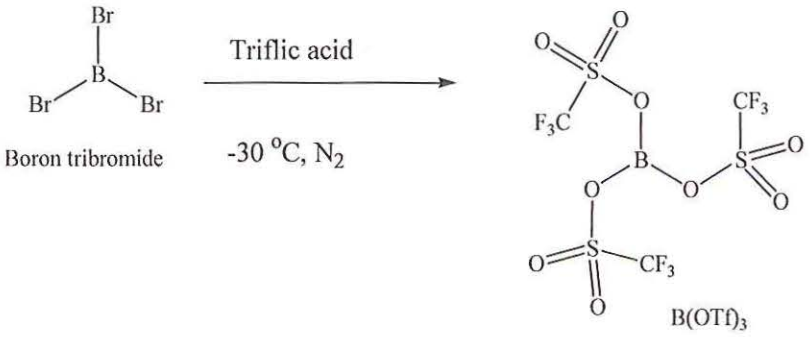

Scheme 4.5. Synthesis of Boron tris(triflate) (B(OTf))

NMR analysis of the $B(OTf)_3$ showed that it forms adducts with solvents such as dimethyl sulfoxide (Figure 4.5) and acetonitrile (Figure 4.6). Triaryl boranes are known to form solvent adducts with acetonitrile.[14]

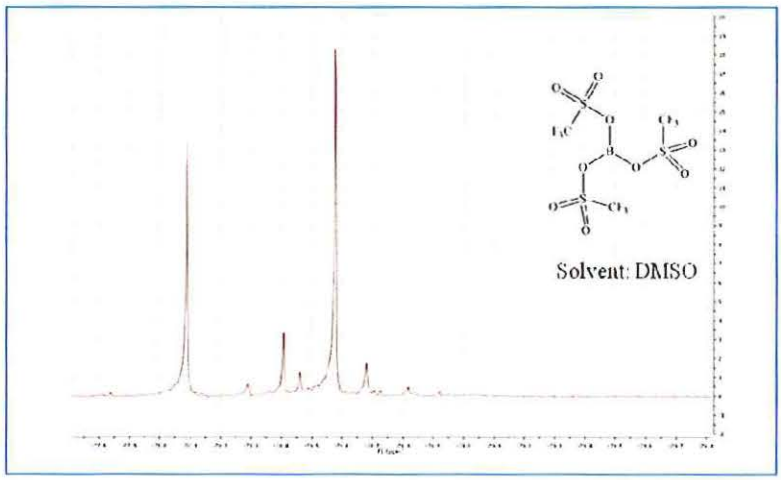

Figure 4.5. ^{19}F NMR of borontristriflate in DMSO.

In acetonitrile solution three ^{19}F peaks peaks were observed at -78.55 (B), -78.39 (C) and -78.09 (D) ppm (Figure 4.7). In order to investigate whether any of the peaks correspond to triflic acid, increasing amount of triflic acid (100 μL) was added to the solution of boron tris(triflate) in acetonitrile . On addition of triflic acid a new peak emerged at -77.7 ppm corresponding to triflic acid which was verified by adding extra amounts of triflic acid (Figure 4.6). The unidentified peaks may correspond to solvent adducts of Boron tris(triflate). Thus boron tris(triflate) is not a suitable candidate for stduying fluoride ion binding due to its moisture sensitivity and reactivity with solvents.

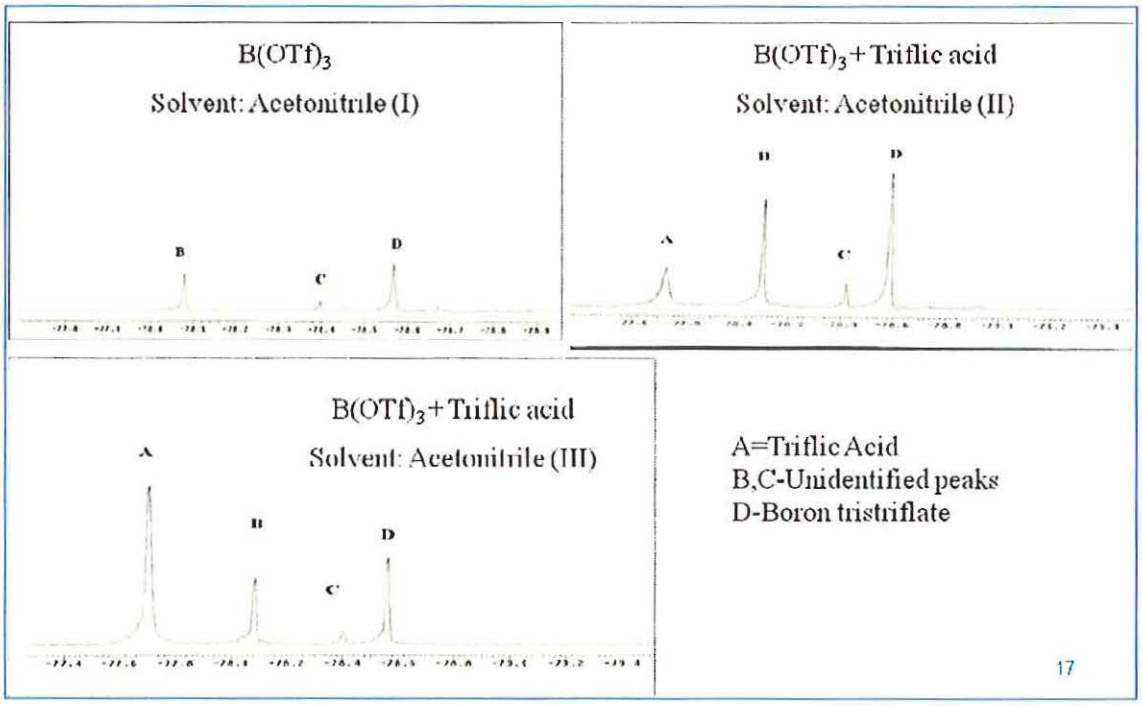

Figure 4.6. ^{19}F NMR of boron tris(triflate) in acetonitrile.

4.2.3 Synthesis and fluoride ion binding studies of Boron tris(trifluoroacetate). Boron tris(trifluoroacetate) was synthesized by slight modification of the reported procedure by Pless and coworkers (Scheme 4.6).[15] To boron tribromide in an RB flask under inert atmosphere, at 0 °C trifluoroacetic acid was added dropwise. Immediately on mixing of the two reagents a white precipitate was formed which was washed with dichloromethane (DCM) 2.3 times (20mL). Removal of any residual solvent in high vacuum gave a white precipitate in 95 % yield. NMR analysis of these compounds in various solvents such as acetonitrile, dimethyl sulfoxide showed that it reacts with solvents (Figure 4.7). Due to its intrinsic Lewis acidity it may be forming adducts with nucleophilic solvents.

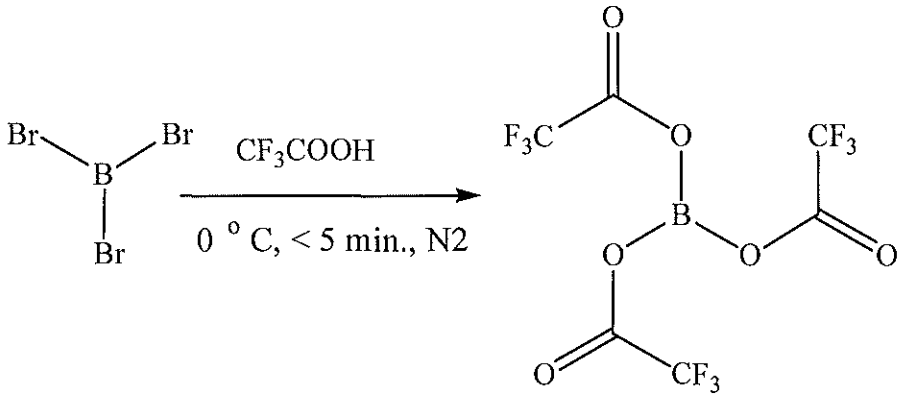

Boron tris(trifluoroacetate)
(BTTA)

Scheme 4.6. Synthesis of Boron tris(trifluoroacetate)

In acetonitrile (Figure 4.7) larger peaks at δ 75.8 corresponds to BTTA and smaller peaks at δ 76.2 and δ 75.5 corresponds to solvent adducts with acetonitrile.

Similarly with DMSO there were three larger peaks at δ 75.1, 75.4 and 75.5 (Figure 4.7). Due to its intrinsic Lewis acidity it may be forming adducts with nucleophilic solvents. It was also found that BTTA polymerizes THF solvent in accordance with the literature reports.[16]

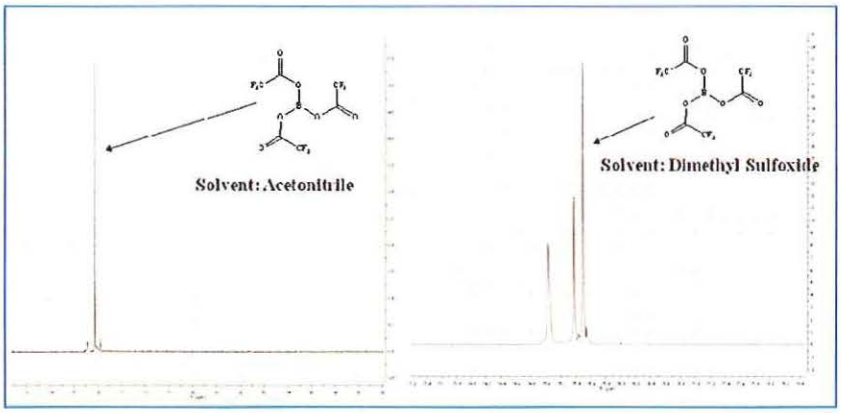

Figure 4.7. ^{19}F NMR of BTTA in acetonitrile (left) and dimethylsulfoxide(right).

In order to determine the fluoride ion binding affinity, BTTA was titrated with, tetrabutyl ammonium fluoride (1.2 equivalents) in acetonitrile and DMSO (Scheme 4.7). NMR analysis of the resultant solution shows that on addition of fluoride ion additional peaks were formed in the range of δ -75.62 to -76.32ppm in acetonitrile and other solvents. UV-Vis spectroscopic titrations also indicated the formation of multiple equilibria. Thus BTTA is not a suitable compound for fluoride ion binding studies using NMR or UV spectroscopy.

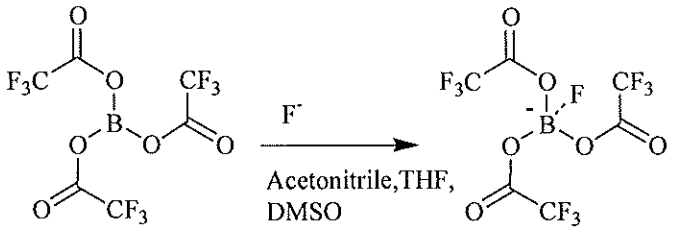

BTTA BTTA-Fluoride

Scheme 4.7. Fluoride ion binding of Borontris(triflate)

4.3 SYNTHESIS AND ANION BINDING STUDIES OF BOROXIN-BASED ANION RECEPTORS.

Boroxines are cyclic trimeric esters of boronic acids. Although boroxin-based polymers have been used as flame retardants and as electrolytes in lithium ion batteries. [17-18] they were never explored as anion receptors. It is well known that they coordinate with N-containing ligands.[19] [20-22] Here we disclose our results on the effect of fluorinated boroxines, tris(2,6-difluorophenyl)boroxin (DF; 23), tris(2,4,6)trifluorophenylboroxin (TF; 24), and tris(pentafluorophenyl)boroxin (PF; 25) as novel anion receptors for potential applications in lithium ion batteries, through *ab-initio* theory, fluoride anion binding studies(Figure 4.8). These cyclic fluorinated boroxines have additional advantages as their Lewis acidity could be readily modulated by varying the number of fluorines on the aromatic rings. Our density functional theory (DFT) calculations substantiate this hypothesis and serves as a predictive tool for identifying the optimal anion receptors.

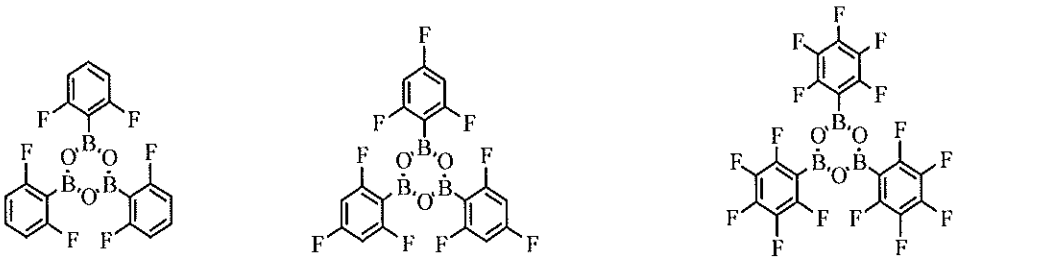

Tris(2,6 -difluorophenyl) boroxin (DF) **23**

Tris(2, 4, 6-trifluorophenyl) Boroxin (TF) **24**

Tris(pentafluorophenyl) Boroxin (PF) **25**

Figure 4.8: Structures of fluorinated boroxines.

4.3.1 Results and Discussions. Boron-based anion receptors such as tris(pentafluorophenyl)borane have recently been used for selective binding of fluoride anions in lithium ion batteries.[23-26] In order to systematically fine tune the binding efficiencies of the boron based anion receptors, we have now synthesized a series of fluorinated arylboroxines – DF (23), TF (24), and PF (25) – by thermal dehydrative cyclizations of the corresponding arylboronic acids. The structures of these compounds were readiy assigned based on ^{19}F- and ^{11}B NMR spectra, which closely match with those calculated by *ab-initio* theory. ^{11}B NMR are especially diagnostic of the structures as deviations of the experimental chemical shifts from GIAO/B3LYP-6-31G** derived values are of too small: $\Delta\delta$ = 1.7 (DF), 0.2 (TF), 0.5 (PF).

The synthetic method adapted is comparatively simple and allows synthesis of a wide variety of fluorinated boroxines from their corresonding arylboronic acids (Scheme 4.8).[27-29] Further, the binding efficiencies of these boroxines can be readily optimized by tailoring the degree of fluorination on the aryl rings, or by incorporating additional electron-withdrawing groups. These anion receptors could be readily monitored for their

anion binding efficiency using ^{19}F and ^{11}B NMR spectroscopy. We have explored fluoride anion binding efficiencies, and binding stoichiometries of these boroxines. These results are further substantiated by *ab-initio* theoretical calculations.

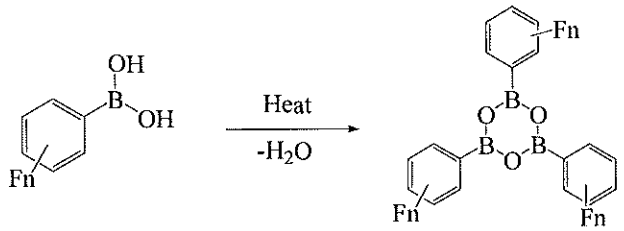

(1)

DF (23); TF (24); PF (25)

Scheme 4.8. Synthesis of fluorinated boroxines.

4.3.2 Structural Characterization. The boroxines 23.25 were characterized by ^{19}F and ^{11}B NMR spectroscopy and the structures were confirmed through comparison of the chemical shifts with those obtained by *ab-initio* GIAO/B3LYP/6-31G**[30] method (Figure 4.9). The ^{19}F NMR spectrum for DF (23) showed a single absorption at -103.0 ppm which is very close to the GIAO/B3LYP/6-31G** of -101.7 ($\Delta\delta$ = 1.3). TF (24) showed two ^{19}F absorptions at $\delta^{19}F$ -99.9 (*ortho*-F), and -106.8 (*para*-F), agreeing with those of DFT-GIAO calculations: -104.8 (*ortho*-F, $\Delta\delta$ = 4.82), -105.5 (*para*-F, $\Delta\delta$ = 2.34). PF (25) showed three absorptions at -132.4 (*ortho*-F), -153.7 (*para*-F), and -163.0 (*meta*-F). The *ortho*-, *meta*- and *para*- fluorine assignments are supported by the *ab-initio* calculated chemical shifts, although the theoretically obtained chemical shifts are deviating from the experimental values by 6 to 10 ppm. Further, the ^{11}B NMR spectra

closely match the experimental values for DF ($\Delta\delta$ = 1.7), TF ($\Delta\delta$ = 0.2) and PF ($\Delta\delta$ = 0.5) showing that the GIAO ^{11}B NMR chemical shifts are reliable indicators of the structural characterization of the boroxines.[31-32]

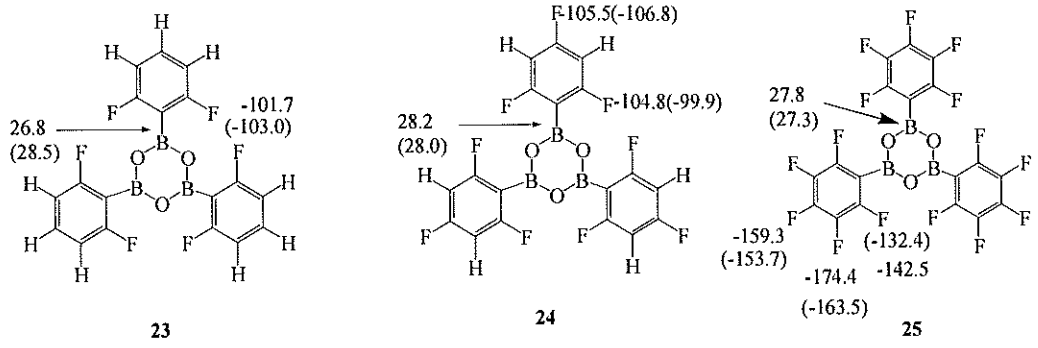

Figure 4.9. Experimental (acetonitrile solvent; in parenthesis) and GIAO/B3LYP/6-31G** calculated $\delta^{19}F$ ($\delta CFCl_3 = 0$) and ^{11}B NMR spectra for DF, TF and PF; DF; $\delta^{11}B$ are shown using arrows ($\delta BF_3.OEt_2 = 0$).

Further, structures of these compounds are confirmed by electron impact ionization mass spectroscopic (EI/MS) studies. A solid probe technique was used for mass spectroscopic studies. The compound was loaded in to solid probe and subjected to electron impact ionization. The EI mass spectrum of DF, TF and PF gave abundant molecular ion peaks indicating that molecular ions are stable under mass spectroscopic conditions. Isotopic abundance measurement confirmed the assignment of molecular ion peaks. EI analysis showed the molecular ion peaks for DF, TF, and PF, at m/z 420, 474 and 581 respectively (Figure 4.10).

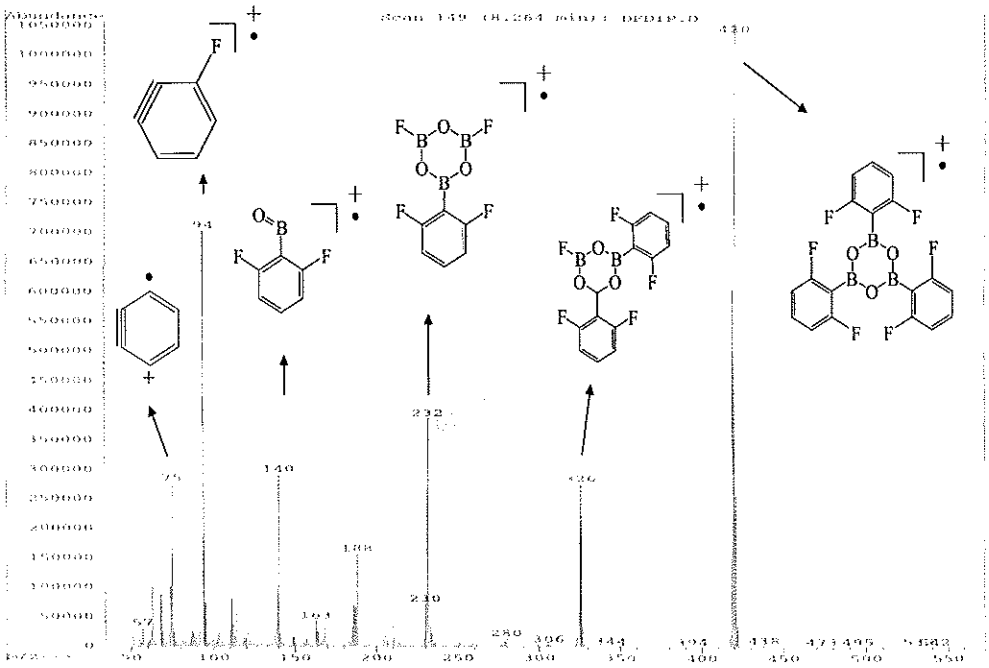

Figure 4.10. EI/MS spectrum of DF recorded at 70eV showing molecular ions and daughter ions.

Mass spectrum of DF showed 5 daughter ions with appreciable abundance at 326, 42, 140, 94, and 75 (Figure 4.10). These m/z values could be readily assigned to fragments 23a, 23b, 23c, 23d and 23e as shown in Scheme 4.9. Loss of fluorobenzyne radical C_6H_3F from molecular ion (m/z 420) gives a fragment at m/z 326 with 26 % abundance relative to molecular ion peak. This fragment is formed by cleavage of boron aryl bond and migration of orthofluorine on phenyl ring to boron centre.

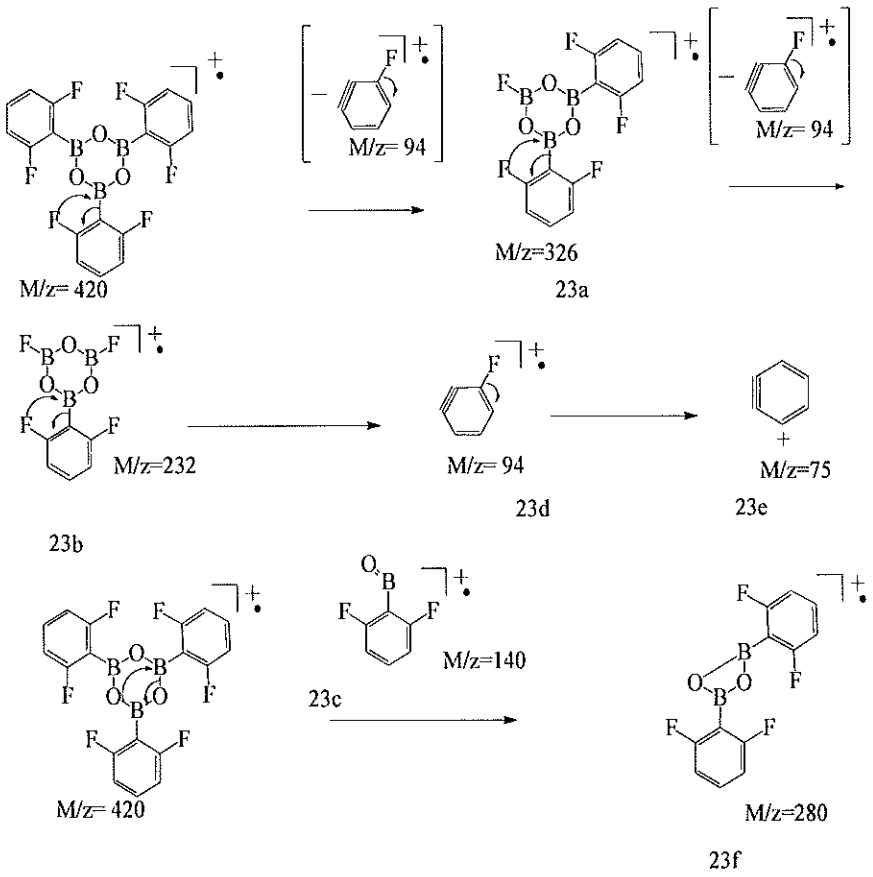

Scheme 4.9. The proposed fragmentation mechanism of DF in EI/MS.

The fragmentation pattern is repeated further. The loss of 2 fluorobenzyne radicals (a loss of $C_{12}H_6F_2$) lead to the formation of fragment at m/z 42 with an abundance of 36%. The peaks at m/z 140 arise by B-O cleavage with an abundance of 29%. The low abundance of these peaks shows the relative thermal stability of boroxines. The relatively intense peak (an abundance of 79%) at m/z 94 is assumed to be due to a fluoorobenzyne radical which was the most abundant daughter ion in the spectrum. It further underwent the cleavage C-F bond to give a fragment at m/z 75(30%), which is probably due to benzyne radical cation, which is unprecedented. The assignments of

peaks are further confirmed by the comparing observed and calculated isotopic pattern (Table 4.1). The peaks at m/z 420, 326 and 42 showed an isotopic pattern corresponding to B3. The M-2, M-1, M, M+ 1 peak are well within the range calculated.

Table 4.1. Isotopic pattern of molecular ions and selected daughter ions of DF.

m/z 420			m/z at 326			m/z at 42		
Mass	Observed %	Calculated %	Mass	Observed %	Calculated %	Mass	Observed %	Calculated %
418	15.0	16.3	324	6.0	17.0	230	21.3	17.7
419	59.2	67.9	325	70.4	69.9	231	74.1	72.1
420	100.0	100.0	326	100.0	100.0	232	100.0	100.0
421	21.7	18.7	327	12.5	12.9	233	9.6	6.9
422	2.6	2.3	328	1.4	1.4	234	6.2	0.8

In some cases the slight difference is from the peaks over lapping due to the loss of proton form the fragments. The fragment at 140 showed an isotopic pattern corresponding to B1. Similarly EI/MS spectrum of TF showed major peaks at m/z 474, 362, 60, 158 and 112.The base peak was molecular ion peaks at m/z 474. Formation of daughter ions can be easily explained using the same mechanism as in the case of DF. The assignments of the peaks are further confirmed by isotopic pattern calculation.

In the case of PF the major peaks were at m/z 581, 434, 286, 194, 148. PF also followed the same fragmentation pattern as DF and TF. The fragmentation pattern shows the possible involvement of a 1,3.sigmatropic migration of the *ortho*-fluorine from the aryl rings to boron in concert with elimination of corresponding fluorobenzyne (Scheme 4.9), which will be discussed later in this section. A similar mechanism was shown by the fluoride adducts of DF, TF and PF (*vide infra*) in ESI/MS studies.

4.3.3 Solvation effect. It has been established through X-ray diffraction studies that tris(pentafluorophenylborane) can form 1:1 adducts with solvents such as acetonitrile.[33] In order to see similar solvation effects on fluorinated boroxines, we have explored the effect of solvents on the stabilization of the boron centers through ^{19}F NMR spectroscopy (Figure 4.11, Figure 4.12 and Figure 4.13) In the relatively non nucleophilic solvent, dichloromethane DF shows a single absorption at $\delta^{19}F$ -104.5, whereas in acetonitrile, dimethylsulfoxide, and ethyl acetate, the absorption has shifted to downfield by 1 ppm to -103. It shows significant solvation effect from these solvents. Similarly, for TF $\delta^{19}F(CH_2Cl_2)$ signals at -101.1(*ortho*-F) and -103.2 (*para*-F) are shifted downfield by 1 ppm for the *ortho*-fluorine, and *para*-fluorine is shifted by 4 ppm upfield in DMSO, acetonitrile and ethyl acetate.

On the other hand, PF (6) shows relatively more sensitivity to solvation effects. In the more coordinating DMSO solvent, the $\delta^{19}F$ (CH_2Cl_2) signals at -132.8 (*ortho*-F), -149.6 (*para*-F), =161.5 (*meta*-F) are split into multiple peaks from -131 to -164 ppm in DMSO indicating the formation of stable PF-DMSO adducts. In acetonitrile and ethyl acetate solvents, the $\delta^{19}F(CH_2Cl_2)$ absorptions are shifted downfield by 0.5 ppm for

ortho-fluorines, upfield by 5 ppm for *para*-fluorines, and upfield by 2 ppm for the *meta*-fluorines.

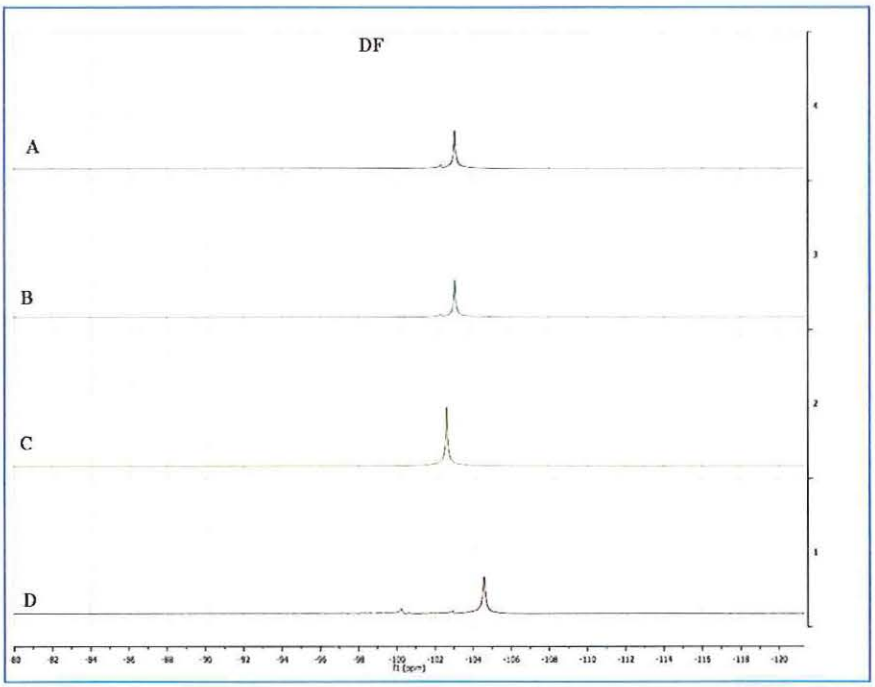

Figure 4.11. ^{19}F NMR spectra of DF (4) in CH_3CN (A), EtOAc (B), DMSO (C), and CH_2Cl_2

The ^{19}F NMR of PF, TF and DF in various solvents thus clearly show the importance of solvation. In case of TF and DF there is rapid exchange of the solvent molecules among the three boron centers of the complex so that only a single ^{19}F NMR absorption is observed for the all the aromatic ortho or *para* fluorines. However, in relatively more polar DMSO solvent, additional distinct absorptions for PF-DMSO adducts could be observed. This indicates relatively slow exchange of the DMSO with

PF. Unlike the starting boroxines, the boroxin-fluoride adducts (in the presence of excess fluoride anion) have similar $\delta^{19}F$ in all the solvents studied (CH_2Cl_2, acetonitrile, and DMSO), showing that the solvent participation is minimal in the case of the fluoride adducts.

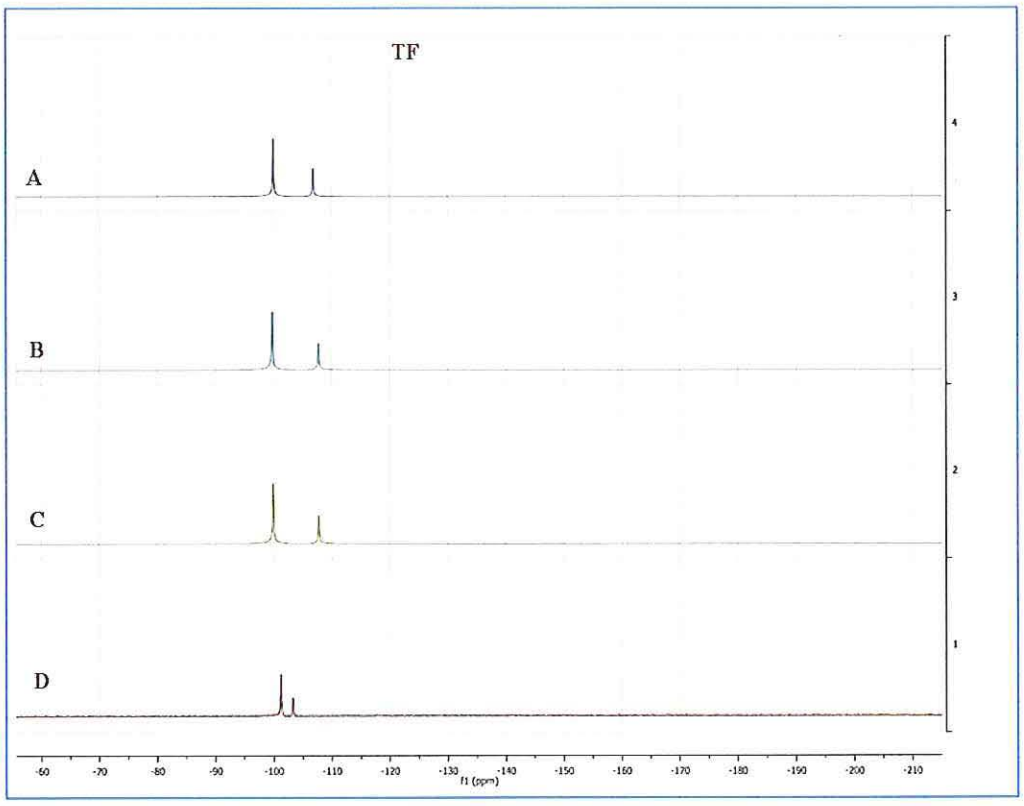

Figure 4.12. ^{19}F NMR spectra of TF (5) in CH_3CN (A), EtOAc (B), DMSO (C), and CH_2Cl_2

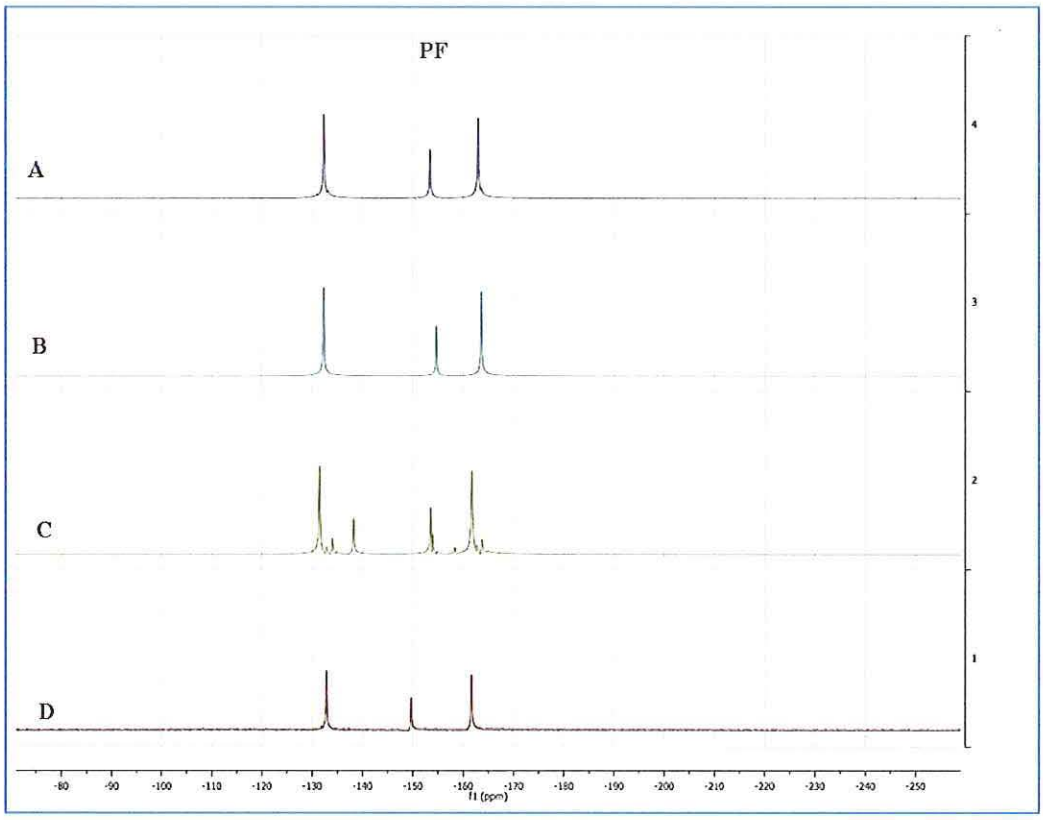

Figure 4.13. ^{19}F NMR spectra of PF (6) in CH_3CN (A), EtOAc (B), DMSO (C), and CH_2Cl_2

4.3.4 Fluoride Anion Binding. Fluoride anion binding to anion receptors helps not only the solubility of the otherwise insoluble lithium fluoride electrolyte in nonaqueous organic solvents, but also dramatically increases the lithium ion conductivities. Reversibility of fluoride anion binding is crucial in the next generation dual ion intercalating lithium ion batteries. In order to understand the structural effects on the fluoride binding to anion receptors we carried out DFT calculations on a series of fluorinated boroxines, and the results are shown in Table 4.2 and Figure 4.14. As can be

seen from (Figure 4.14) fluoride anion binding is correlated with the number of the fluorines on the aryl rings: the more the number of fluorines in the aryl rings, the higher the binding efficiency of the boronic anhydrides (boroxines). Because there is more than one boron capable of anion capture we estimated the binding energies for the second and third fluoride and report the data in Table 4.2. These calculations are less reliable because they involved highly charged species. Nonetheless it appears than multiple bindings are favorable (exothermic). Second and third anion binding energies do not follow the same trend as a function of fluorination that the first anion binding follows.

To understand the binding abilities of the fluorinated boroxines with fluoride anion we have carried out ^{19}F NMR spectroscopic studies for solutions of boroxines with varied amounts of TBAF. A series of samples of boroxines (23.25) were prepared in acetonitrile, dichloromethane, and DMSO, containing 0, 1, 2, and 3 equivalents of TBAF and $CFCl_3$ ($\delta CFCl_3 = 0$) as the internal reference, and the spectra were recorded in the unlocked mode. The ^{19}F and ^{11}B NMR spectra of the boroxin-fluoride complexes (26-28) in acetonitrile are summarized in Figure 4.16 and Figure 4.17 respectively. DF-Fluoride complex, 26 (with two equivalents of TBAF), shows a single absorption, $\delta^{19}F$ -110.4 (*ortho*-F). TF-fluoride complex, 27 (with two equivalents of TBAF), also shows only a single ^{19}F absorption at -107.9 ppm, due to the coincidental merging of the *ortho*- and *para*- fluorines; i.e., the *ortho*- fluorines are shielded much farther than the *para*-fluorine, with respect to the corresponding neutral boroxin. PF-fluoride complex, 28 (with one or two equivalents of TBAF), shows three ^{19}F absorptions at -139.3 (*ortho*-F), -155.3 (*meta*-F), -162.9 (*para*-F).

Table 4.2. Fluoride (F^-) anion binding energies (B3LYP, LACVP**), solvation energies and degree of fluorination for various fluorinated arylboroxines.

Compound	Degree of Fluorination	Binding Energy(Kcal/mol)
tris(pentafluorophenyl)boroxin (25)	15	74.1
(2,6-difluorophenyl)-bis(pentafluorophenyl)boroxin*	12	73.1
bis(2,6-difluorophenyl)-(pentafluorophenyl)boroxin*	9	71.0
bis(2,6-difluorophenyl)-(pentafluorophenyl)boroxin*	9	70.0
tris(2,4,6-trifluorophenyl)boroxin (24)	9	69.3
tris(2,6-difluorophenyl)boroxin (23)	6	67.5
tris(4.fluorophenyl)boroxin	3	61.6
Second Anion Captured		
*(2,6-difluorophenyl)-bis(pentafluorophenyl**)boroxin*	13	49.1
bis(2,6-difluorophenyl)-(pentafluorophenyl*)boroxin*	10	45.9

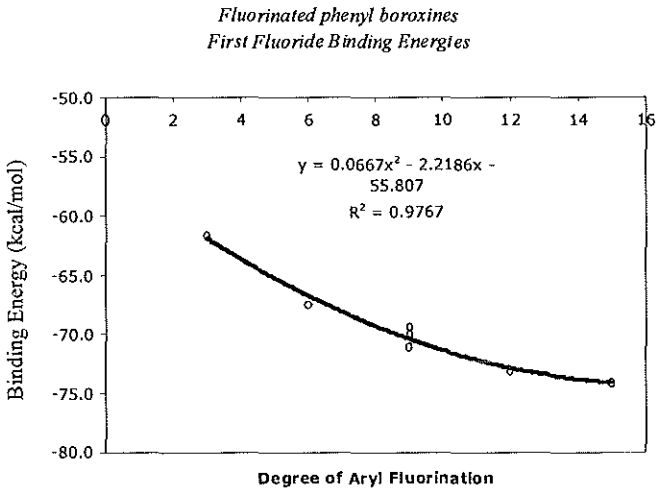

Figure 4.14. Effect of degree of aryl fluorination on the fluoride anion binding energies of arylboroxines from DFT (B3LYP).

The assignments of the chemical shifts of these boroxin-fluoride complexes, 26, 27, and 28, could be readily confirmed through their DFT-GIAO chemical shifts (Figure 4.15). The DFT-GIAO derived $\delta^{19}F$ for the *ortho*- fluorines in these complexes vary slightly from each other, whereas they show single absorptions in solution NMR, indicating rapid rotation across the B-aryl bonds in the solution phase. Further, the DFT values also reflect different chemical environments for the two sets of aryl groups. In solution, due to the rapid intramolecular exchange of the fluoride anion among the three borons, a single $\delta^{19}F$ absorption is observed (*vide infra*). The DFT-GIAO predicts a $\delta^{19}F$ of -166.7, -168.8, and -164.6 for the B-F fluorine in structures 26, 27, and 28, respectively. These absorptions could not be observed in solution, perhaps due to the rapid intramolecular fluoride anion exchange (*vide infra*).

Upon addition of 1 mol equivalent of TBAF to PF (25), in acetonitrile solvent, complete disappearance of the ^{19}F NMR peaks for the starting material was observed, and a three line ^{19}F NMR spectrum for PF-fluoride complex, 28, was observed: $\delta^{19}F$ -139.3, -155.3, -162.9 (Figure 4.16). However, for DF (23) and TF (24), upon addition of one mol equivalent of TBAF, a complex spectrum resulted with multiple absorptions corresponding to the boroxin-fluoride complexes (26 and 27), presumably because of their equilibration with unreacted boroxines. Addition of two mol equivalents of TBAF to these solutions resulted in surprisingly simplified spectra showing only one absorption (less than 0.1% of starting material could be observed by ^{19}F NMR).

These results show that PF has relatively stronger fluoride affinity as compared to those of DF and TF. The data in (Table 4.2) is also in accordance with these results; i.e., the higher the aryl-fluorination the stronger the fluoride binding. At first glance we would have expected distinct ^{19}F absorptions for the two sets of aromatic rings for complexes 26-28; i.e., the aryl rings bound to sp^3-hybridized boron are chemically different than those attached to sp^2-hybridized boron. The observation of a single *ortho*-^{19}F (or *para*-^{19}F) absoption for each of these complexes (with excess fluoride in case of DF and TF) shows that there is a rapid intramolecular fluoride exchange between the three borons (equation 2) with an upper limit of free energy of activation of 12.5, 12.4, and 12.0 kcal/mol for boroxin-fluoride compexes 26, 27, and 28 respectively (corresonding to exchange rate constants of 4400 s^{-1}, 4800 s^{-1} and 9200 s^{-1}, respectively).[34] Presumably due to this low barrier for exchange the $\delta^{19}F$ for B-F fluorine could not be observed in solution (*vide supra*).

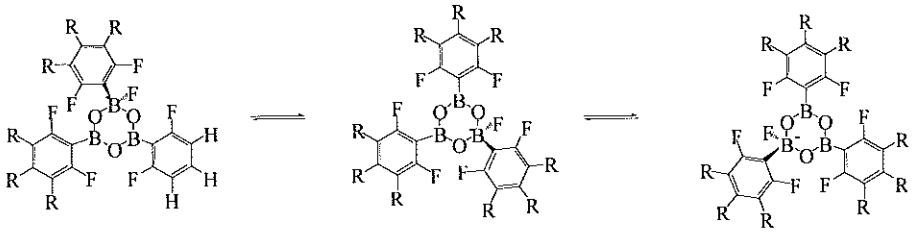

(2)

R = H; DF (**23**)

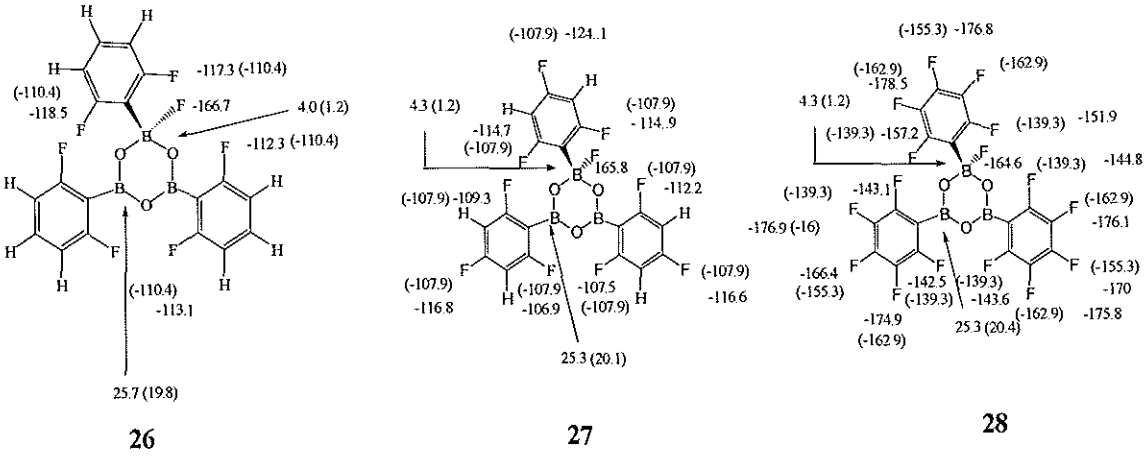

Figure 4.15. Experimental (acetonitrile solvent; $\delta^{19}F$ in parenthesis) and GIAO/B3LYP/6-31G** calculated $\delta^{19}F$ ($\delta CFCl_3 = 0$) for the boroxin-fluoride complexes (26-28); $\delta^{11}B$ are shown using arrows ($\delta BF_3OEt_2 = 0$).

Anion receptor PF (6), in acetonitrile, in the presence of 1 mol equivalent of fluoride, showed three new absorptions at -139.3 (*ortho*-F), -155.3 (*para*-F), -162.9 (*meta*-F) corresponding to the PF-fluoride complex, and the absorptions for PF have completely disappeared (Figure 4.16). Further addition of TBAF (2 to 3 mol equivalents) resulted in no change of the spectra, showing that the stoichiometry of the PF-fluoride complex is 1:1. The formation of the fluoride complex is essentially irreversible as the

absorptions corresonding to the starting PF could not be observed even after addition of one mol equivalent of TBAF. The *ortho*- fluorines are relatively more shielded in the PF-fluoride complex (28) as compared to the *meta*- and *para*-fluorines, as expected due to the proximity of the negatively charged boron.

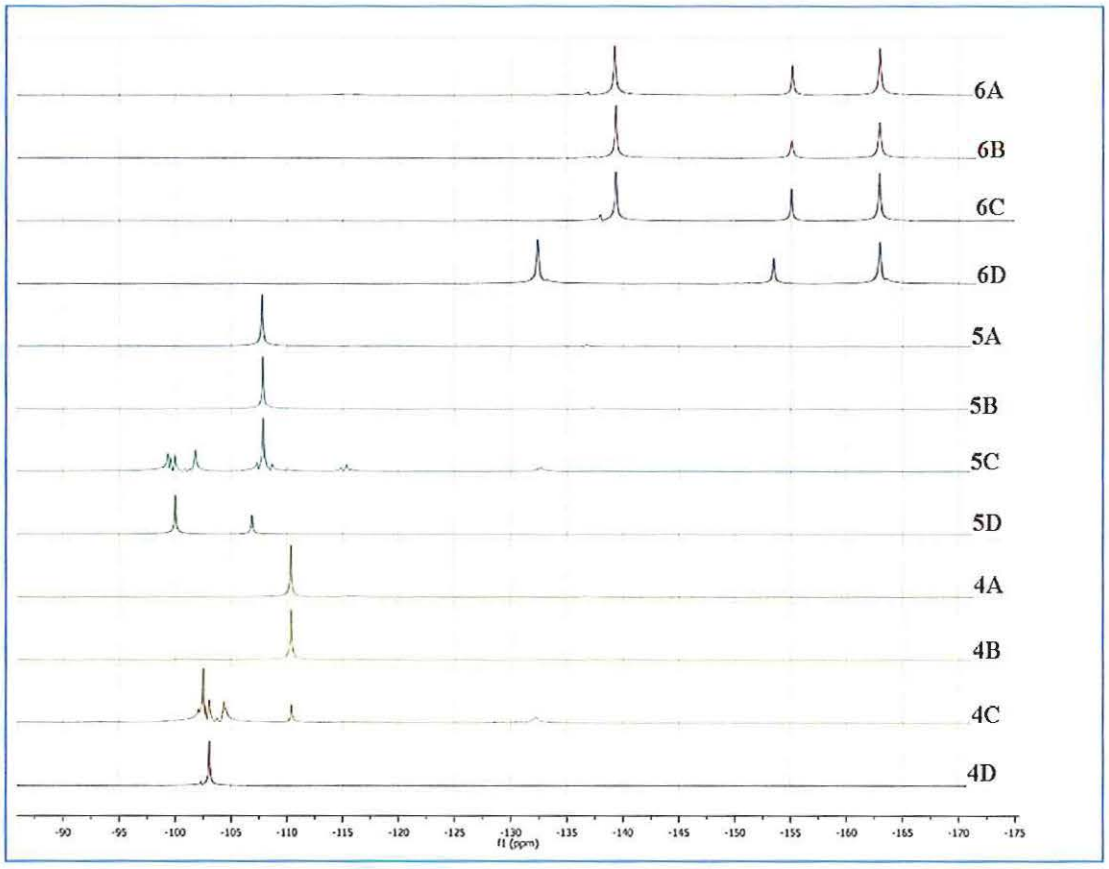

Figure 4.16. ^{19}F NMR (376MHz) spectra of DF (23), TF (24), and PF (25) in acetonitrile at various molar equivalents of TBAF: boroxin : TBAF = 1:3 (A); boroxin : TBAF = 1:2 (B); boroxin : TBAF = 1:1 (C); boroxin without added TBAF (D).

4.3.5 ^{11}B NMR Studies and GIAO Calculations. The ^{11}B NMR for the fluoride complexes (26, 27, and 28) are shown in Figure 4.17. DF-fluoride complex (26) shows two ^{11}B absorptions at δ^{11}B 19.8 (sp^2-B) and 1.2 (sp^3-B). TF-fluoride complex and PF-fluoride complexes similarly show two ^{11}B absorptions: δ^{11}B (TF): 20.1 (sp^2-B) and 1.2 (sp^3-B); δ^{11}B (PF): 20.4 (sp^2-B) and 1.2 (sp^3-B). The DFT-GIAO derived chemical shifts are in reasonably close agreement ($\Delta\delta$ = 2.8 to 5.9) with experimental values so that the assignments of the ^{11}B absorptions in the complexes could be confirmed.

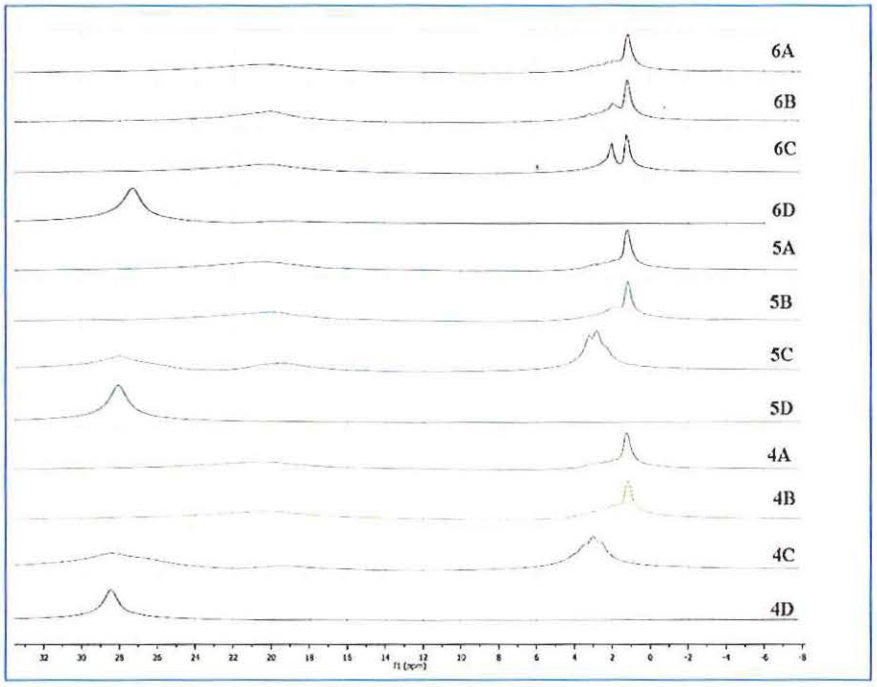

Figure 4.17. ^{11}B NMR (128 MHz) spectra of DF (23), TF (24), and PF (25) in acetonitrile at various molar equivalents of TBAF: boroxin : TBAF = 1:3 (A); boroxin : TBAF = 1:2 (B); boroxin : TBAF = 1:1 (C); boroxin without added TBAF (D).

In the presence of 1 mol equivalent of TBAF, about 20% of the unreacted starting materials could be observed in case of DF and TF, in addition to the above two ^{11}B absorptions for the fluoride complexes, 26 and 27, showing their equilibration with residual boroxines. Further, the chemical shifts of the sp^3-hybridized boron in complexes 26 and 27 is shielded by 2 ppm in the presence of two equivalents of TBAF, presumably due to the weak binding of the second fluoride anion to these complexes.

Addition of 1 mol equivalent of TBAF to PF, however, resulted in instantaneous complete disappearance of the starting material as monitored by ^{11}B NMR spectroscopy. The PF-fluoride complex, 28, showed three relatively broad signals at $\delta^{11}B$ 20.4 (sp^2-B) , 2.2 (sp^3-B),1.4 (sp^3-B) (Figure 4.15). Further addition of TBAF to this solution resulted gradual broadening of the peak at 2.2 ppm. Although we cannot clearly rationalize this unexpected observation for PF, perhaps a second fluoride anion binding may be involved in this case. In accordance with this expectation, UV-vis studies also show possible existence of multiple equilibria, i.e., co-existence of more than one PF-fluoride complex (*vide infra*). Upon further addition of up to 3 mol equivalents of TBAF the spectra for boroxin-fluoride complexes, 26, 27, and 28 remained unchanged.

4.3.6 UV-Vis Studies. UV-vis spectroscopy is commonly used to identify the stoichiometry of host-guest complexes.[35] In order to further confirm the ^{19}F NMR derived stoichiometry for the boroxin-fluoride complexes, we have carried out UV-vis studies for these complexes using continuous variation method (Job's plots).

UV-Vis spectra were recorded for a series of DF/TBAF (PF/TBAF) solutions; the mol ratios of DF to fluoride (PF to fluoride) were continually varied while keeping the total concentration of each of their solutions constant. The measured UV-vis absorbances at 265, 265, 260, and 64 nm (multiplied by mol fraction of boroxines) were plotted against mol fractions of the TBAF (Figure 4.18).[36-37] Through these Job's plots, stoichiometry of the DF-fluoride complex was determined as 1:1. In case of DF 1:1 stoichiometry is consistently observed at all wavelengths: 269, 265, 260, and 64 nm (Figure 4.18B) Stoichiometry of host-guest complexation is independent of UV-vis wavelength in Job's plots, if a single complex is formed. On the other hand, dependence of Job's maxima on wavelength is indicative of the co-existence of more than one complex.[35],[38-39] The Job's plots for PF, show deviations from 1:1 stoichiometry at different wavelengths, indicating the possible co-existence of more than one complex for PF (Figure 4.18C) (*vide supra*).

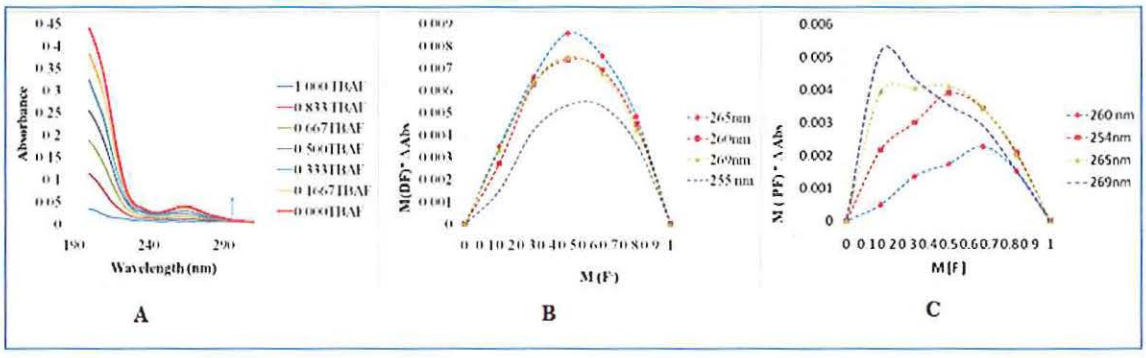

Figure 4.18. UV-Vis Spectra (in acetonitrile) obtained from continuous variation method (A), and Job's plots for DF(B) and PF(C); B and C are the overlay plots for absorbances at 269, 265, 260 and 65 nm.

4.3.7 *Ab initio* Structures of Boroxin-Fluoride Complexes. We have optimized structures of symmetrically bound and unsymmetrically bound fluoride anion complexes of DF at B3LYP/6-31G** level in order to clarify the nature of the fluoride anion binding to the cyclic boroxines. Aldridge and coworkers have earlier shown that a related tribora-macrocyclic compound, 1,4,7-trifloro-1,4,7-triboracyclononane (30) (Figure 4.19) and its perfluorinated analog have symmetrical fluoride anion binding to all three boron atoms, at HF/6-31+G* level.[40]

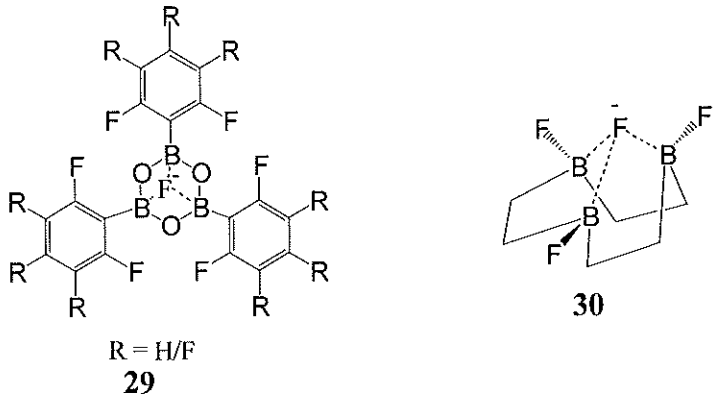

Figure 4.19. Structures of fluorinated boroxin and 1,4,7-trifloro-1,4,7-triboracyclononane showing symmetircal fluoride binding.

However, we have found at higher DFT levels of calculations at B3LYP/6-311G** that the symmetyrical C_{3v} structure for the complex, 29, is relatively 12.5 kcal/mol higher in energy as compared to that of the unsymmetrically bound species, 26. Structures 26 and 29 are energy minima on the potential energy surface at this level of theory (Figure 4.20). The relatively low energy for the unsymmetric structure (26) implies its entropic advantage over the symmetric structure, 29. The fluoride bound

complex, 26, shows significantly upfield shifted ^{19}F signals for the fluorine atoms attached to aromatic rings. However, we were not able to observe the absorptions corresponding to the fluoride anion attached to boron.

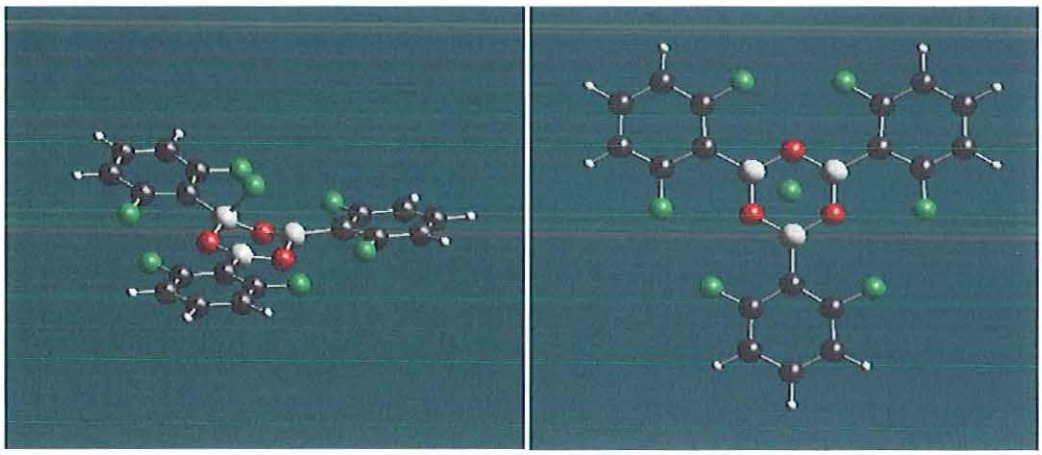

Figure 4.20. B3LYP/6-311G** structures of asymmetic and symmetrically bridged [DF-F]$^-$ complexes, coresonding to structures 26 (left) and 29 (right).

The lack of detection of the boron-bound fluoride absorption indicates that there is rapid equilibrium between three unsymmetrical structures relative to the NMR time scale at ambient temperature with an estimated free energy of activation of 12.0 to 12.5 kcal/mol (*vide supra*). Geometries for the PF and [PF-F]$^-$ are shown in (Figure 4.21). In the neutral form the PF anion receptor is a propeller shape molecule with a small angle (36.4 degrees) between the boroxin ring and the phenyl groups. In the charged state [PF-F]$^-$ the boron atom that captures the fluoride anion becomes more tetragonal and the propeller angle increases significantly (79.7 degrees).

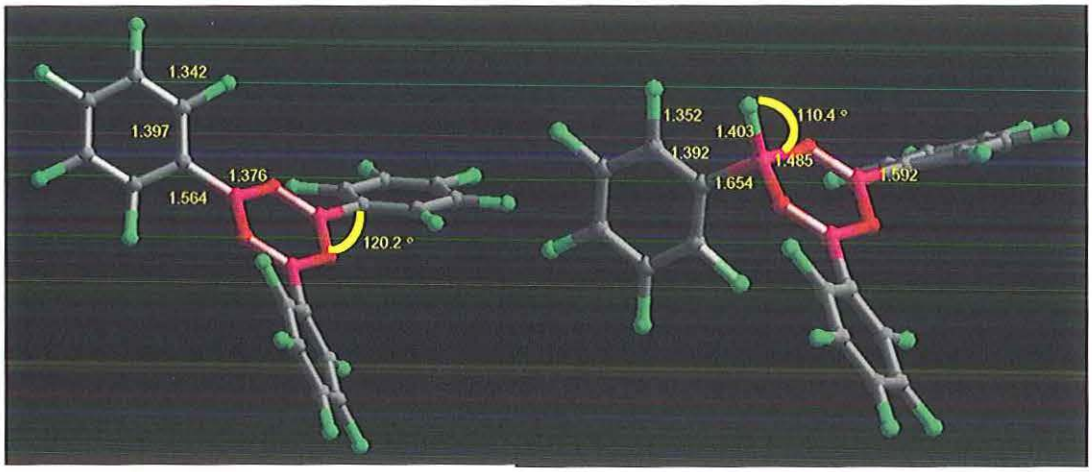

Figure 4.21. B3LYP/6-311G** solution (propylene carbonate) geometry-optimized structures of neutral PF (left) and the corresponding charged $[PF\text{-}F]^-$ complex (right).

4.3.8 Tandem Mass spectroscopic Studies of Boroxin Fluoride Complex. In light of the importance of the selective binding of the electrolyte materials to the anion receptors, it is useful to characterize the structural details of the boroxin-anion complexes. Electrospray ionization mass spectroscopy in the negative ion mode is ideally suited for characterization of the stoichiometry of the fluoride anion complexes.[41-42] Competitive ESI-MS studies also would provide quantitative information on the relative bidning affinities. Further, the tandem mass spectrometric fragmentations would reveal the mechanistic aspects of the rearrangements involved in the fragmentations. We now report the electrospray mass spectrometric characterization of the molecular ion complexes for these fluorinated boroxines, also substantiated by the DFT studies. Electrospray ionization mass spectroscopy (ESI-MS) is expected to show the molecular ion peaks for the boroxin anion complexes, and thus direct characterization of the anion

complexes could be achieved. The molecular ion peaks for the fluoride anion adducts for DF, TF, and PF, corresponding to m/z of 439, 493 and 601, respectively were observed. The observed isotopic ratios for MF-2, MF-1, MF, and MF+1 for DF-F$^-$, TF-F$^-$, and PF-F$^-$ are generally in accordance with the calculated ratios, confirming these peaks as the molecular ion peaks for the fluoride adducts(Figure 4.22).

Tandem mass spectrometry is useful in the characterization of the fragmentation mechanisms. The fragmentation mass spectrum obtained by the collision induced dissociation (CID) of the DF-fluoride (26) molecular ion peak at 439 showed appearance of the peaks at m/z 345, 61, 113 (Figure 4.23). These m/z values could be readily assigned to the anion species 26a, 26b, and 26c arising from the successive eliminations of 3.fluorobenzyne and 1,3,5-trifluoroboroxin, as shown in (Scheme 4.11). Similar fragmentation pattern was observed in case of other boroxines fluoride complexes, TF-F$^-$ and PF- F$^-$.

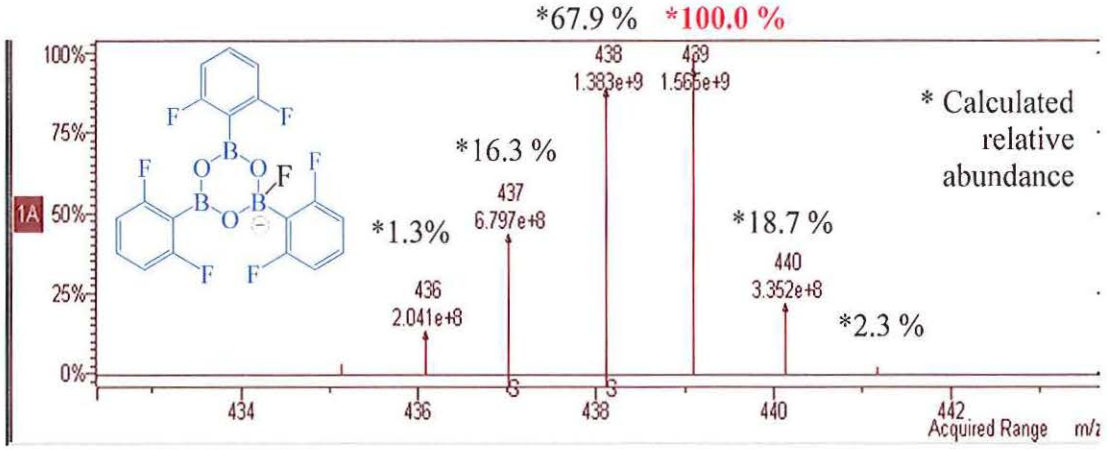

Figure 4.22. Electron spray ionization mass spectrum (ESI/MS) of DF-Fluoride complex showing isotopic pattern.

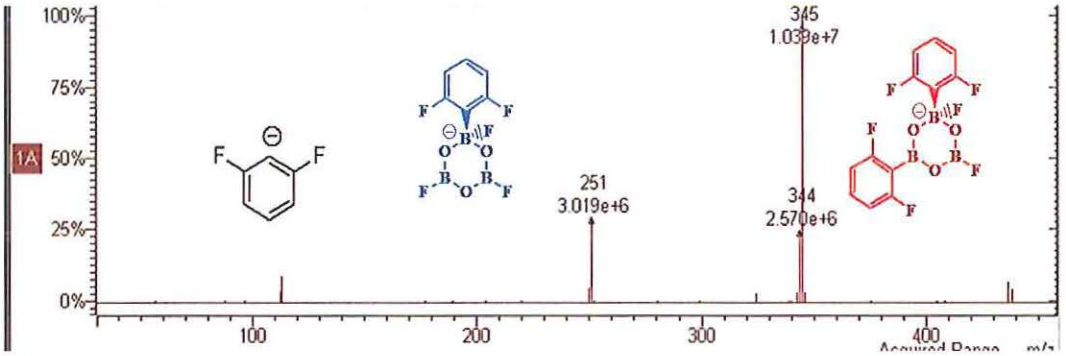

Figure 4.23. ESI/MS spectra showing the molecular ion peaks for the boroxin-fluoride complexes, DF-F$^-$, TF-F$^-$, and PF-F$^-$.

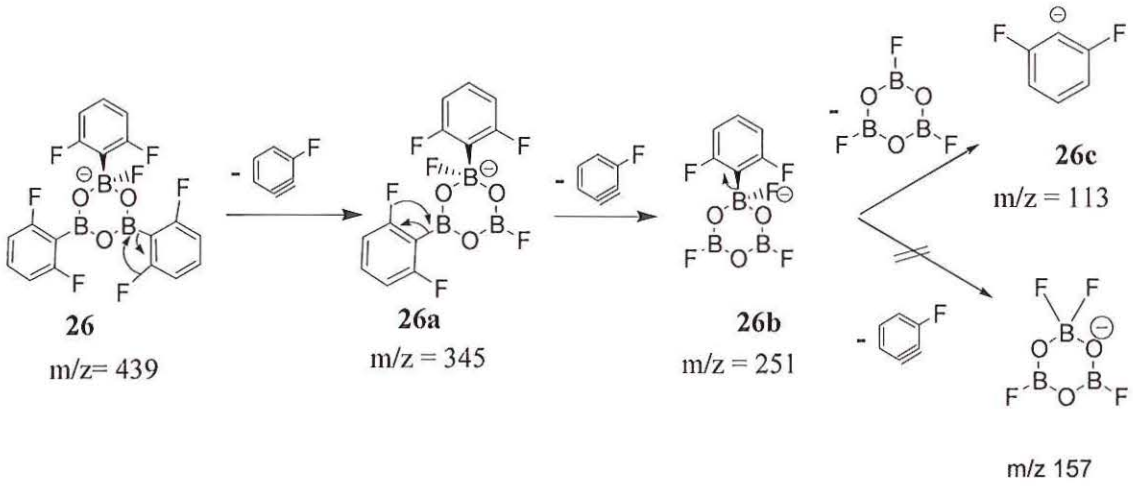

Scheme 4.10. Proposed mechanism for the mass spectral fragmentation of DF-fluoride complex.

4.3.9 Theoretical Studies: 1,3-sigmatropic Rearrangement. The fragmentation pattern of the ESI-MS/MS of the DF, TF, and PF fluoride anion complexes show the involvement of a 1,3.sigmatropic migration of the *ortho*-fluorine from the aryl rings to boron in concert with elimination of fluorobenzyne (Scheme 4.10). Such 1,3.fluoride migrations to boron have not been reported to date to the best of our knowledge, although several such shifts have been observed for the allyl fluorides.[43-45] The 1,3.sigmatropic fluorine sifts to silicon have also been reported in the 2.phoshspha-1,3.disilallyl fluoride derivative.[46] Recent DFT theoretical studies indicate that this allowed suprafacial rearrangement proceeds with a four membered C_s transition state in which migrating fluorine has a charge of -0.6e.[47] The 1,3.sigmatropic fluorine migrations to boron have never been reported to the best of our knowledge. In order to probe the nature of the 1,3.sigmatropic shift of fluoride to boron we have calculated the transition structures for these sigmatropic shifts for $[DF\text{-}F]^-$ anion complexes using structures 31 as a small molecule model compound. We have also carried out similar calculations on the negatively charged model compound 31, in order to see if fluoride migrations can take place to the sp^3-B center.

The calculated transition structures (Figure 4.24) have a single negative eigen value and the negative imaginary frequency corresponded to the migrating fluorine bonds, as shown by the IR spectral animations. The activation barriers for the 1,3.shift of fluorine for compounds 31 and 32 at B3LYP/6-311G** were found to be 32.3 and 56.2 kcal/mol, respectively (equations 3 and 4).

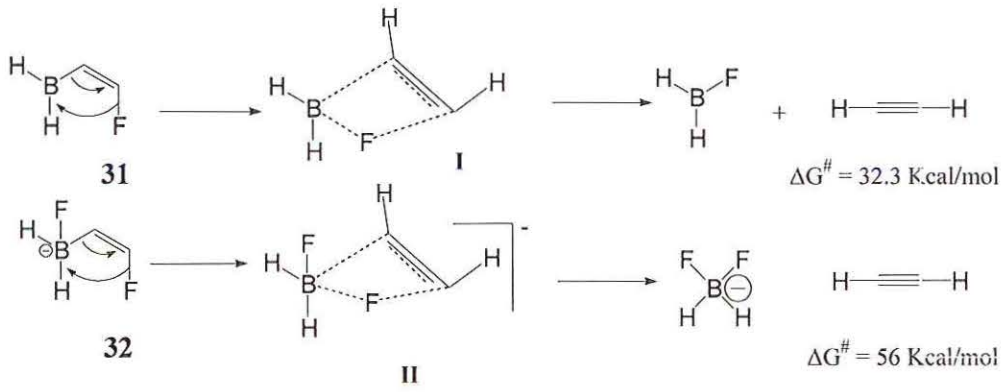

Thus expectedly, the 1,3.shift of fluorine to the electrophilic sp^2 B (in compound 31) is relatively much faster than that of the sp^3 B center (in compound 32). In accordance with these DFT computations, the fragment ion 26b gave anion 26c by the cleavage of the boron-aryl bond, and the corresponding 1,3-sigmatropic fluorine migration was not observed(Scheme 4.11).

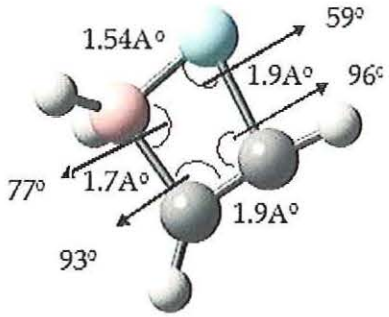

Figure 4-24. Transition state for fluoride migration (II)

4.3.10 Competition Binding Studies of Boroxin- Fluoride Complexes. Earlier DFT computations show that as the number of fluorine atom on the aryl rings of boroxines increase their binding efficiency increases.[48] The isodesmic reactions for the competitive binding of fluoride to DF, TF, and PF, at B3LYP/6-311G**, show that the PF-fluoride complex is more stable than DF-fluoride and TF-fluoride complexes by 6.6 kcal/mol, and 4.8 kcal/mol, respectively, implying insignificant amounts of DF-fluoride and TF-fluoride complexes (0.0014% and 0.029%, respectively) in an equilibrium mixture of all these three boroxines in the presence of fluoride anion (equations 5 and 6).

Expected ratio: PF-F]⁻ : DF-F]⁻ = 99.998 : 0.0014 (5)

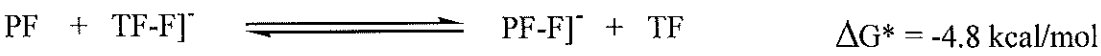

(6)

Expected ratio: PF-F]⁻ : TF-F]⁻ = 99.97 : 0.029

Indeed, when an equimolar mixture of DF, TF, PF in the presence of of 0.33 mol equivalent TBAF was subjected to ESI mass spectrometric analysis, the appearance of exclusively PF-fluoride complex at m/z 601(Figure 4.25) was found. The mass peaks due to the DF-floride and TF-fluoride complexes were observed under these conditions, which is in accordance with these calculations.

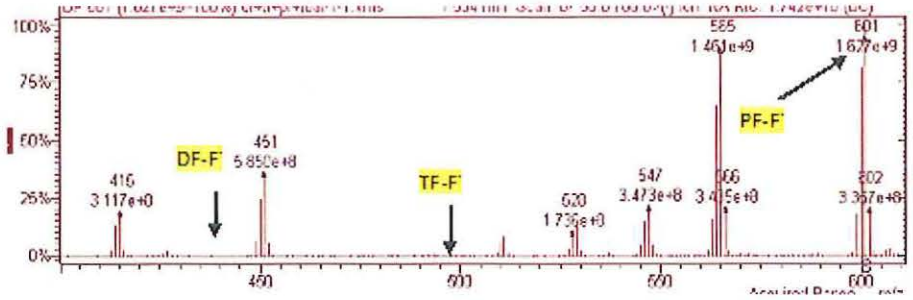

Figure 4.25. ESI/MS spectrum of equimolar mixture of DF, TF and PF in the presence of 0.33 equivalents of TBAF.

Lithium hexafluorophosphate is commonly added as supporting electrolyte in the lithium ion batteries, and therefore it is interesting to compare its relative binding efficiency with anion receptors. It would be also informative to compare the fluoride anion binding strength with that of other commonly used halide anions.

Thus, we have extended these anion binding studies to other halide anions (chloride, bromide, and iodide anions), and hexafluorophosphate. When each of these boroxines was separately mixed with TBACl, TBABr, TBAI, and $TBAPF_6$ and subjected to negative ion ESI mass spectrometry, we have not been able to observe the corresponding molecular ion peaks for the anion adducts(equation 7, 8 and 9, (No detectable MX]- peaks) in ESI-MS).

$$DF \xrightleftharpoons{BuN^{+}X^{-}} DF\text{-}X]^{-} \quad (7)$$

$$X = Cl^{-}, Br^{-}, PF_6^{-}$$

$$TF \xrightleftharpoons{BuN^{+}X^{-}} TF\text{-}X]^{-} \quad (8)$$

$$X = Cl^{-}, Br^{-}, PF_6^{-}$$

$$PF \xrightleftharpoons{BuN^{+}X^{-}} PF\text{-}X]^{-} \quad (9)$$

$$X = Cl^{-}, Br^{-}, PF_6^{-}$$

The ESI mass spectrum of an equimolar mixture of the DF, TBACl, TBABr, TBAI, TBAF, on the other hand, showed exclusively the molecular ion peak for the DF-F anion complex (Figure 4.26). These results imply the extremely weak binding affinities of chloride, bromide, iodide, and hexafluoroposphate anions to the boroxines.

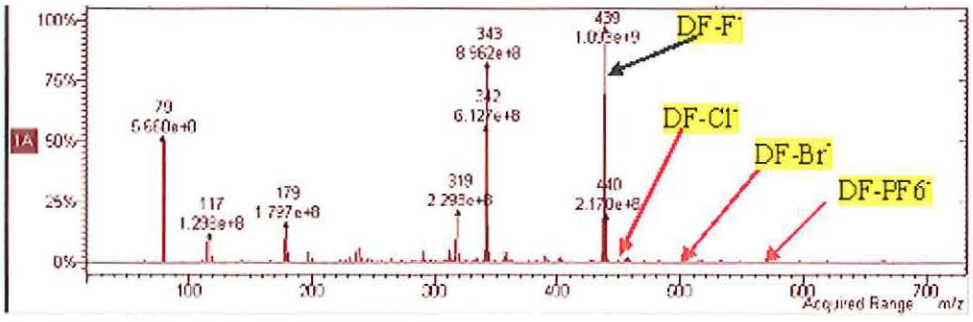

Figure 4.26. ESI/MS spectrum of an equimolar mixture of DF , TBACl, TBABr, TBAI, TBAF.

4.3.11 NMR Studies of Anion Binding. ^{19}F NMR titration of DF with tetrabutyl ammonium salts of anions such as tetrabutylammonium chloride (TBACl), tetrabutyl ammonium bromide (TBABr), tetrabutylammonium iodide(TBAI), and tetrabutylammonium phosphate ($TBAPF_6$) resulted in no upfield shift of peaks due to anion binding even at DF: anion ratio of 1:2 , indicating that there is either no binding or week binding. The relatively small downfield shift may be due to salt effect (Figure 4.27).In summary, fluorinated arylboroxines are efficient anion receptors, comparable to the state-of- the-art PFPB anion receptor.[24-25, 33] The structures of the fluoride complexes DF, TF, and PF are confirmed by matching the experimental ^{19}F and ^{11}B NMR chemical shifts with those obtained from DFT calculations. Further EI/MS studies confirmed the structure of these boroxines.Our *Ab-initio* calculations show that the symmetrically bound fluoride complex, 29, is, unexpectedly, less favorable as compared to the unsymmetrically bound species, 26, by 12.5 kcal/mol. The coalescence of the ^{19}F NMR signals of these boroxines at ambient temperature shows relatively rapid equilibration of the fluoride anion among the three boron atoms in these boroxines, with an estimated upper limit of about 12 kcal/mol.

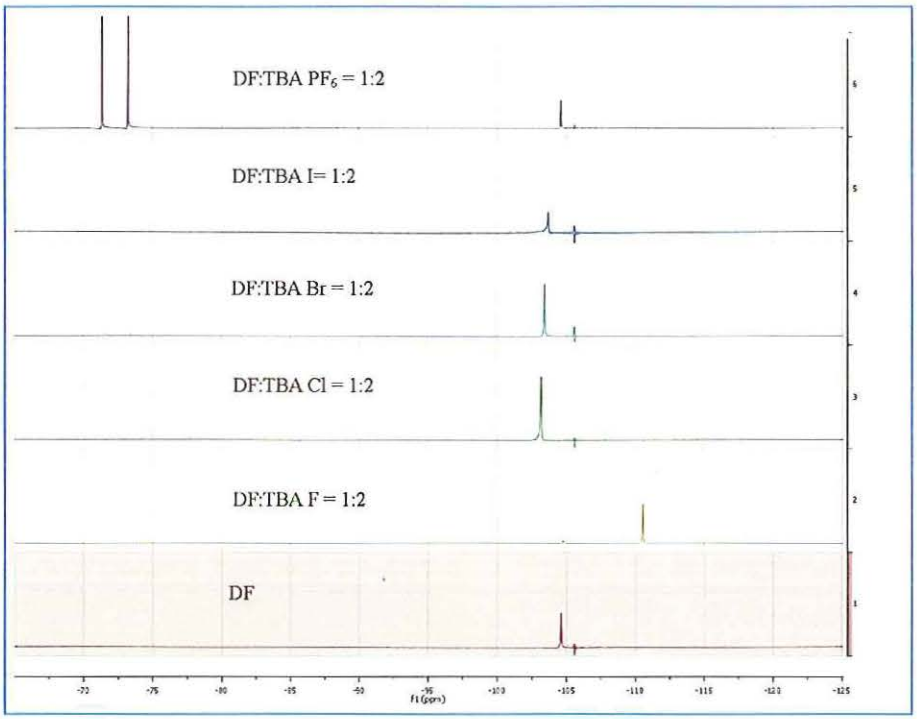

Figure 4.27. ^{19}F (376 MHz) NMR spectra of DF in dichloromethane in the presence of 2 equivalents of tetrabutyl ammonium salts of anions , TBAF, TBACl, TBABr, TBAI, and $TBAPF_6$.

Our electrospray mass spectroscopic studies in combination with *ab intio* DFT theory show that the fluorinated boroxines are highly selective to fluoride anion binding, and their relative binding to other halide anions and hexafluorophosphate is insignificant. Using tandem ESI mass spectroscopy we have characterized the fragmentation patterns for the fluorinated boroxin-fluoride anion complexes and identified the first 1,3.sigmatropic shift of fluorine to boron. The activation barriers for the 1,3.fluoride anion migration to boron has been estimated as 32.3 kcal/mol at B3LYP/6-311G**.

4.4 EXPERIMENTAL SECTION

4.4.1 Materials. Acetonitrile (anhydrous, >99.8%), dimethylsulfoxide (>99.6%, dichloromethane (>99.8%), ethyl acetate (>99.5%), and tetrabutylammonium fluoride hydrate (>98%) were obtained from Aldrich and used as received. The fluorinated boroxines DF (23), TF (24), and PF (25) were obtained by thermal dehydration of the corresponding arylboronic acids, at 100 °C for about one hour.[27] The products were obtained essentially pure as confirmed by their ^{19}F NMR and ^{11}B NMR spectra (*vide infra*). Further confirmation of the structures were provided by matching the observed chemical shifts with those obtained at GIAO/B3LYP/6-31G** level.[30]

4.4.2 NMR Spectra. ^{19}F NMR spectra (at 376 MHz) and ^{11}B NMR spectra (128 Hz) were obtained on a Varian Inova 400 MHz spectrometer in anhydrous CH_3CN (in unlocked mode) or CD_3CN solutions. ^{19}F NMR spectra referenced to $CFCl_3$ ($\delta^{19}F = 0$), and ^{11}B NMR spectra are referenced to $BF_3.OEt_2$ ($\delta^{11}B = 0$). All the NMR spectra were processed using MestReNova 6.2.0 software.

A series of solutions (about 200 mM) of boroxines (DF, TF, and PF) were prepared by dissolving each of the boroxines in various solvents (acetonitrile, DMSO, ethyl acetate, and dichloromethane), and appropriate amounts of tetrabutylammonium fluoride (TBAF) was added to them so that the resulting solutions had mol ratios of boroxin:fluoride as 1:0, 1:1, 1:2 and 1:3. These homogenous solutions were transferred into 5 mm NMR tubes, $CFCl_3$ was added as an internal reference, and ^{19}F NMR spectra were recorded at ambient temperature. ^{11}B NMR spectra were obtained for the same solutions using $BF_3.$etherate as external reference.

The reaction of boroxines (DF, TF, and PF) with fluoride anion was exothermic. A clear homogeneous solutions resulted immediately after the addition of TBAF to DF and TF. However, reaction of PF with TBAF gave homogeneous solutions only in DMSO, acetonitrile and dichloromethane, but not in ethyl acetate. The ^{11}B and ^{19}F NMR spectra for the boroxines and their fluoride complexes 26, 27, and 28 (1:1 mol ratio) in acetontrile are as follows:

DF: $\delta^{19}F$ -103.0 (broad s); $\delta^{11}B$ 28.5.

TF: $\delta^{19}F$ -99.9 (apparent triplet, J = 7.5 Hz, *ortho*-F), 106.8 (t, J = 8 Hz; *para*-F); $\delta^{11}B$ 28.0.

PF: $\delta^{19}F$ -132.4 (m, *ortho*-F), -153.7 (t, J = 19 Hz, *para*-F), -163.5 (m, *meta*-F). $\delta^{11}B$ 27.3 (broad s), 20.4 (broad s).

Complex 26: $\delta^{19}F$ -110.4 (broad s, *ortho*-F); (additional small peaks, $\delta^{19}F$ -102 to -105, were observed, presumably corresponding to multiple fluoride exchange equilibria).; $\delta^{11}B$ 28.5(broad s), 20.4(broad s), 3.0(m).

Complex 27: δ^{19} -107.9 (m, *ortho*- and *para*-F) (additional small peaks, $\delta^{19}F$ -98 to -115, were observed, presumably corresponding to multiple fluoride exchange equilibria); $\delta^{11}B$ 28.0(broad s) , 20.1(broad s), 2.8(m).

Complex 28: PF: $\delta^{19}F$ -139.3 (m, *ortho*-F), -155.3 (t, *para*-F), -162.9 (m, *meta*-F). $\delta^{11}B$ 20.4(broad s), 1.95 (broad s), 1.2 (m).

Addition of 2 mol equivalents of TBAF simplified the ^{19}F NMR spectra of the complexes 7 and 8. There was no apparent change in the spectra of complex 9. The $\delta^{19}F$ remained constant upon further addition of up to 3 mol equivalents of TBAF to each of these complexes (7, 8, and 9). The ^{19}F and ^{11}B NMR spectra of these complexes with two mol equivalents of fluoride anion are as follows:

Complex 26 (with excess TBAF): $\delta^{19}F$ -110.4 (broad s); $\delta^{11}B$ 20.4 (broad s), 1.2 (broad s).

Complex 27 (with excess TBAF): $\delta^{19}F$ -107.9 (m, *ortho*- and *para*-F); $\delta^{11}B$ 20.4, 1.2.

Complex 28 (with excess TBAF): $\delta^{19}F$ PF: $\delta^{19}F$ -139.3 (m, *ortho*-F), -155.3 (t, J = 19 Hz, *para*-F), -162.9 (m, *meta*-F); $\delta^{11}B$ 20.4 (broad s), 1.2 (broad s).

4.4.3 UV-Vis Spectroscopic Studies. UV-Vis spectroscopic studies were carried out on a Cary-50 UV-vis spectrophotometer equipped with a 1.cm path-length quartz cell by monitoring the absorbances between 200 to 300 nm. The micropipettes used were capable of delivering 1 mL solutions, having adjustable ranges between 100 μL – 1000 μL. All UV-Vis measurements were performed at ambient temperature. 1 x 10^{-5} M Stock solutions of DF (23), PF (25), and tetrabutylammonium fluoride (TBAF) were prepared in acetonitrile. Stoichiometry of the DF-fluoride (PF-fluoride) complexes was determined using Job's continuous variation method as follows:

A series of solutions consisting of DF (PF) and TBAF were prepared by mixing the above stock solutions so that the total concentration of the combined solutions was maintained constant at 1 x 10^{-5} M, and the UV absorbances were recorded separately for

each solution. Stoichiometry of the complexes was determined by a plot of the absorbances (multiplied by mol fraction of boroxines) versus mol fractions of the TBAF.

4.4.4 *Ab- Initio* Calculations. We conducted thermodynamic calculations, in the form of electronic energies, solvation free energies in propylene carbonate, and binding energetics using Quantum Mechanical Density Functional Theory (B3LYP)[49] for reactions of fluoride anion binding to novel fluorinated phenyl boroxin anion receptors. We performed full geometry optimizations with solvation effects obtained through a continuum dielectric model.[50] The molecular solvation surface of the anion receptor was defined with the molecular radius (2.7Å) and dielectric constant of propylene carbonate (ε=64.5). All wave functions are open shell (UDFT), calculated with a high level basis set (LACVP**) which translates to 6-311 G** basis for main group elements. *Ab-initio* calculations were carried out on a Dell Linux Cluster (80 node/160 core, Single Core Xeon, 3.06GHz) running Linux/OSCAR, with 160GB of RAM, and 8.6TB of disk space. ^{11}B and ^{19}F NMR chemical shifts were calculated using density functional theory, at B3LYP/6-311G** level) for the various fluorinated receptors and fluoride complexed anions. The geometries were fully optimized (basis set 6-311G**) in a continuum dielectric medium appropriate for propylene carbonate (PC). The ^{19}F and ^{11}B NMR chemical shifts are computed with respect to $CFCl_3$ ($\delta^{19}F = 0.0$) and BF_4^- ($\delta^{11}B = 0.0$), respectively. The latter $\delta^{11}B$ (BF_4^-) are re-converted to $\delta^{11}B(BF_3.Et_2O)$. ($\delta^{11}B(BF_4^-) = -2.2$ with respect to $\delta^{11}B$ ($BF_3.OEt_2$; $\delta^{11}B = 0$).

4.4.5 Mass Spectroscopic Studies. EI/MS spectra were obtained on Hewlett Packard 59892A Mass spectrometer. The HP 59882A direct insertion probe provided the way to introduce solid in to the EI ion source. Approximately 1mg of the sample was placed in a piece of glass capillary tubing and is loaded in to the tip of the probe.The probe was inserted in to the MS engine ion source. EI/MS spectra were recorded at 70eV. The oven temperature was ramped from 50 ^{0}C to 280 ^{0}C at 20 ^{0}C/min and then heated for 5 minutes at 280 ^{0}C.ESI/ MS/MS studies were carried out on a Varian 1200L Quadrupole MS/MS spectrometer. All the experiments were done in negative ion detection scan mode (m/z = 50 to 600). Needle voltage of -4500 Volts, drying gas temperature of 50 ^{0}C to 100 ^{0}C, and a flow rate was 50 µL/min were used. Nitrogen was used as the nebulizing gas.The parent molecular ion (M^-) in ESI/MS was used for Tandem MS analysis. The instrumentation conditions are as follows: negative ion detection, scan mode, needle voltage = 4500, detector voltage = 1600 Volts, syringe solvent flow rate = 50 µL/min, nebulizing gas = nitrogen, collision gas = argon. The drying gas temperature was varied between 50 ^{o}C and 100 ^{o}C for optimal conditions; The ESI-MS molecular ion peaks for the DF, TF, and PF fluoride complexes are as follows: DF-Fluoride complex (MF^-), m/z = 439; MF-2:MF-1:MF: MF+1 = 43:88:100:21 (calculated ratio 16:68:100:19); TF-Fluoride complex (MF^-), m/z= 493, MF-2:MF-1:MF:MF+1 = 32:98:100:21 (calculated ratio 16:68:100:19); PF-Fluoride complex (MF^-), m/z= 601, MF-2:MF-1:MF:MF+1 = 38:98:100:35 (calculated ratio 16:68:100:19). The CID-MS/MS of the DF-Fluoride ion complex at m/z 439 showed peaks at m/z 345, 61 and 113; The CID-MS of the TF-Fluoride ion complex at m/z 493 showed peaks at m/z 369,281 and 131; The CID-MS of the PF-Fluoride ion complex at m/z 601 showed peaks at m/z 453, 305 and 167.

4.5 REFERENCES

[1] J. L. Sessler, P. A. Gale, W.-S. Cho, *Anion Receptor Chemistry*, **2006**.

[2] C. R. Wade, A. E. J. Broomsgrove, S. Aldridge, F. o. P. Gabbai□, Fluoride Ion Complexation and Sensing Using Organoboron Compounds, *Chem. Rev.* **2010**, *110*, 3958.

[3] K. Severin, Self-assembled organometallic receptors for small ions, *Coord. Chem. Rev.* **2003**, *245*, 3.

[4] W. C. West, J. F. Whitacre, N. Leifer, S. Greenbaum, M. Smart, R. Bugga, M. Blanco, S. R. Narayanan, Reversible intercalation of fluoride-anion receptor complexes in graphite, *J. Electrochem. Soc.* **2007**, *154*, A929.

[5] A. Bianchi, K. Bowman-James, E. Garcia-Espana, Editors, *Supramolecular Chemistry of Anions*, **1997**.

[6] D. F. Shriver, M. J. Biallas, Observation of the chelate effect with a bidentate Lewis acid, F2BCH2CH2BF2, *Journal of the American Chemical Society* **1967**, *89*, 1078.

[7] H. E. Katz, Hydride sponge: complexation of 1,8-naphthalenediylbis(dimethylborane) with hydride, fluoride, and hydroxide, *Journal of Organic Chemistry* **1985**, *50*, 5027.

[8] H. E. Katz, Hydride sponge: 1,8-naphthalenediylbis(dimethylborane), *Journal of the American Chemical Society* **1985**, *107*, 1420.

[9] H. E. Katz, 1,8-Naphthalenediylbis(dichloroborane) chloride: the first bis boron chloride chelate, *Organometallics* **1987**, *6*, 1134.

[10] V. C. Williams, W. E. Piers, W. Clegg, M. R. J. Elsegood, S. Collins, T. B. Marder, New Bifunctional Perfluoroaryl Boranes. Synthesis and Reactivity of the ortho-Phenylene-Bridged Diboranes 1,2-[B(C6F5)2]2C6X4 (X = H, F), *Journal of the American Chemical Society* **1999**, *121*, 3244.

[11] S. Sole, P. Gabbai Francois, A bidentate borane as colorimetric fluoride ion sensor, *Chemical communications (Cambridge, England)* **2004**, 1284.

[12] M. Melaimi, P. Gabbai Francois, A heteronuclear bidentate Lewis acid as a phosphorescent fluoride sensor, *J Am Chem Soc* **2005**, *127*, 9680.

[13] G. A. Olah, K. Laali, O. Farooq, Chemistry in superacids. 6. Perfluoroalkanesulfonic acid-boron perfluoroalkanesulfonates: new superacid systems for generation of carbocations and catalysts for electrophilic transformations of hydrocarbons, *J. Org. Chem.* **1984**, *49*, 4591.

[14] C. Bergquist, B. M. Bridgewater, C. J. Harlan, J. R. Norton, R. A. Friesner, G. Parkin, Aqua, Alcohol, and Acetonitrile Adducts of Tris(perfluorophenyl)borane: Evaluation of Bronsted Acidity and Ligand Lability with Experimental and Computational Methods, *J. Am. Chem. Soc.* **2000**, *122*, 10581.

[15] J. Pless, W. Bauer, Boron tris(trifluoroacetate) for cleaving protective groups in peptide chemistry, *Angew. Chem.* **1973**, *85*, 142.

[16] G. A. Olah, O. Farooq, C. X. Li, M. A. M. Farnia, J. J. Aklonis, Cationic ring-opening polymerization of tetrahydrofuran with boron, aluminum, and gallium tristriflate, *J. Appl. Polym. Sci.* **1992**, *45*, 1355.

[17] P. v. R. Schleyer, H. Jiao, N. J. R. van Eikema Hommes, V. G. Malkin, O. Malkina, An Evaluation of the Aromaticity of Inorganic Rings: Refined Evidence from Magnetic Properties, *Journal of the American Chemical Society* **1997**, *119*, 12669.

[18] D. W. Lamb, R. I. Keir, G. L. D. Ritchie, Polarizability and magnetizability anisotropies of trimethylboroxine, Me3B3O3. Comparison of boroxine and benzene ring systems, *Chemical Physics Letters* **1998**, *291*, 197.

[19] H. R. Snyder, M. S. Konecky, W. J. Lennarz, Aryl boronic acids. II. Aryl boronic anhydrides and their amine complexes, *Journal of the American Chemical Society* **1958**, *80*, 3611.

[20] J. Kua, P. M. Iovine, Formation of Para-Substituted Triphenylboroxines: A Computational Study, *Journal of Physical Chemistry A* **2005**, *109*, 8938.

[21] W. L. Fielder, M. M. Chamberlain, C. A. Brown, Formation of an adduct of triphenylboroxin and p-phenylenediamine, *Journal of Organic Chemistry* **1961**, *26*, 2154.

[22] J. F. Mariategui, K. Niedenzu, Boron-nitrogen compounds. CXX. Complexes of B-triethylboroxin with ethylenediamine and derivatives thereof, *Journal of Organometallic Chemistry* **1989**, *369*, 137.

[23] B. Xie, H. S. Lee, H. Li, X. Q. Yang, J. McBreen, L. Q. Chen, New electrolytes using Li2O or Li2O2 oxides and tris(pentafluorophenyl) borane as boron based anion receptor for lithium batteries, *Electrochem. Commun.* **2008**, *10*, 1195.

[24] X. Sun, H. S. Lee, X.-Q. Yang, J. McBreen, The compatibility of a boron-based anion receptor with the carbon anode in lithium-ion batteries, *Electrochem. Solid-State Lett.* **2003**, *6*, A43.

[25] X. Sun, H. S. Lee, S. Lee, X. Q. Yang, J. McBreen, A novel lithium battery electrolyte based on lithium fluoride and a tris(pentafluorophenyl) borane anion receptor in DME, *Electrochem. Solid-State Lett.* **1998**, *1*, 239.

[26] Z. Chen, K. Amine, Bifunctional electrolyte additive for lithium-ion batteries, *Electrochem. Commun.* **2007**, *9*, 703.

[27] H. J. Frohn, N. Y. Adonin, V. V. Bardin, V. F. Starichenko, Polyfluoroorganoboron-oxygen compounds. 1. Polyfluorinated aryl(dihydroxy)boranes and tri(aryl)boroxins, *Z. Anorg. Allg. Chem.* **2002**, *628*, 2827.

[28] H. Zeng, R. Hua, Palladium-Catalyzed Hydrophenylation of Alkynes with Sodium Tetraphenylborate under Mild Conditions, *J. Org. Chem.* **2008**, *73*, 558.

[29] B. M. Rambo, J. J. Lavigne, Defining Self-Assembling Linear Oligo(dioxaborole)s, *Chem. Mater.* **2007**, *19*, 3732.

[30] Y. Cao, M. D. Beachy, D. A. Braden, L. Morrill, M. N. Ringnalda, R. A. Friesner, Nuclear-magnetic-resonance shielding constants calculated by pseudospectral methods, *J. Chem. Phys.* **2005**, *122*, 224116/1.

[31] D. Hong, P. J. Carroll, L. G. Sneddon, Synthesis and structural characterization of an 11-vertex nido-diphosphaborane, 7,9-Ph2-nido-7,9-P2B9H9, *J. Organomet. Chem.* **2003**, *680*, 61.

[32] M. E. Bluhm, M. G. Bradley, R. Butterick, III, U. Kusari, L. G. Sneddon, Amineborane-Based Chemical Hydrogen Storage: Enhanced Ammonia Borane Dehydrogenation in Ionic Liquids, *J. Am. Chem. Soc.* **2006**, *128*, 7748.

[33] H. Jacobsen, H. Berke, S. Doering, G. Kehr, G. Erker, R. Froehlich, O. Meyer, Lewis Acid Properties of Tris(pentafluorophenyl)borane. Structure and Bonding in L-B(C6F5)3 Complexes, *Organometallics* **1999**, *18*, 1724.

[34] X. Zhu, G. Perry, M. A. Smith, Two hits and you're out? A novel mechanistic hypothesis of Alzheimer disease, *Adv. Behav. Biol.* **2008**, *57*, 191.

[35] K. A. Connors, *Binding Constants: The Measurements of Molecular Complex Stability*, John Wiley, New York, **1987**.

[36] K. Hirose, A practical guide for the determination of binding constants, *J. Inclusion Phenom. Macrocyclic Chem.* **2001**, *39*, 193.

[37] A. S. Karikari, B. D. Mather, T. E. Long, Association of Star-Shaped Poly(D,L-lactide)s Containing Nucleobase Multiple Hydrogen Bonding, *Biomacromolecules* **2007**, *8*, 302.

[38] G. F. Atkinson, Equilibrium composition, additive properties, and stoichiometry, *J. Chem. Educ.* **1974**, *51*, 792.

[39] W. C. Vosburgh, G. R. Cooper, Complex ions. I. The identification of complex ions in solution by spectrophotometric measurements, *J. Am. Chem. Soc.* **1941**, *63*, 437.

[40] S. Aldridge, I. A. Fallis, S. T. Howard, Anion binding by multidentate Lewis acids: a DFT study, *Chem. Commun. (Cambridge)* **2001**, 231.

[41] M. H. Mohamed, L. D. Wilson, J. V. Headley, K. M. Peru, Electrospray ionization mass spectrometry studies of cyclodextrin-carboxylate ion inclusion complexes, *Rapid Commun. Mass Spectrom.* **2009**, *23*, 3703.

[42] B. Kralj, A. Smidovnik, J. Kobe, Mass spectrometric investigations of alpha - and beta - cyclodextrin complexes with ortho-, meta- and para-coumaric acids by negative mode electrospray ionization, *Rapid Commun. Mass Spectrom.* **2009**, *23*, 171.

[43] M. G. Barlow, R. N. Haszeldine, C. J. Peck, Valence-bond isomer chemistry. Part 11. Thermal arrangement of the Diels-Alder adduct of hexafluorobicyclo[2.2.0]-2,5-hexadiene and 2,3-dimethyl-1,3-butadiene: a [1,3] sigmatropic shift of fluorine, *J. Fluorine Chem.* **1981**, *18*, 601.

[44] M. G. Barlow, R. N. Haszeldine, C. J. Peck, Valence-bond isomer chemistry. Part 12. Pyrolysis of the hexafluorobicyclo[2.2.0]hexa-2,5-diene-diazomethane adduct. Sigmatropic fluorine shifts and elimination of difluorocarbene from hexafluorocycloheptatrienes, *J. Fluorine Chem.* **1982**, *20*, 771.

[45] J. Burdon, A. Childs, I. W. Parsons, T. W. Rimmington, The sigmatropic migration of fluorine, *J. Fluorine Chem.* **1981**, *18*, 75.

[46] M. Driess, S. Rell, H. Pritzkow, R. Janoschek, R2Si:PSiR2R: 1,3-sigmatropic migration of fluorine in a 2-phospha-1,3-disilaallyl derivative capable of conjugation and its conversion to phosphadisilacyclopropanes, *Angew. Chem., Int. Ed. Engl.* **1997**, *36*, 1326.

[47] E. Chamorro, J. C. Santos, B. Gomez, R. Contreras, P. Fuentealba, Topological analysis of the electron localization function applied to the study of the [1,3] sigmatropic shift of fluorine in 3-fluoropropene, *J. Chem. Phys.* **2001**, *114*, 23.

[48] N. G. Nair, M. Blanco, W. West, F. C. Weise, S. Greenbaum, V. P. Reddy, Fluorinated Boroxin-Based Anion Receptors for Lithium Ion Batteries: Fluoride Anion Binding, Ab Initio Calculations, and Ionic Conductivity Studies, *J. Phys. Chem. A* **2009**, *113*, 5918.

[49] A. D. Becke, Density-functional thermochemistry. III. The role of exact exchange, *J. Chem. Phys.* **1993**, *98*, 5648.

[50] D. J. Tannor, B. Marten, R. Murphy, R. A. Friesner, D. Sitkoff, A. Nicholls, B. Honig, M. Ringnalda, W. A. Goddard, III, Accurate First Principles Calculation of Molecular Charge Distributions and Solvation Energies from Ab Initio Quantum Mechanics and Continuum Dielectric Theory, *J. Am. Chem. Soc.* **1994**, *116*, 11875.

VITA

Nanditha Govindan Nair was born in Kerala, India on May 31st, 1982. She was awarded the Bachelor of Science in chemistry from Kannur University, India in 2002. To further her education she decided to pursue her Master of Science at Cochin University of Science and Technology. After completing the Masters program in Applied Chemistry, she was accepted as a graduate student at Missouri University of Science and Technology, Rolla, Missouri, USA. Under the guidance of Dr. V. Prakash Reddy, Associate professor, Department of Chemistry, Missouri University of Science and Technology, she started her graduate research in Chemistry, while being a teaching assistant. She received her doctorate degree in Chemistry in Spring 2011.